RADIATION DOSIMETRY AND MEDICAL PHYSICS CALCULATIONS USING MCNP 5

A Thesis

by

RANDALL ALEX REDD

Submitted to the Office of Graduate Studies of
Texas A&M University
in partial fulfillment of the requirements for the degree of

MASTER OF SCIENCE

May 2003

Major Subject: Health Physics

RADIATION DOSIMETRY AND MEDICAL PHYSICS CALCULATIONS USING MCNP 5

A Thesis

By

RANDALL ALEX REDD

Submitted to the Office of Graduate Studies of
Texas A&M University
in partial fulfillment of the requirements for the degree of

MASTER OF SCIENCE

Approved as to style and content by:

_____	_____
Ian S. Hamilton	John W. Poston Sr.
(Chair of Committee)	(Member)
_____	_____
John R. Ford	Edward D. Harris
(Member)	(Member)
	_____
	William E. Burchill
	(Head of Department)

May 2003

Major Subject: Health Physics

ABSTRACT

Radiation Dosimetry and Medical Physics Calculations Using MCNP 5. (March 2003)
Randall Alex Redd, B.S., Texas A&M University
Chair of Advisory Committee: Dr. Ian S. Hamilton

Six radiation dosimetry and medical physics problems were analyzed using a beta version of MCNP 5 as part of an international intercomparison of radiation dosimetry computer codes, sponsored by the European Commission committee on the quality assurance of computational tools in radiation dosimetry. Results have been submitted to the committee, which will perform the inter-code comparison and publish the results independently. A comparison of the beta version of MCNP 5 with MCNP 4C2 is made, as well as a comparison of the new Doppler broadening feature. Comparisons are also made between the *F8 and F6 tallies, neutron tally results with and without the use of the S(α,β) cross sections, and analytically derived peak positions with pulse height distributions of a Ge detector obtained using the beta version of MCNP 5.

The following problems from the study were examined:

Problem 1 was modeled to determine the near-field angular anisotropy and dose distribution from a high dose rate ^{192}Ir brachytherapy source in a surrounding spherical water phantom.

Problem 2 was modeled to find radial and axial dose in an artery wall from an intravascular brachytherapy ^{32}P source.

Problem 4 was modeled to investigate the response of a four-element TLD-albedo personal dosimeter from neutrons and/or photons. Significant differences in neutron response with S(α,β) cross sections compared to results without these cross sections were found.

Problem 5 was modeled to obtain air kerma backscatter profiles for 150 and 200 kVp X-rays upon a water phantom. Air kerma backscatter profiles were determined along the apothem and diagonal of the front face of the phantom. A comparison of experimental results is also made.

Problem 6 was modeled to determine indirect spectral and energy fluences upon two neutron detectors within a calibration bunker. The largest indirect contribution was found to come from low energy neutrons with an average angle of 47^{o} where 0^{o} is a plane parallel to the floor.

Problem 7 was modeled to obtain pulse height distributions for a germanium detector. Comparison of analytically derived peaks with peak positions in the spectra are made. An examination of the Doppler broadening feature is also included.

ACKNOWLEDGMENTS

I would like to thank Dr. Tim Goorley for his patience through all my questions and for his willingness to continue working on this project after my summer work was complete. It was not easy to send this work back and forth through email or to get the computer time to run all of these problems. I would also like to thank Dr. Elizabeth Selcow-Stein and Dr. Ian Hamilton for their wonderful mentoring during this project. I also greatly appreciate the support of Dr. John Poston, Dr. John Ford, Dr. Edward Harris, Dr. Wendy Keeney-Kennicutt, the faculty and staff of the Department of Nuclear Engineering, and the First Year Chemistry Program.

I greatly appreciate the help, support and understanding of my family and friends. May everyone be safe and well.

TABLE OF CONTENTS

LIST OF FIGURES

LIST OF TABLES

INTRODUCTION

MCNP is a general-purpose Monte Carlo N-Particle code that can be used for neutron, photon, electron, or coupled neutron/photon/electron transport within an arbitrary three-dimensional configuration of materials in geometric cells. Unlike a deterministic method, which solves the transport equation for the average particle behavior, the Monte Carlo method obtains an answer by simulating individual particles, tallying the results, and inferring the average behavior of particles in a physical system from the average behavior of simulated particles using the central limit theorem (Briesmeister 2000).

Six problems involving radiation dosimetry and medical physics have been modeled in this study. These problems are a part of an international intercomparison of radition dosimetry computer codes, sponsored by the European Commission committee on the quality assurance of computational tools in radiation dosimetry, QUADOS. This study does not attempt to compare the different computational codes, but does compare the beta version of MCNP 5 with previous versions of MCNP, specifically MCNP 4C2.

In addition, a comparison of results with the new Doppler broadening feature, obtained in the context of the problems given by QUADOS with and without this feature, has been made. This new feature should improve the accuracy of modeling low energy photon transport.

Finally, a comparison between analytically derived results and the results with and without the new Doppler broadening feature is made. The Compton edge in a pulse height distribution can be analytically determined, as well as any X-ray escape peak energies. These analytically derived values will be compared with the values obtained using a model of a Ge detector to obtain pulse height distributions.

Throughout this work, the beta version of MCNP 5 was securely maintained within Los Alamos such that input files were sent to Dr. Tim Goorley and run at his convenience with the results being sent back for analysis and reporting. All reports have gone through the security offices at LANL for clearance before release.

Each problem is discussed separately so that there are several different results and conclusion sections as they apply to each individual problem.

This thesis follows the style and format of Health Physics.

BACKGROUND

QUADOS

The international intercomparison consists of eight benchmark problems. The results were originally due 15 October 2002, but were extended to 20 January 2003, for participants who worked on multiple problems. These benchmark problems are intended to:

- provide a snapshot of the methods and codes currently in use,
- furnish information on the methods used to assess the reliability of computational results,
- disseminate "good practice" throughout the radiation dosimetry community,
- provide the users of computational codes with an opportunity to quality assure their own procedures,
- inform the radiation safety and medical physics communities about the benefits to be obtained from sensitivity and uncertainty analysis, and
- inform the above communities about the more sophisticated computational dosimetry approaches that may be available to them (Siebert 2003).

The eight problems suggested in the QUADOS study are:

1. ^{192}Ir brachytherapy source problem
2. Endovascular radiotherapy problem
3. Dose distribution of a proton beam in a water phantom
4. Neutron and/or photon response of a TLD-albedo personal dosimeter on an ISO slab phantom
5. Air kerma backscatter profiles for two ISO photon expanded and aligned fields impinging on the ISO water phantom
6. Calibration of neutron detectors in a bunker
7. Peak efficiencies and pulse height distributions of a photon germanium spectrometer in the energy range below 1 MeV
8. Constancy check source.

Seven of these problems were attempted. Problems three and eight could not be accomplished because the first involves proton dose to a spherical water phantom, which cannot be modeled in MCNP version 5 because it lacks the capability to transport either protons or alpha particles. There was also not enough information provided in problem eight to complete it.

Results of the intercomparison will hopefully point out which methods and codes are more reliable, accurate, and perhaps easier to use in the context of these problems. It may also point out some of the weaknesses of various codes. For example, MCNP is not very good at transporting low energy photons. The germanium spectrometer problem has shown that a 15 keV photon incident upon the

detector will produce only the most significant of interactions. Other interactions result in either no tally within the given bin or a result with significant error. While the new Doppler broadening feature attempts to address this lack of accuracy for low energy photons, additional computational methods are needed, like perhaps the $S(\alpha,\beta)$ cross sections employed with the physics of low energy neutrons. Other codes may already take this into account and may produce more accurate results for the same problem. By knowing which programs will work best in which areas we will be able to further increase the accuracy of our modeling.

MCNP vs. Deterministic Method

Deterministic transport methods solve a transport equation for the average particle behavior throughout the phase space of the problem. For example, the discrete ordinates method will divide phase space into many small boxes for particles to travel within. As the volumes of the boxes are decreased, these particles will take a differential amount of time to move a differential distance in space. In the limit this approaches the integro-differential transport equation, which has derivatives in space and time. The Monte Carlo method obtains an answer by simulating individual particles and tallying certain aspects of their behavior such as the number of ^{6}Li neutron capture reactions, $^{6}Li(n,t)^{4}He$. The average behavior of particles in a physical system is then inferred from the average behavior of the simulated particles using the central limit theorem. The tallied aspects of the simulated particles' behavior are then the obtained answer. This method transports particles in space and time so it is sometimes said this solves the integral transport equation, which does not have time or space derivatives (Briesmeister 2000).

Doppler Broadening

When incoherent scattering of an incident photon occurs, producing a Compton electron and a scattered photon, the effect of the electron binding energy on the energy of the scattered photon has been ignored in previous MCNP versions. The electron binding energy will also affect the angle of the scattered photon, but this has already been taken into account by modifying the Klein-Nishina differential cross section with a form factor. The effect of binding energy on the energy of the scattered photon is to broaden the energy spectrum due to the precollision momentum of the electron. A new feature takes this into account by using the Hartree-Fock Compton profile to sample the projected momentum and to directly calculate the final energy of the scattered photon (Sood 2002).

PROBLEM ONE: ^{192}Ir BRACHYTHERAPY SOURCE

Description of Problem

The first two problems are high-dose brachytherapy devices. Brachytherapy is a medical procedure in which a radioactive source is placed within a body cavity or tumor (interstitial), or in close proximity to a tumor (intercavitary) (Bast et al. 2000). These two problems specifically focus on endovascular or vascular brachytherapy use following balloon angioplasty to prevent restenosis caused by intimal hyperplasia, or the re-closing of the plaque, which would again block the artery.

The different brachytherapy devices are designed to provide a high dose, typically 12 Gy, to the plaque and surface of the artery with very little dose to surrounding tissue, making it a more attractive choice than for example, an external beam. This is possible due to the physical configuration of the catheters. An algorithm has been developed to calculate near-field dose with these devices, but has been reported to contain errors in the radial dose and anisotropy functions. Problem one repeats work that has been previously published pointing out these errors with MCNP 4A (Wong et al. 1999).

This brachytherapy device uses a gamma source, ^{192}Ir, to deliver a high dose-rate in the near-field (defined to be < 5 cm by the author of the problem, Dr. Robert Price) to surrounding water. The dose is determined for both radial and anisotropic distributions using a beta version of MCNP 5. This version did not include the Doppler broadening feature. The anisotropic distribution is in ten-degree increments from 0^o to 180^o with 0^o defined to be the axis through the center of the device along the woven steel cable. The anistropic dose distribution was determined by cutting the surrounding sphere into wedges with 10^o width and tallying within these cells as shown in Fig. 1, below.

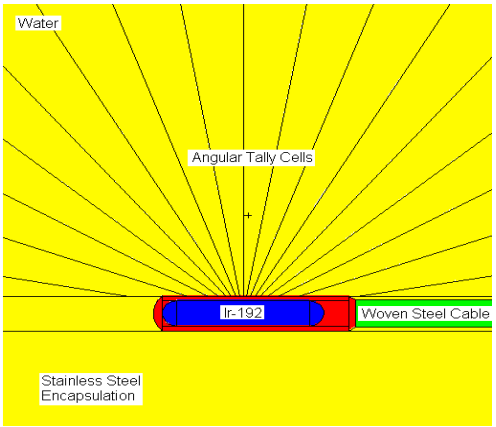

Fig. 1. Side view of anisotropic brachytherapy model. The angular tally cells are wedges of a sphere cut at 10^o increments. Radius of ^{192}Ir core is 0.065 cm.

The radial distribution was determined with concentric cylinders about the source cylinder as shown in Fig. 2, below. APPENDIX A contains example input files for all of the problems.

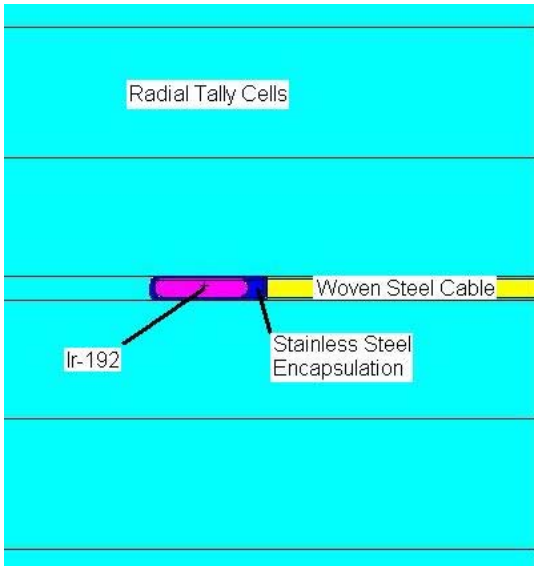

Fig. 2. Side view of radial brachytherapy model. The radial tally cells are cylinders with increasing radii of 0.5 cm.

Geometry Specifications

The ^{192}Ir brachytherapy device, which is shown in Fig. 3 on the next page, is an ^{192}Ir core cylinder with radius 0.0325 cm geometrically centered at the origin. It is capped at both ends by half spheres with the same radii to give a total length of 0.36 cm. This ^{192}Ir core is encased in a stainless steel cylinder, radius 0.045 cm, with a half sphere cap, radius 0.061 cm, at one end and a cone that connects to the woven steel cable to give a maximum length of 0.45 cm to the steel encapsulation. The material of the capsule and cable is the same steel but with different densities. It has been assumed that the demarcation between the two different densities is at the smaller end of the cone. A 5 cm radius sphere filled with water surrounds the device, which also serves as the boundary of the problem (Siebert 2003).

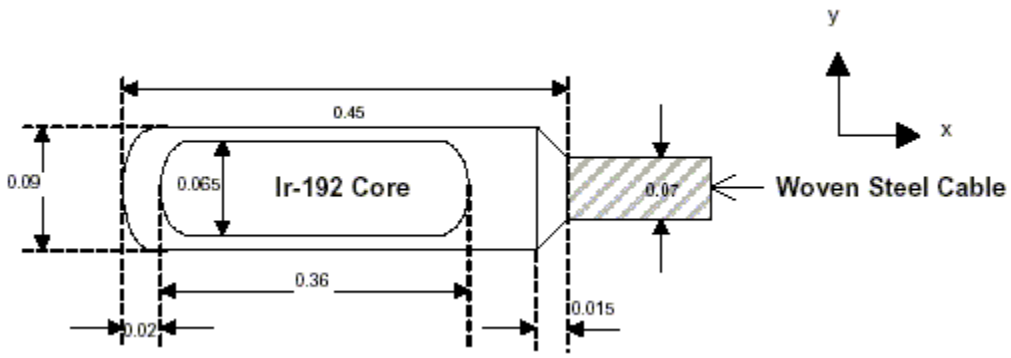

Fig. 3. Geometry of ^{192}Ir brachytherapy device (Siebert 2003).

Source Specifications

The source contains a cylinder with two half spherical caps at the ends, which were all included in the same cell description, cell 1. The source was then defined as a cylindrical source with radius equal to the radius of the ^{192}Ir cylinder and spheres. The extent was defined as the distance from the center to the outer edge of the caps. By including cell 1 in the source definition card (SDEF card), only the source points sampled within cell 1 are used, which makes the source geometry appropriate for the source with two half spherical end caps. This description, therefore, gives a uniform distribution of source points within a cylinder as well as within cell 1 that is inside of this cylinder.

Some biasing of the source was originally tested, but it was found that particles, probably from the center of the source, had a high weight that would sometimes affect large changes in the variance of the variance. The variance of the variance is an indication of the relative statistical uncertainty in the estimated relative error and is very sensitive to large history-score fluctuations or large changes in the tally (Briesmeister 2000).

Tally Specifications

The radial dose distribution was determined by placing cylinders about the ^{192}Ir core and steel encapsulation in 0.5 cm radial increments up to the 5 cm radius sphere. The anisotropic dose distribution was originally set up for five-degree increments, but the results did not converge in a reasonable timeframe. The variance of the variance also fluctuated, indicating a high weight/low probability event was not being sampled enough. The wedges were increased to ten-degree increments to try to offset this.

Both the F6 and *F8 tallies were used in the anisotropic and radial dose determinations. The F6 tallies, which give results in MeV g^{-1}, were converted to Gray (Gy) with the tally multiplier card (FM card). The *F8 tallies, which give results in MeV, were later converted to Gy by dividing by the mass

within the cell and multiplying by 6.02E-10 to convert the units from MeV g^{-1} to J kg^{-1} (Gy). The mass within the cell was determined by multiplying the density of material in the cell by the volume of the cell.

Results

The radial and angular anisotropic dose distributions have been determined with each result normalized to one source particle. The radial dose distribution is given in Table 1 below. Note that in the discussion it is recommended that the results for the anisotropic distribution be kept to three significant figures, but the tables actually include four to allow readers to compare between the F6 and *F8 tally results.

Table 1. Radial dose distribution for ^{192}Ir brachytherapy device.

Average Distance Within the Bin from Origin (center of source cylinder)	F6 Tally Result (Gy)	Standard Deviation (±)	*F8 Converted Tally Result (Gy)	Standard Deviation (±)	Difference Between F6 and *F8 Tally Results (%)	Standard Deviation (±)
0.25	1.343E-13	1.3E-17	1.343E-13	8.10E-17	0.00	- - -
0.75	4.673E-14	4.7E-18	4.679E-14	2.30E-17	0.13	0.050
1.25	2.681E-14	2.7E-18	2.684E-14	1.60E-17	0.11	0.061
1.75	1.828E-14	1.8E-18	1.831E-14	1.10E-17	0.16	0.061
2.25	1.356E-14	1.4E-18	1.359E-14	8.20E-18	0.22	0.061
2.75	1.058E-14	1.1E-18	1.060E-14	6.40E-18	0.19	0.061
3.25	8.531E-15	8.5E-19	8.547E-15	6.00E-18	0.19	0.071
3.75	7.040E-15	7.0E-19	7.050E-15	4.90E-18	0.14	0.070
4.25	5.910E-15	5.9E-19	5.913E-15	5.30E-18	0.051	0.090
4.75	5.061E-15	1.0E-18	5.059E-15	6.10E-18	0.040	0.12

Fig. 4, below, is a graph of the results of the radial dose profile. The angular anisotropic dose distribution is given in Table 2 on the following page.

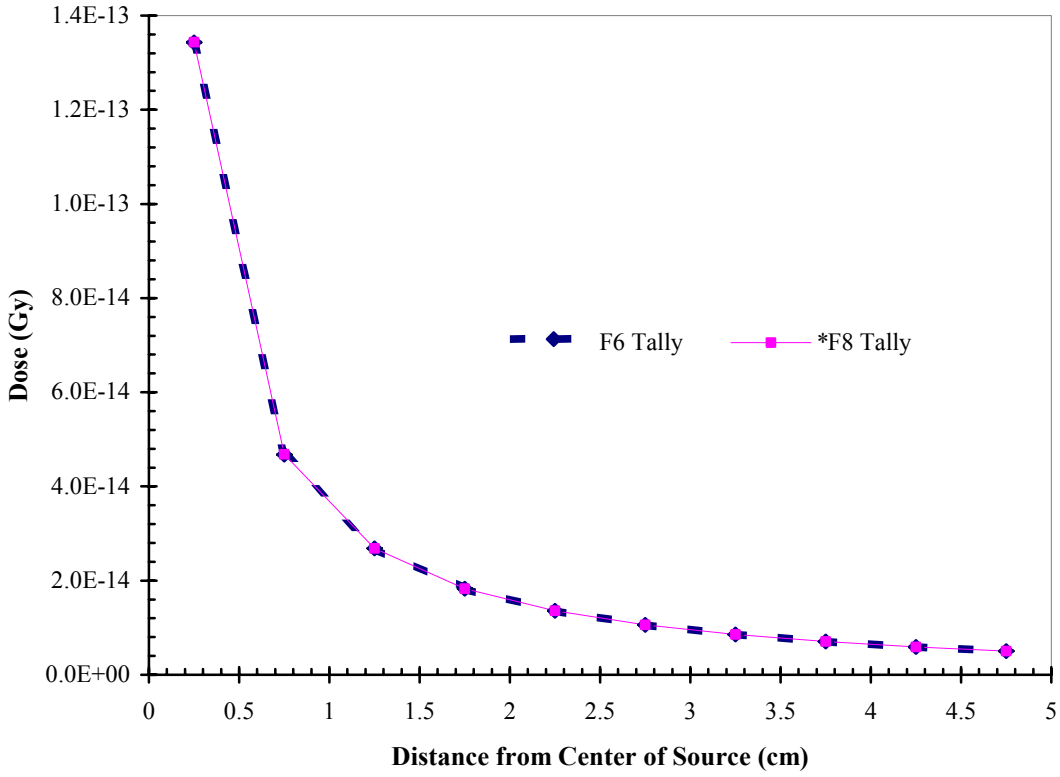

Fig. 4. Radial dose profile from center of source for ^{192}Ir brachytherapy device. The statistical error indicates one standard deviation and is smaller than the size of the data points.

Table 2. Angular dose distribution for ^{192}Ir brachytherapy device.

Average Angle (degrees)	F6 Tally Result (Gy)	Standard Deviation (±)	*F8 Tally Converted to Dose (Gy)	Standard Deviation (±)	Difference Between F6 and *F8 Tally Results (%)	Standard Deviation (±)
5	1.329E-14	6.6E-18	1.331E-14	1.3E-17	0.15	0.11
15	1.392E-14	7.0E-18	1.392E-14	1.4E-17	0.00	- - -
25	1.431E-14	7.2E-18	1.435E-14	1.4E-17	0.28	0.11
35	1.453E-14	5.8E-18	1.453E-14	1.5E-17	0.00	- - -
45	1.463E-14	5.9E-18	1.464E-14	1.3E-17	0.07	0.098
55	1.470E-14	5.9E-18	1.472E-14	1.3E-17	0.14	0.097
65	1.473E-14	5.9E-18	1.477E-14	1.3E-17	0.27	0.097
75	1.476E-14	5.9E-18	1.478E-14	1.3E-17	0.14	0.097
85	1.476E-14	5.9E-18	1.476E-14	1.3E-17	0.00	- - -
95	1.477E-14	5.9E-18	1.479E-14	1.3E-17	0.14	0.097
105	1.475E-14	5.9E-18	1.479E-14	1.3E-17	0.27	0.097
115	1.473E-14	5.9E-18	1.474E-14	1.3E-17	0.068	0.097
125	1.470E-14	5.9E-18	1.471E-14	1.3E-17	0.07	0.097
135	1.464E-14	5.9E-18	1.463E-14	1.3E-17	0.07	0.098
145	1.452E-14	5.8E-18	1.454E-14	1.5E-17	0.14	0.11
155	1.432E-14	7.2E-18	1.434E-14	1.4E-17	0.14	0.11
165	1.395E-14	7.0E-18	1.396E-14	1.4E-17	0.072	0.11
175	1.339E-14	6.7E-18	1.340E-14	1.3E-17	0.075	0.11

A graph of these results is given in Fig. 5 on the following page.

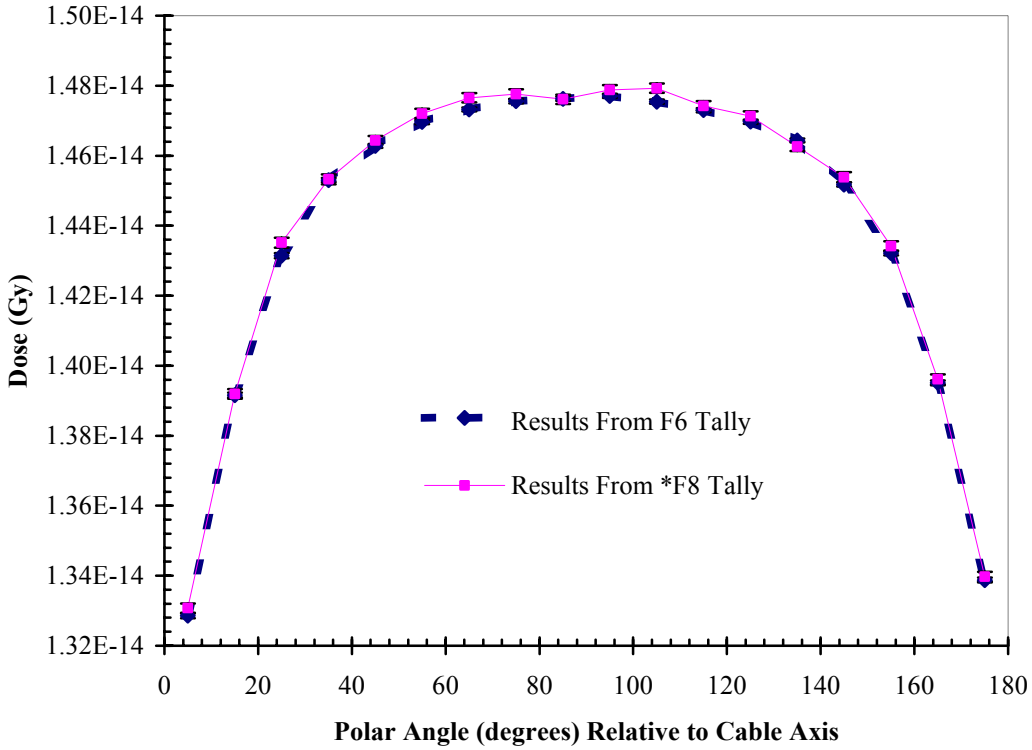

Fig. 5. Angular anisotropic dose profile for ^{192}Ir brachytherapy device. The statistical error indicates one standard deviation and is smaller than the size of the data points.

Fig. 6 on the following page shows a closer view of the angular anisotropic dose profile from 40^{o} to 140^{o} to better show the difference between the two tallies.

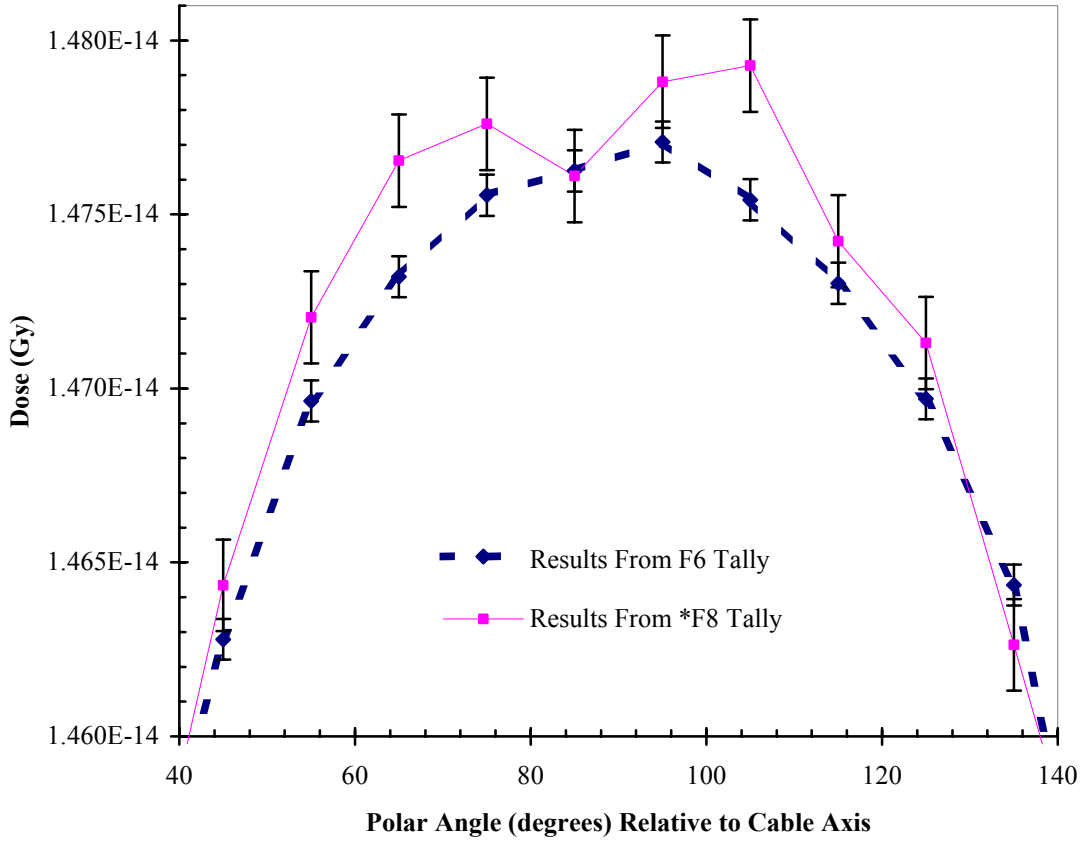

Fig. 6. Close-up of angular anisotropic dose profile for ^{192}Ir brachytherapy device. The statistical error indicates one standard deviation.

Discussion

The volume of the wedges had to be calculated and input by hand for the tallies in the anisotropic dose determination because the F6 tally uses this volume to determine mass within the given cell. Mass within the cells is calculated by the MCNP program by multiplying the volume of the cell times the density of the material within the cell. An exact calculation of the cell volumes could not be performed because the wedges have a cylinder, that runs unevenly through them. Furthermore, the cylinder is capped at both ends by the 5 cm sphere so the caps are not right angles to the cylinder. Assuming the length of the cylinder to be 10 cm the volume is therefore, 0.0636 cm^3. The volume of each wedge, neglecting the cylinder, is 14.5444 cm^3. At most, only half of the cylinder volume might exist in the wedge and these would be the wedges from 0^o-10^o and 170^o-180^o. So for these, a volume of 14.5444 cm^3 – 0.0318086 cm^3

= 14.5126 cm^3 was used while for the rest the 14.5444 cm^3 volume was used. This introduces some error, but if the results are limited to three significant figures it should not make any difference.

The graph in Fig. 3 uses the same volumes in the calculations of the F6 and *F8 tallies allowing the two to be compared. In this problem, the two tallies compared well with differences in tally results after the third significant figure. The percent-difference in the radial dose distribution ranged from 0.0 – 0.22%, while the range for the angular anisotropic distribution went from 0.0 – 0.28%. However, both had significant error associated with the percent-difference as shown in Tables 1 and 2. It is interesting to note that the standard deviation for the F6 tally results were often outside the standard deviation for the *F8 tally results. The precision of the F6 tally was found to be smaller by about a half an order of magnitude than the *F8 tally.

PROBLEM TWO: ^{32}P BRACHYTHERAPY SOURCE

Description of Problem

The second problem uses a ^{32}P source to provide beta dose to the arterial wall. The following was determined:

- the dose rate was measured at a depth of 1 mm into the artery wall from the inside surface along the source longitudinal axis;
- the radial dose rate profile; and
- the dose rate at 1 mm depth inside the artery wall at the center of the source longitudinal axis.

To obtain a good profile of the dose rate along the source longitudinal axis, the blood and artery wall were divided into rings so the weight window generator could be applied. Originally, the source was biased so that more particles were sampled at the ends of the source cylinder. This was found to give erroneous results near the center of the source cylinder because of a low sampling frequency. This was corrected by rerunning without any source biasing.

Geometry Specifications

For this problem the balloon apparatus, which would center the catheter, was not modeled, as directed by the author of the problem, Dr. Robert Price. The ^{32}P source is a cylinder geometrically centered on the origin along the y-axis with radius 0.012 cm and length 2.7 cm. It is surrounded by a NiTi tube of inner radius 0.0154 cm and outer radius 0.023 cm (wall thickness of 0.0076 cm). A symmetric air space exists between the ^{32}P source cylinder and the NiTi cylinder wall. At the closed end of the ^{32}P source is a tungsten marker of length 0.1 cm followed by a NiTi plug also of length 0.1 cm. Both the marker and plug are the same radius as the ^{32}P source. Beyond the NiTi plug is a NiTi hemispherical weld. The radius is assumed to be the same radius as the outside wall of the NiTi tube, 0.023 cm. At the other end of the source cylinder is the NiTi guide wire. It has a radius equal to the inner radius of the NiTi tube, 0.0154 cm. The wire contacts the ^{32}P source with another half sphere that is assumed to be of the same radius as the wire, 0.0154 cm. The wire and tube both continue to the end of the phantom. Outside of the NiTi tube is the blood which ends at the inner wall of the artery, also a cylinder with radius 0.15 cm and outer wall radius 0.35 cm. Beyond the artery wall is the water phantom that extends to a radius of 15 cm and length of 30 cm. Outside of the water phantom is defined as outside of the problem, or void (Siebert 2003). A geometry plot, Fig. 7, using the Visual Editor of the side view is on the following page.

Source Specifications

The source was defined to be an isotropic cylinder source emitting beta particles. Since beta particles are emitted over a spectrum of energies, probabilities associated with these energies (as given by the author) were included in the source definition (Price 2002).

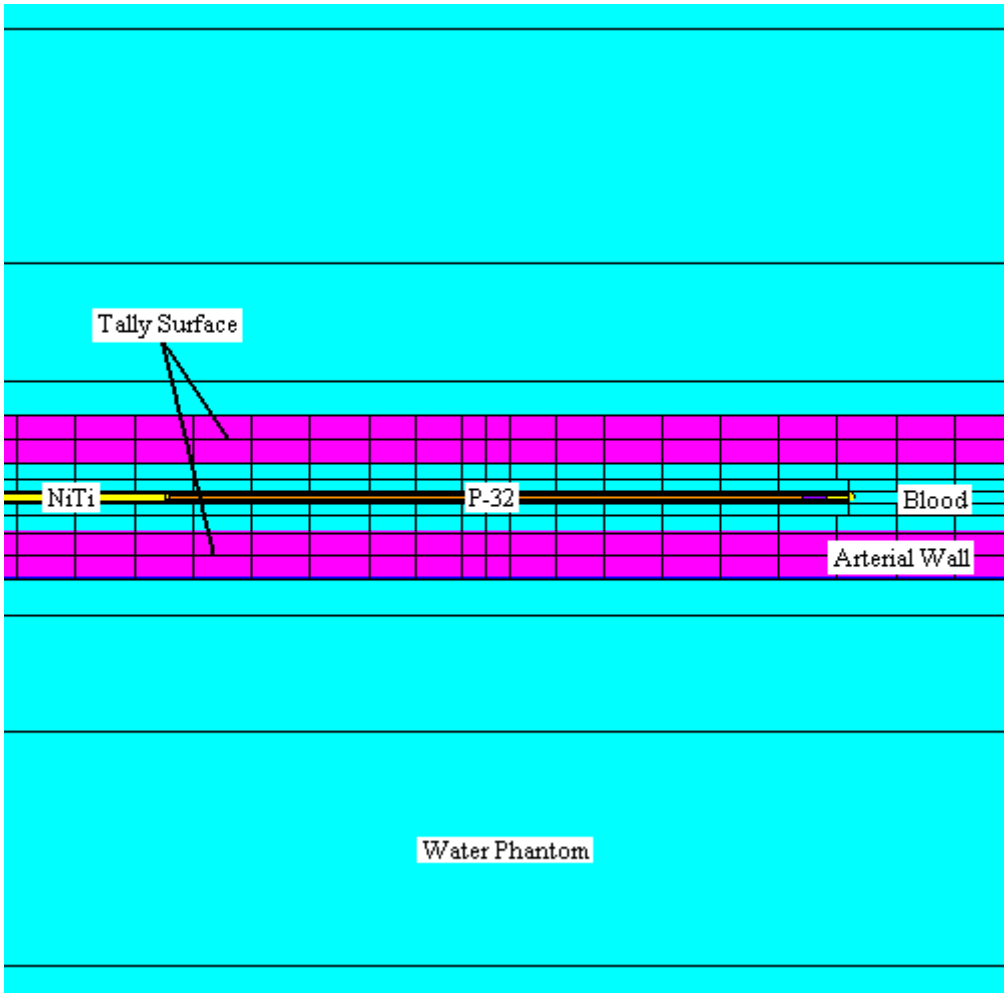

Fig. 7. Color modified Visual Editor geometry plot of the side view of ^{32}P brachytherapy device. Dose rate at 1 mm within the artery wall is determined by tally of flux across the surface indicated. From the edge of the arterial wall to the tally surface is 1 mm.

An axial MCNP geometry plot is shown on the following page as Fig. 8 to better show the cylindrical nature of this problem.

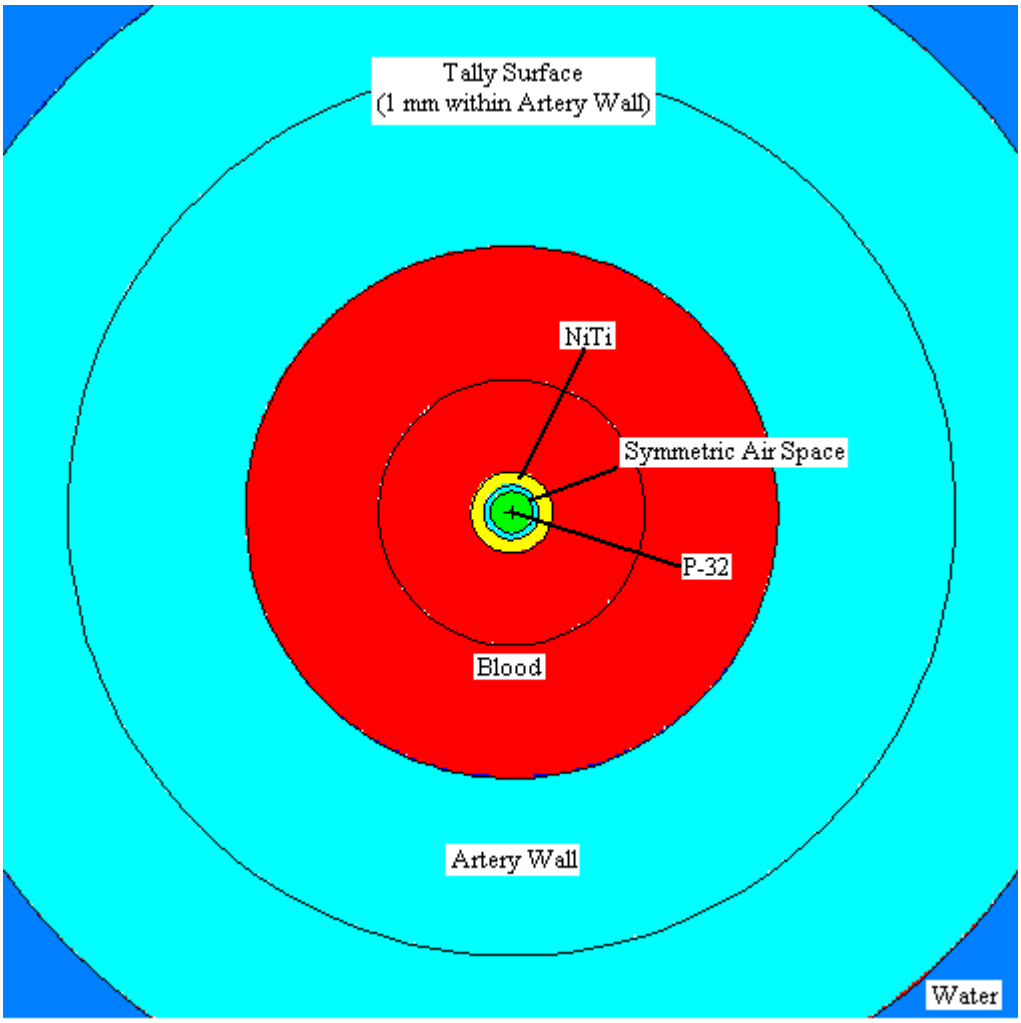

Fig. 8. Color modified MCNP geometry plot of axial view of ^{32}P brachytherapy device. The radial dose rate was determined by measuring dose within cylinders about the source axis. From the edge of the arterial wall to the tally surface is 1 mm.

Tally Specifications

In order to measure the dose rate at 1 mm depth within the artery wall along the wall, the surface of a cylinder was segmented using the FS card. The SD card was also used to indicate the surface area of the segments. It should be noted when looking at the output that because of the segmentation, the tally fluctuation chart will have a value of zero for the F4 tallies. This is because the tally fluctuation chart is an indication of the first bin only. In this case, the first bin is the segment that is actually in the void resulting in all zeros.

DE and DF cards were also used to convert MeV cm^{-2} to Gy. Values used in the DE and DF cards are the electron energy and mass collison stopping powers for adipose tissue (ICRP), respectively. Adipose tissue was the closest material in atomic composition with available mass collision stopping powers (Attix 1986).

Variance Reduction

To better sample the far ends of the cylinder of the artery wall, the cells were divided into rings. The weight window generator was then used to optimize electron flux on surface 24, which is the cylinder 1 mm into the artery wall from the inside. To further assist in getting a good weight window, the densities of all of the materials were lowered and the energy of the source electron changed to 10 MeV so that the electrons would travel further. The material densities and particle energy were changed back after generating the weight window mesh file.

Results

The input file was run twice. The first run included the biasing of the source with greater frequency of source particles occurring at the ends of the cylinder. The radial dose distribution from the center of the source cylinder was obtained from this result along with a better idea of the axial dose profile. The second run was used to obtain the dose profile along the axis of the artery wall. Results for the radial dose profile are given in Table 3, on the next page. The slope of the radial dose rate profile did not meet the statistical criteria of >3 with a value of 2.55. The slope is one of the statistical checks indicating whether enough particles have been simulated to satisfy the central limit theorem. Other statistical checks did pass. Results for the second run are given in Table 4, on the following page, with a graph of the results from both runs in Fig. 9. In all cases, the dose was normalized to a single particle, but later multiplied by 7E09 to convert to a 7 GBq source.

Table 3. Radial dose rate distribution for ^{32}P brachytherapy device.

Average Distance (cm)	Radial Dose Rate (Gy s^{-1})	Standard Deviation (±)
0.049	1.00E-04	9.5E-07
0.1125	4.50E-05	6.1E-07
0.2	1.91E-05	2.4E-07
0.3	8.36E-06	1.6E-07
0.425	4.87E-06	1.7E-07
0.75	2.35E-06	1.1E-07
1.5	1.00E-06	5.4E-08
3.5	3.42E-07	2.2E-08
10	5.87E-08	4.0E-09

Table 4. Dose rate distribution at 1 mm depth in artery wall along the source axis. The source is geometrically centered at 0,0,0.

Average Distance (cm)	Dose Rate (Gy s^{-1})	Standard Deviation (±)
-1.625	1.62E-03	5.42E-05
-1.375	8.77E-02	3.68E-04
-1.125	2.03E-01	5.48E-04
-0.875	2.09E-01	5.65E-04
-0.625	2.10E-01	5.67E-04
-0.4	2.10E-01	6.29E-04
-0.2	2.09E-01	6.27E-04
0	2.09E-01	1.11E-03
0.2	2.09E-01	7.32E-04
0.4	2.10E-01	6.29E-04
0.625	2.09E-01	5.65E-04
0.875	2.10E-01	5.67E-04
1.125	2.04E-01	5.50E-04
1.375	8.76E-02	3.68E-04
1.625	1.52E-03	5.56E-05

Dose rate at 1 mm within the artery wall along the midway point of the source cylinder is 2.09E-01 ± 1.11E-03 Gy s^{-1}. This was the average dose to the surface of a 0.2 cm width ring about the center of the source cylinder 1 mm within the artery wall.

Fig. 9, below, gives the results of the dose rate at 1 mm within the artery wall along the axis. The biased source decreases in dose rate near the center of the catheter while at the same time increasing in error. The unbiased source remains fairly flat throughout the length of the source.

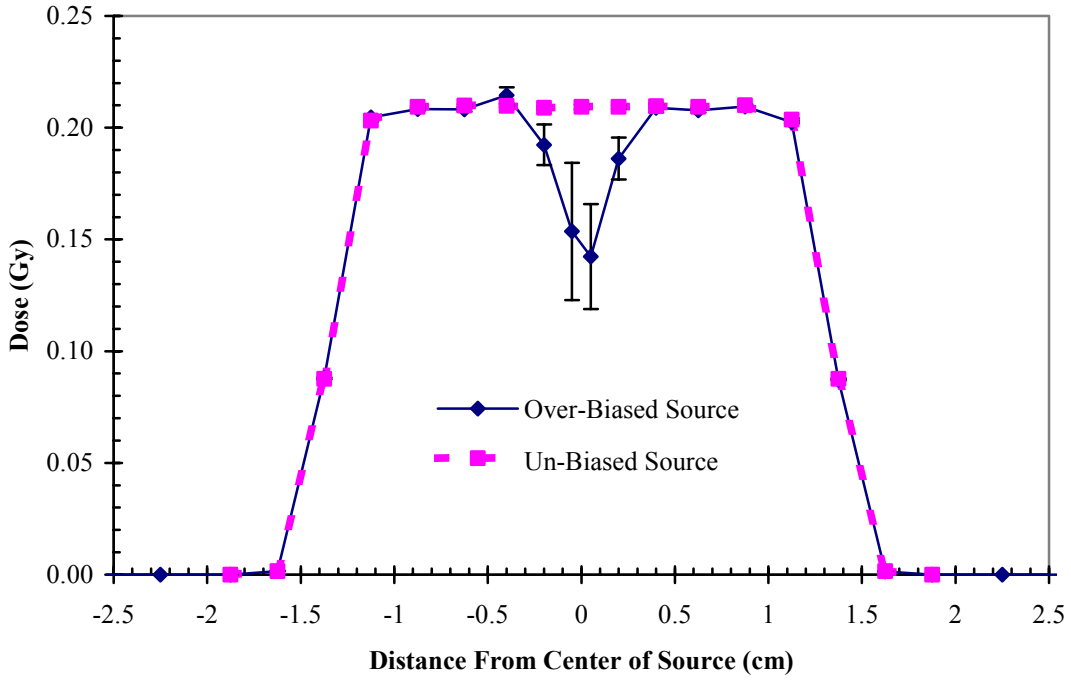

Fig. 9. Dose rate at 1 mm within artery wall for 7 GBq ^{32}P Source. The F2 tally was modified with DE and DF cards using mass collision stopping powers, converted to Gy (1.602E-10), and changed to a 7 GBq source (7E09). The statistical error is smaller than the size of the data points in most cases, but would otherwise indicate ± one standard deviation.

Discussion

The dose at 1 mm within the artery wall along the axis was very even with no peaks along the length of the source. It then quickly dropped off. The flat distribution could mean that the electrons passing through 1 mm arterial wall depth still have sufficient energy to continue on before depositing a relatively large amount of energy in the Bragg peak; or, possibly the Bragg peak for these electrons may

be insufficient to affect the distribution significantly. If the axial dose were studied further away from the source this might start to change the even profile to include a positive peak at the center.

The biased source dropped at the center of the source but the increasing relative error indicated erroneous results. In this case, the standard deviation of the biased source was outside of the standard deviation of the unbiased results.

PROBLEM FOUR: NEUTRON AND PHOTON RESPONSE OF A TLD-ALBEDO PERSONAL DOSIMETER ON AN ISO SLAB PHANTOM

Problem Description

Photon and neutron responses in a four-element TLD-albedo personal dosimeter located on the center of the front face of an ISO water filled slab phantom were determined using a beta version of MCNP 5. This version did not include the Doppler broadening feature. Photon response for photons of energy 33 keV, 48 keV, 100 keV, 248 keV, 662 keV, and 1.25 MeV were determined as energy absorbed in the TLD, which was assumed to be proportional to light output. Neutron response for neutrons with energies of 0.0253 eV, 1 eV, 10 eV, 100 eV, 1 keV, 10 keV, 100 keV, 1 MeV, 10 MeV, and 20 MeV were determined as the number of $^{6}Li(n,t)^{4}He$ capture reactions, which was again assumed to be proportional to the light output.

Comparisons of photons at energies of 33 kev, 48 keV, 100 keV, 248 keV and 1.25 MeV between versions 4C2 and 5beta3.23 were made with each run ending at 50 million histories. These comparisons began at the same random number and tracked. In addition, the 33 kev photon source was also run in versions 4C3 and 5beta4.9 to compare computer time, ctm, only.

Neutron results using the $S(\alpha,\beta)$ cross sections were compared with results obtained without these cross sections. The $S(\alpha,\beta)$ cross sections replace the free gas treatment of the particle physics at low neutron energies with some consideration of bond energies and their effect upon elastically scattered neutrons. In this problem, the bond energies of oxygen and hydrogen in water were taken into account in the water of the slab phantom.

TLDs are often used in personal dosimetry throughout the radiation industry. The elements offer a small and light device for measuring dose and when used with certain shielding materials, can approximate different types of doses such as surface dose and neutron dose. For example, this problem contains both ^{6}Li and ^{7}Li chips which would normally be compared to determine neutron dose. LiF elements also offer a close match in effective atomic number, which when compared to that of soft tissue, give a strong correlation to dose equivalent and exposure over a wide range of photon energies (Knoll 2000).

Geometry Specifications

The geometry is specified by two distinct portions, the slab phantom and the TLD. A side view of the MCNP geometry plot is given in Fig. 10 on the following page.

The phantom is a standard ISO water filled slab phantom with external dimensions 30 cm x 30 cm x 15 cm. The front wall of the phantom is 0.25 cm thick polymethyl methacrylate, PMMA, (8%

hydrogen, 32% oxygen, and 60% carbon) while the remaining walls are all 1 cm thick PMMA. The phantom is filled with water.

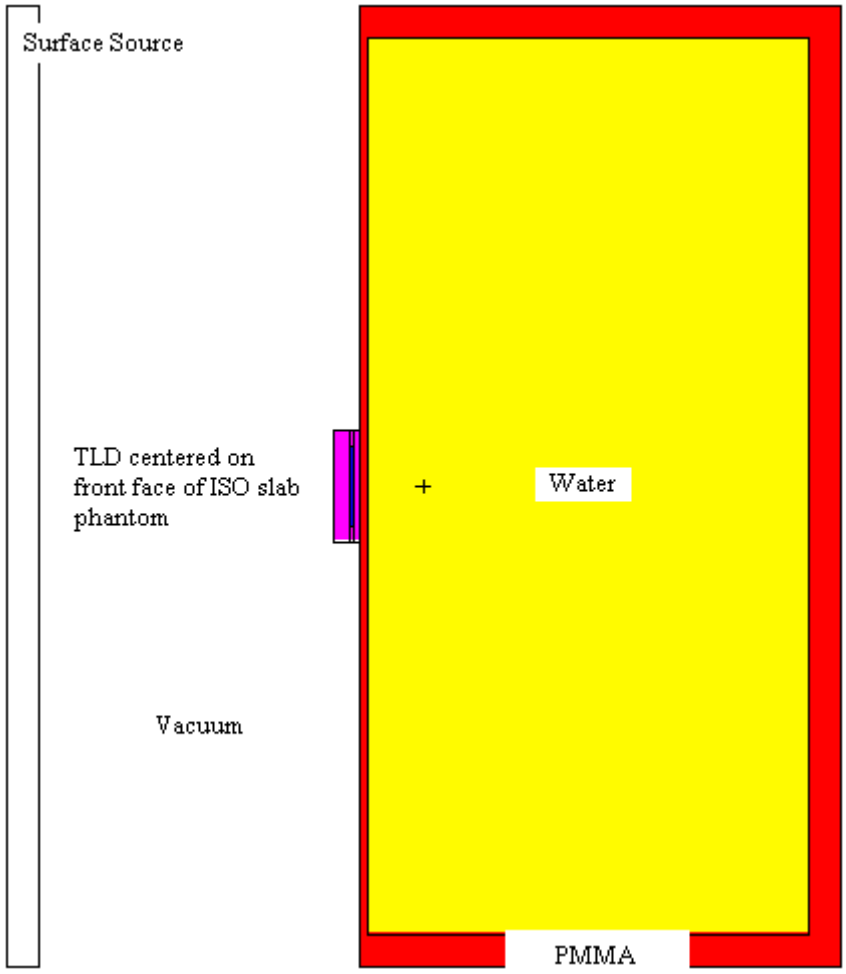

Fig. 10. Side view of MCNP geometry plot for problem 4.

The TLD model is centered on the front face of the phantom with the long axis vertical. The holder, which is polyethylene, is 35.0 mm x 55.0 mm x 7.9 mm. The top two TLD elements are ^{6}Li and ^{7}Li elements. Centered on these elements are 1.0 cm diameter cylindrical holes through the polyethylene, $(CH_2)_n$, holder. The bottom two elements are also ^{6}Li and ^{7}Li with a 1.0 cm cylindrical hole, containing vacuum, behind them that extends back to the front face of the phantom. 1 mm thick aluminum disks, also with 1.0 cm diameters, are located in front of the bottom two chips. The four elements are embedded in an

aluminum plate that is 25.0 mm x 45.0 mm x 0.9 mm. The elements are each 3.2 mm x 3.2 mm x 0.9 mm (Siebert 2003).

A front view of the TLD and depth view from the front surface are given to show shielding in Fig. 11, below.

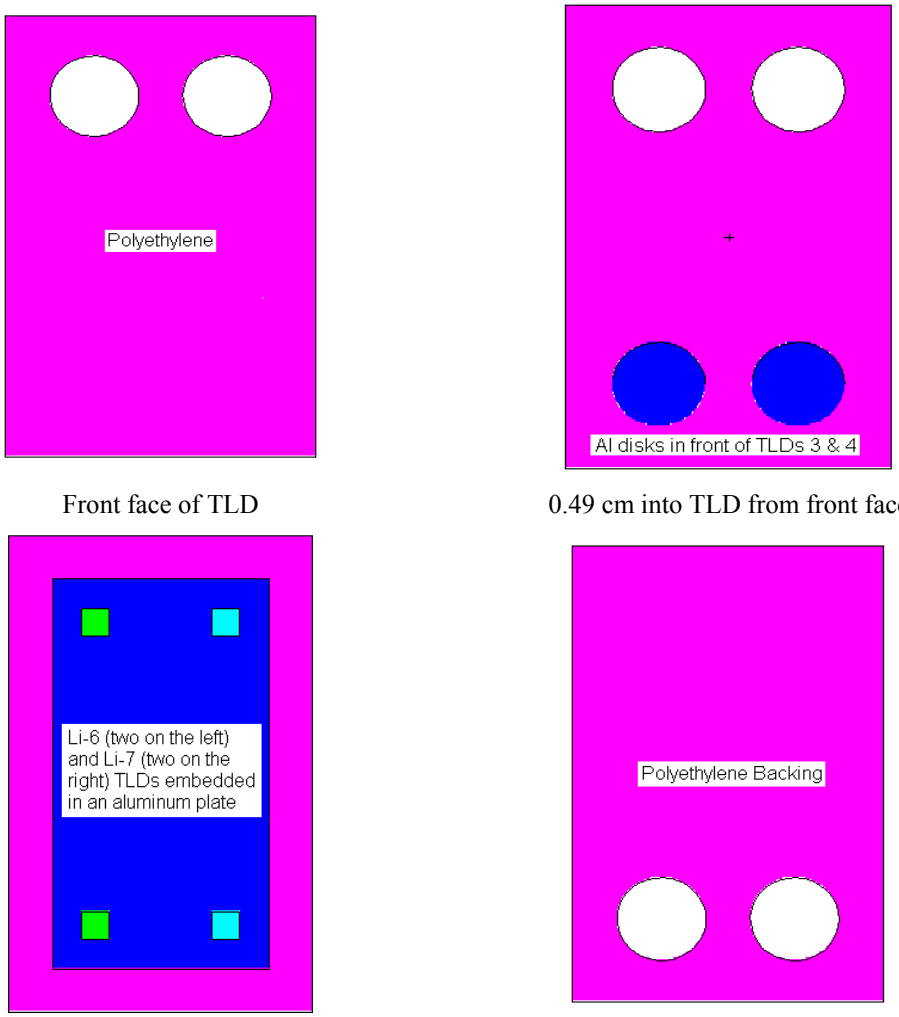

Front face of TLD

0.49 cm into TLD from front face

0.5 cm into the TLD from front face

0.59 cm into the TLD from front face

Fig. 11. MCNP geometry plot of front view of TLD followed by planar views within the TLD.

Source Specifications

The source is a surface source with the same dimension as the front face of the phantom, which emits particles normal to the front face of the slab phantom and TLD. To better sample the photons and

neutrons about the TLD, the source was biased so that more particles started out directed towards the TLD.

Photons of energies 33 keV, 48 keV, 100 keV, 248 keV, 662 keV, and 1.25 MeV were individually examined and neutrons of energies 0.0253 eV, 1 eV, 10 eV, 100 eV, 1 keV, 100 keV, 1 MeV, 10 MeV, and 20 MeV were also individually examined.

Tally Specifications

F6 tallies for the cells corresponding to the TLD elements were used to determine photon energy deposition while neutron response was measured as the number of $^{6}Li(n,t)^{4}He$ capture reactions. To count the number of capture reactions the tally multiplier card, FM, was used in conjunction with the F4 tally to specify which reaction to count. The result was then multiplied by the volume within the cell and a factor to convert the density from atoms cc^{-1} to atoms $(barns\text{-}cm)^{-1}$. The FM card requires an input of density which was not in the correct units for all of the neutron results.

Variance Reduction

Since the TLD badge was small compared to the size of the slab phantom, very few particles made it to the smaller LiF elements. Changing the importances of the cells was found to be insufficient to increase the number of particles passing through the elements. A mesh was therefore created and used to generate weight windows. This greatly improved the method with photon results usually converging within 50 million source particles. The neutrons, however, often took up to 300 million source particles to converge.

Results

Photon response was measured by determination of the amount of energy absorbed using the F6 tally. The results were multiplied by the mass within the cell to provide an answer in MeV. The results for each of the photon energies are given in Table 5 on the following page. Each result is normalized to one source particle.

Table 5. Photon response in TLD determined as energy absorbed, MeV.

	Source Photon Energy (MeV)	Energy Deposited (MeV)	Standard Deviation (±)
Element 1 (^{6}Li) Top Left	0.033	9.92E-07	4.8E-09
	0.048	5.93E-07	3.7E-09
	0.100	5.43E-07	3.6E-09
	0.248	1.33E-06	5.6E-09
	0.662	3.42E-06	7.5E-09
	1.250	5.69E-06	1.5E-08
Element 2 (^{7}Li) Top Right	0.033	9.92E-07	7.0E-09
	0.048	6.01E-07	5.5E-09
	0.100	5.37E-07	4.2E-09
	0.248	1.33E-06	8.3E-09
	0.662	3.42E-06	1.2E-08
	1.250	5.68E-06	3.0E-08
Element 3 (^{6}Li) Bottom Left	0.033	7.86E-07	9.5E-09
	0.048	5.48E-07	7.6E-09
	0.100	5.29E-07	6.9E-09
	0.248	1.29E-06	1.2E-08
	0.662	3.36E-06	2.0E-08
	1.250	5.60E-06	5.0E-08
Element 4 (^{7}Li) Bottom Right	0.033	7.76E-07	1.0E-08
	0.048	5.48E-07	7.9E-09
	0.100	5.16E-07	6.2E-09
	0.248	1.28E-06	1.5E-08
	0.662	3.35E-06	1.9E-08
	1.250	5.53E-06	5.4E-08

Fig. 12 on the following page shows these results of photon response (as energy absorbed) vs. the log of the source photon energy.

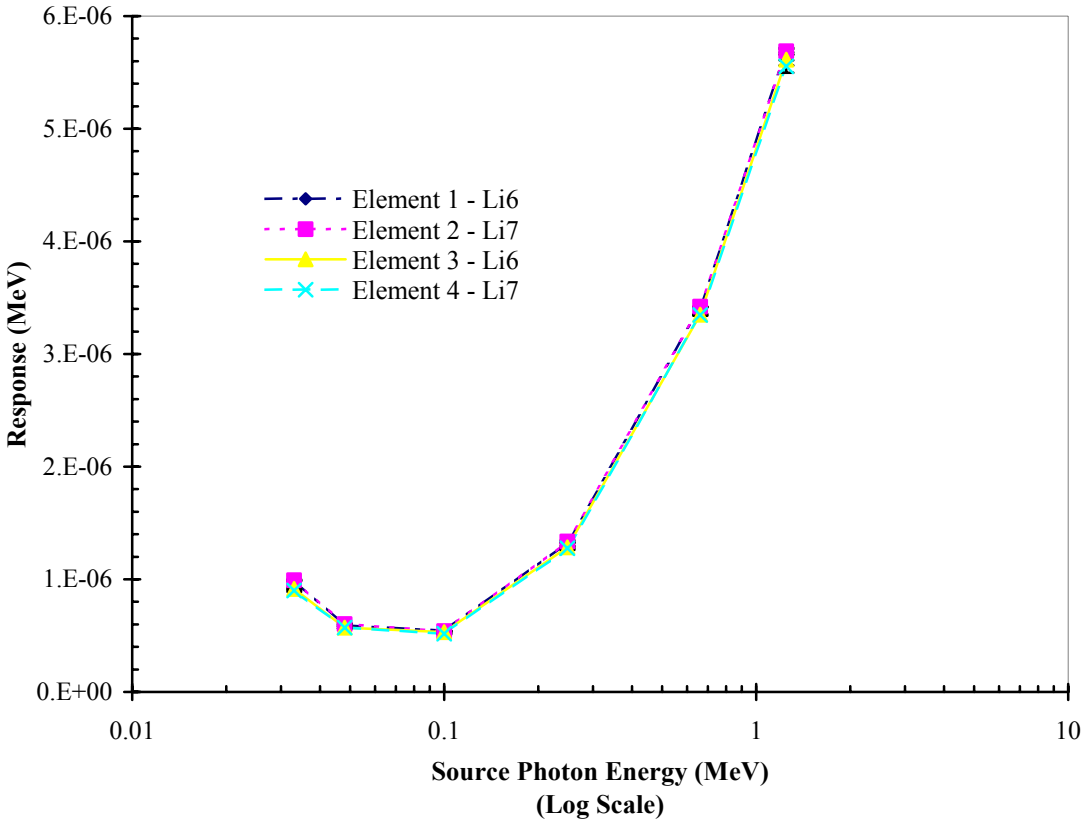

Fig. 12. Photon response in TLD determined as energy absorbed. Statistical errors indicate one standard deviation and are in most cases smaller than the size of the data points.

The results for the neutron response, as measured by the number of ^{6}Li capture reactions, are given in Table 6 on the following pages. These results include the S(α,β) cross sections.

Table 6. Neutron response in TLD determined as number of $^{6}Li(n,t)^{4}He$ capture reactions.

	Source Neutron Energy (MeV)	Number of Captures	Standard Deviation (±)
Element 1 (^{6}Li) Top Left	2.53E-08	1.90E-02	3.0E-05
	0.000001	1.14E-02	2.5E-05
	0.00001	5.86E-03	1.4E-05
	0.0001	3.25E-03	1.3E-05
	0.001	2.00E-03	1.2E-05
	0.01	1.26E-03	9.6E-06
	0.1	7.55E-04	4.9E-06
	1	3.07E-04	4.2E-06
	10	4.60E-05	8.8E-07
	20	2.18E-05	1.2E-06
Element 2 (^{7}Li) Top Right	2.53E-08	6.06E-05	3.6E-08
	0.000001	1.12E-05	1.5E-08
	0.00001	5.03E-06	9.0E-09
	0.0001	2.85E-06	8.8E-09
	0.001	1.81E-06	7.8E-09
	0.01	1.20E-06	5.6E-09
	0.1	7.45E-07	2.8E-09
	1	3.24E-07	2.3E-09
	10	5.13E-08	8.5E-10
	20	2.55E-08	6.9E-10
Element 3 (^{6}Li) Bottom Left	2.53E-08	1.66E-03	2.7E-05
	0.000001	5.81E-03	5.8E-05
	0.00001	7.56E-03	6.4E-05
	0.0001	6.50E-03	7.6E-05
	0.001	5.14E-03	8.6E-05
	0.01	3.64E-03	6.6E-05
	0.1	2.61E-03	3.6E-05
	1	1.28E-03	3.2E-05
	10	2.16E-04	6.4E-06
	20	1.18E-04	9.6E-06

Table 6. Continued.

	Source Neutron Energy (MeV)	Number of Captures	Standard Deviation (±)
	2.53E-08	5.33E-06	5.5E-08
	0.000001	1.09E-05	9.7E-08
	0.00001	1.33E-05	1.1E-07
	0.0001	1.19E-05	1.2E-07
Element 4 (^{7}Li)	0.001	9.43E-06	1.1E-07
Bottom Right	0.01	7.47E-06	1.1E-07
	0.1	5.41E-06	5.5E-08
	1	2.89E-06	4.9E-08
	10	5.84E-07	1.4E-08
	20	2.56E-07	1.4E-08

Fig. 13, on the next page, shows the results for elements 1 and 3. These elements contained 95.6% ^{6}Li and 4.4% ^{7}Li. All of the elements are embedded in an aluminum plate. Elements 1 and 2 have nothing in front but air with borated polyethylene behind. Elements 3 and 4 have borated polyethylene followed by 1 mm thick aluminum disks in front. These elements have a vacuum behind them.

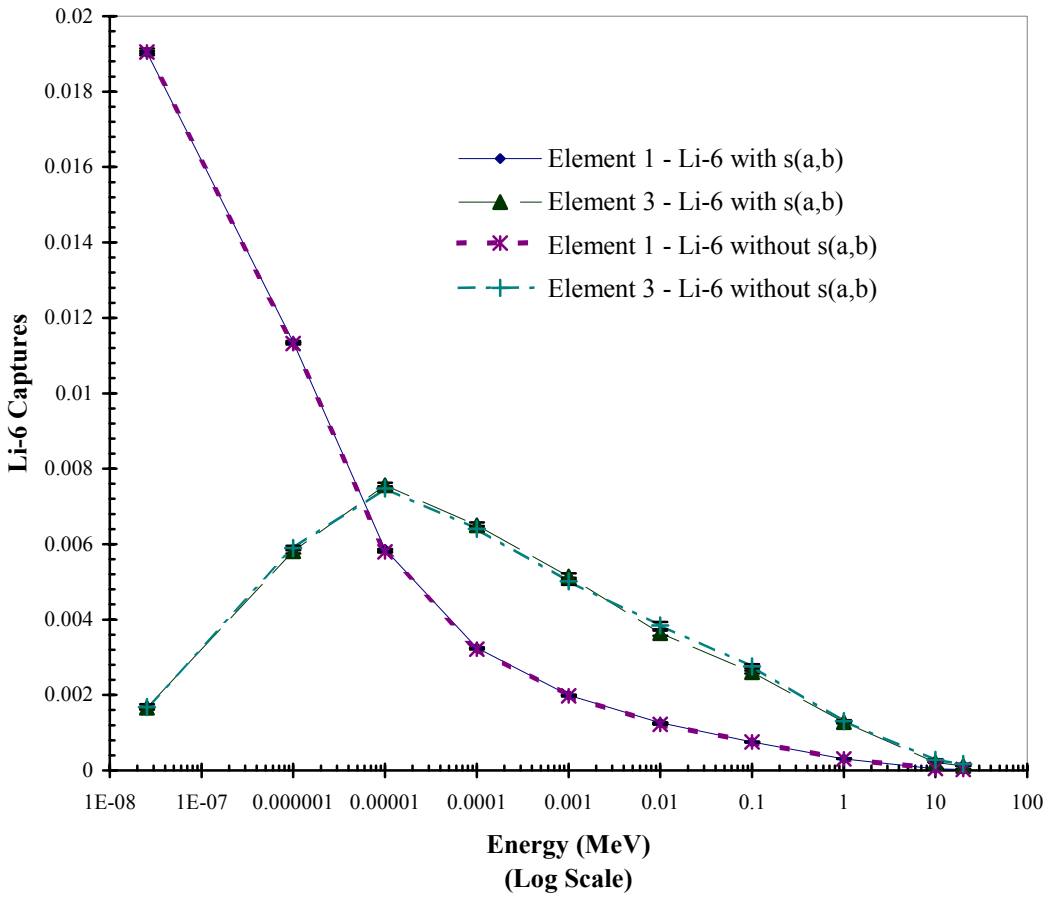

Fig. 13. ^{6}Li(n,t)^{4}He capture reactions per source neutron for ^{6}Li elements. Statistical errors indicating one standard deviation are in most cases smaller than the size of the data points.

Fig. 14, on the next page, shows the results for elements 2 and 4. These elements contained 99.93% ^{7}Li and 0.07% ^{6}Li. All of the elements are embedded in an aluminum plate. Elements 1 and 2 have nothing in front but air with borated polyethylene behind. Elements 3 and 4 have borated polyethylene followed by 1 mm thick aluminum disks in front. Vacuum is located behind elements 3 and 4 to the surface of the slab phantom.

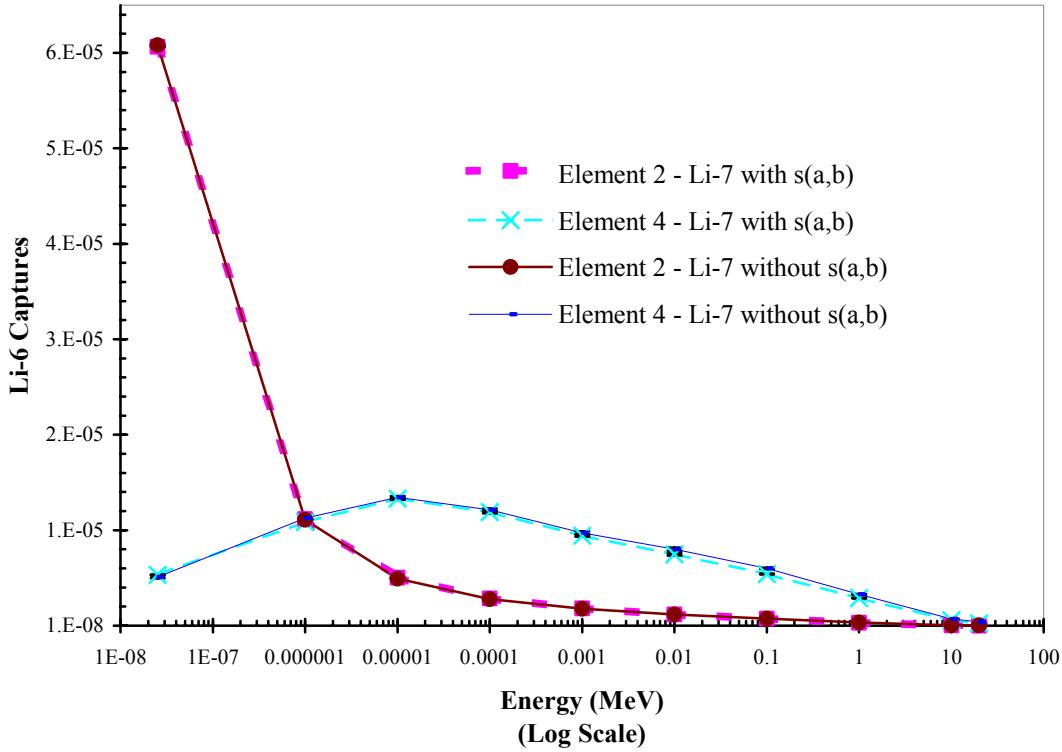

Fig. 14. ^{6}Li(n,t)^{4}He capture reactions per source neutron for ^{7}Li elements. Statistical errors indicating one standard deviation are in most cases smaller than the size of the data points.

Discussion

Two of the photon problems and 1 neutron problem did not converge completely. The 662 keV photon and 1.25 MeV photon had slopes below three. The 10 eV neutron and 10 MeV neutron also had slopes below three.

When comparing MCNP versions 4C2 and 5beta3.23 with each run starting at the same random number and tracking to end at 50 million histories, it was found that the tally results, slope, vov, error, nrn, and collisions were all identical. The only difference was the ctm, which was found to be running 58% longer in version 5beta3.23 when compared to 4C2.

These problems were also rerun with the S(α,β) cross section modifications. The two different results for the neutron tallies along with the percent-difference between the two are given in Table 7, on the following page. Elements 3 and 4, which were both behind aluminum disks and the borated polyethylene, had greater increases in the percent-difference between the tally results with S(α,β) and the tally results without S(α,β) than elements 1 and 2. The magnitude in error increased significantly along

with the percent-difference. This may reflect how few neutrons are absorbed after slowing down such that any difference in the cross sections will result in a large difference in comparison.

Table 7. Comparison of tally results with S(α,β) and without S(α,β) for each of the source neutrons.

		With S(α,β)		Without S(α,β)			
	MeV	Captures	Standard Deviation (±)	Captures	Standard Deviation (±)	% Difference	Standard Deviation (±)
Element 1 (^{6}Li) Top Left	2.53E-08	1.90E-02	3.0E-05	1.91E-02	8.8E-05	0.04	0.49
	0.000001	1.14E-02	2.5E-05	1.13E-02	2.5E-05	0.37	0.31
	0.00001	5.86E-03	1.4E-05	5.79E-03	1.4E-05	1.14	0.34
	0.0001	3.25E-03	1.3E-05	3.22E-03	1.3E-05	1.05	0.56
	0.001	2.00E-03	1.2E-05	1.98E-03	1.6E-05	0.90	1.00
	0.01	1.26E-03	9.6E-06	1.22E-03	1.3E-05	2.96	1.26
	0.1	7.55E-04	4.9E-06	7.51E-04	5.7E-06	0.47	1.00
	1	3.07E-04	4.2E-06	3.09E-04	4.8E-06	0.74	2.08
	10	4.72E-05	1.7E-06	4.72E-05	1.7E-06	0.00	-
	20	2.18E-05	1.2E-06	2.69E-05	1.6E-06	23.1	9.07
Element 2 (^{7}Li) Top Right	2.53E-08	6.06E-05	3.6E-08	6.08E-05	1.0E-07	0.25	0.18
	0.000001	1.12E-05	1.5E-08	1.11E-05	1.4E-08	0.58	0.18
	0.00001	5.03E-06	9.0E-09	4.95E-06	8.9E-09	1.59	0.25
	0.0001	2.85E-06	8.8E-09	2.79E-06	8.4E-09	1.84	0.43
	0.001	1.81E-06	7.8E-09	1.77E-06	9.1E-09	1.75	0.66
	0.01	1.20E-06	5.6E-09	1.17E-06	7.3E-09	2.00	0.77
	0.1	7.45E-07	2.8E-09	7.43E-07	3.5E-09	0.33	0.60
	1	3.24E-07	2.3E-09	3.30E-07	2.5E-09	1.86	1.06
	10	5.62E-08	1.1E-09	5.62E-08	1.1E-09	0.00	-
	20	2.55E-08	6.9E-10	3.17E-08	8.9E-10	24.0	4.46

Table 7. Continued.

		With S(α,β)		Without S(α,β)			
	MeV	Captures	Standard Deviation (±)	Captures	Standard Deviation (±)	% Difference	Standard Deviation (±)
Element 3 (^{6}Li) Bottom Left	2.53E-08	1.66E-03	2.7E-05	1.68E-03	7.2E-05	1.14	4.66
	0.000001	5.81E-03	5.8E-05	5.90E-03	6.0E-05	1.53	1.43
	0.00001	7.56E-03	6.4E-05	7.48E-03	6.4E-05	1.14	1.19
	0.0001	6.50E-03	7.6E-05	6.41E-03	7.6E-05	1.46	1.66
	0.001	5.14E-03	8.6E-05	5.02E-03	9.3E-05	2.38	2.47
	0.01	3.64E-03	6.6E-05	3.84E-03	9.5E-05	5.51	3.18
	0.1	2.61E-03	3.6E-05	2.76E-03	5.4E-05	5.81	2.50
	1	1.28E-03	3.2E-05	1.30E-03	3.0E-05	1.93	3.46
	10	2.79E-04	1.6E-05	2.79E-04	1.6E-05	0.00	-
	20	1.18E-04	9.6E-06	1.69E-04	1.4E-05	42.3	14.55
Element 4 (^{7}Li) Bottom Right	2.53E-08	5.33E-06	5.5E-08	5.12E-06	1.5E-07	3.89	2.93
	0.000001	1.09E-05	9.7E-08	1.13E-05	1.1E-07	3.65	1.35
	0.00001	1.33E-05	1.1E-07	1.35E-05	1.1E-07	1.08	1.20
	0.0001	1.19E-05	1.2E-07	1.21E-05	1.4E-07	2.08	1.56
	0.001	9.43E-06	1.1E-07	9.75E-06	1.6E-07	3.34	2.09
	0.01	7.47E-06	1.1E-07	8.03E-06	1.7E-07	7.47	2.67
	0.1	5.41E-06	5.5E-08	6.01E-06	7.4E-08	11.1	1.71
	1	2.89E-06	4.9E-08	3.28E-06	6.1E-08	13.5	2.71
	10	7.27E-07	3.0E-08	7.27E-07	3.0E-08	0.00	-
	20	2.56E-07	1.4E-08	3.99E-07	2.2E-08	55.8	10.78

Fig. 15 on the following page shows the percent-difference with and without the S(α,β) cross sections.

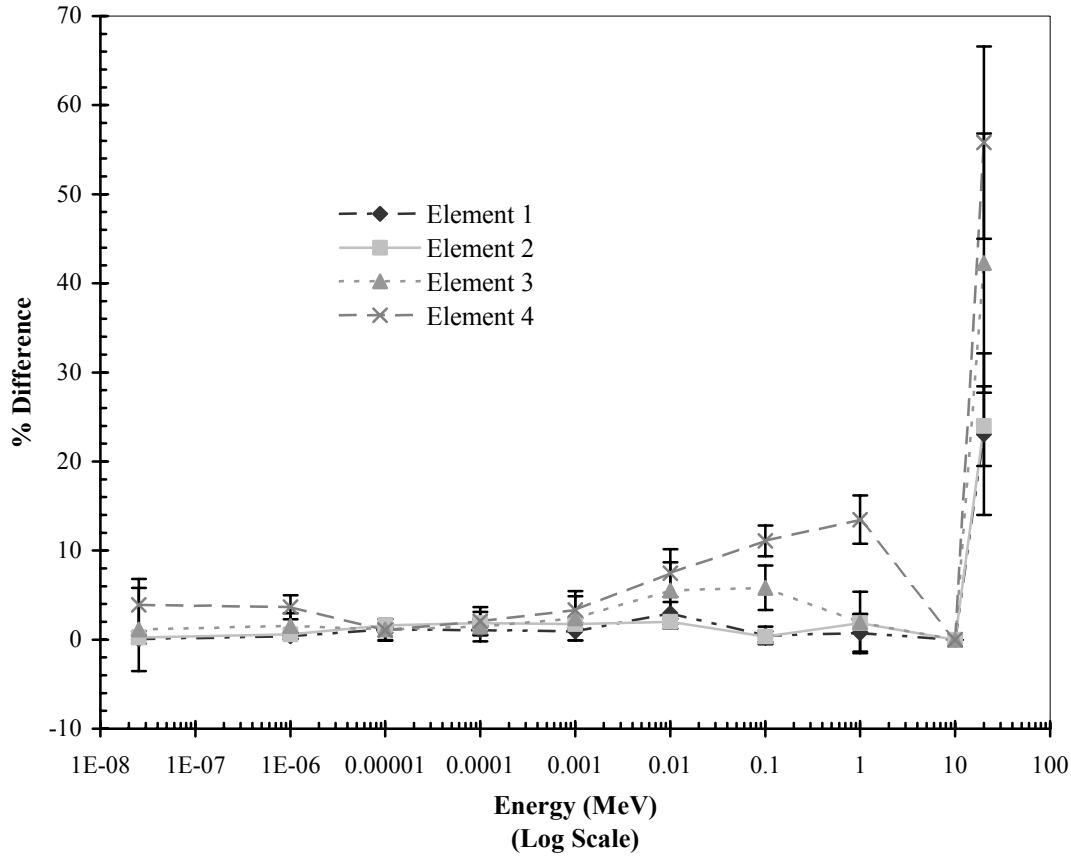

Fig. 15. Comparison of tally results with and without S(α,β) cross sections. Statistical error indicates one standard deviation.

The use of the S(α,β) cross sections is limited to neutrons and only a few materials. These cross sections may potentially have a great effect upon the results of low energy photons. By improving the low energy physics and including resonances in the cross sections that take into account molecular properties like bond vibrations and rotations, the results will, hopefully, be more accurate for low energy photons.

PROBLEM FIVE: AIR KERMA BACKSCATTER PROFILES FOR TWO ISO PHOTON EXPANDED AND ALIGNED FIELDS IMPINGING ON AN ISO SLAB PHANTOM

Description of Problem

Air kerma backscatter profiles along the apothem and diagonal of an ISO slab phantom were determined on the front face of the phantom using a beta version of MCNP 5. This version did not include the Doppler broadening feature. Two source photon spectra were used. The first was an ISO narrow spectrum series – tube voltage 200 kV (filtration 4.0 mm Al + 2.0 mm Cu + 3.0 mm Sn + 1.0 mm Pb). The second was an ISO wide spectrum series – tube voltage 150 kV (filtration 4.0 mm Al + 1.0 mm Sn). The air kerma backscatter profiles were determined along the diagonal and apothem on the front face.

The surface of the front face was segmented using spheres each with a radius of 0.2 cm. Energy fluence was tallied through these circles (a plane segmented with spheres will result in segmented circles) and modified using mass energy transfer coefficients for air (Gualdrini 2003) and a multiplication factor of 1.602E-10 to convert to Gy. Fig. 16 on the following page shows an example of the segmenting of the surface in order to determine the profiles along the apothem and diagonal. Backscatter was then determined using the following two equations, the second of which was the *F2 tally output:

$$B = \frac{K_a(phantom\ present)}{K_a(free\ in\ air)}$$

$$K_a = \int_{E_{\min}}^{E_{\max}} \Phi(E)(\mu_{tr}/\rho)_{air} EdE$$

K_a (free in air) was determined by replacing the materials within the slab with vacuum. The mass energy transfer coefficients for air were still used.

Geometry Specifications

The phantom is a standard ISO water filled slab phantom with external dimensions 30 cm x 30 cm x 15 cm. The front wall of the phantom is 0.25 cm thick polymethyl methacrylate, PMMA, while the remaining walls are all 1 cm thick PMMA. The remainder of the geometry is vacuum (Siebert 2003).

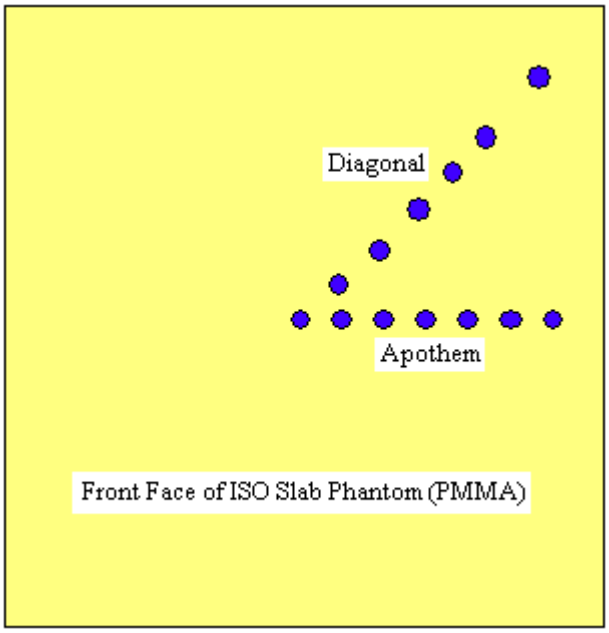

Fig. 16. Hand drawn example of segmented regions. Air kerma backscatter was determined within each of the segmented circles. Not to scale.

Source Specifications

The two source photon spectrums used, ISO narrow spectrum series – tube voltage 200 kV (filtration 4.0 mm Al + 2.0 mm Cu + 3.0 mm Sn + 1.0 mm Pb) and ISO wide spectrum series – tube voltage 150 kV (filtration 4.0 mm Al + 1.0 mm Sn) were graphed and compared to the published graph (Siebert 2002) to confirm no mistakes were made in the data entry. Particles began at a surface source located directly in front of and normal to the front face of the phantom with the same dimensions as the phantom front face. The source was located within the vacuum. The particles were all directed uniformly at the phantom with normal incidence upon the phantom front face.

Tally Specifications

This problem specifically required backscatter at the surface so a surface energy fluence tally had to be used, *F2. In addition, the surface had to be segmented to determine the profile along the apothem and diagonal. Point detectors were tried, but would not converge quickly and were abandoned. The surface was segmented using the SF and SD cards.

Segments not important as tally regions were given areas of 1, which is not correct, so the input file would run. In this case the first segment of the surface is the tally region. Since the ten statistical

checks performed by MCNP are only performed on the first bin, or segment in this case, this proved to be a good way to perform the segmentation.

Results

The results were all normalized to a single source particle. The determinations of K_a (phantom present) with both the narrow and wide spectrums failed to pass all statistical checks. After 1 billion histories the results had slopes about 2.4 and 2.6 for the narrow and wide spectrums, respectively. The resulting air kerma backscatter profiles for the narrow and wide spectrums along the apothem is given in Table 8, below. The standard deviation was calculated using error propagation (Knoll 2000).

Table 8. Air kerma backscatter profile along the apothem.

	Narrow Spectrum		Wide Spectrum	
Distance from Center (cm)	Backscatter	Standard Deviation (±)	Backscatter	Standard Deviation (±)
0.0	1.37	0.0065	1.53	0.0075
0.5	1.37	0.0065	1.54	0.0076
1.0	1.36	0.0063	1.54	0.0076
1.5	1.37	0.0065	1.53	0.0074
2.0	1.38	0.0065	1.54	0.0076
2.5	1.36	0.0064	1.54	0.0076
3.0	1.36	0.0064	1.54	0.0074
3.5	1.37	0.0065	1.54	0.0076
4.0	1.37	0.0065	1.53	0.0073
4.5	1.36	0.0064	1.53	0.0074
5.0	1.36	0.0064	1.53	0.0075
6.0	1.36	0.0064	1.52	0.0075
7.0	1.35	0.0064	1.52	0.0075
8.0	1.34	0.0063	1.50	0.0074
9.0	1.34	0.0063	1.50	0.0074
11.0	1.31	0.0062	1.45	0.0071
13.0	1.26	0.0059	1.38	0.0068

Table 9, below, contains the air kerma backscatter profiles along the diagonal for both photon spectrums. The standard deviation was calculated using error propagation (Knoll 2000).

Table 9. Air kerma backscatter profile along the diagonal.

	Narrow Spectrum		Wide Spectrum	
Distance from Center (cm)	Backscatter	Standard Deviation (±)	Backscatter	Standard Deviation (±)
0.0	1.37	0.0065	1.53	0.0075
0.707	1.37	0.0065	1.54	0.0076
1.41	1.37	0.0065	1.55	0.0076
2.12	1.37	0.0065	1.54	0.0076
2.83	1.37	0.0065	1.54	0.0076
3.54	1.36	0.0064	1.53	0.0075
4.24	1.37	0.0065	1.53	0.0075
4.95	1.37	0.0065	1.53	0.0075
5.66	1.38	0.0065	1.53	0.0074
6.36	1.35	0.0064	1.52	0.0075
7.07	1.35	0.0064	1.51	0.0072
8.49	1.34	0.0063	1.50	0.0073
9.90	1.33	0.0063	1.50	0.0074
11.3	1.33	0.0063	1.47	0.0073
12.7	1.30	0.0061	1.44	0.0071
15.6	1.25	0.0059	1.38	0.0067
18.4	1.20	0.0056	1.29	0.0064

Fig. 17 on the following page plots the air kerma backscatter profiles for both spectrums of photons along the apothem and diagonal.

Discussion

K_a values for the narrow and wide spectrum with vacuum replacing the materials in the ISO slab were converted to pGy·cm^2 by multiplying times the area of the slab, 900 cm^2, and 1E12. This resulted in values of 0.675 pGy·cm^2 and 0.40 pGy·cm^2 for the narrow and wide spectrums in air, respectively. The source was actually a spectrum of photons, but the conversion coefficients in ICRP 74 have values of

0.372 pGy·cm^2, 0.600 pGy·cm^2 and 0.856 pGy·cm^2 for source photon energies of 0.100 MeV, 0.150 MeV, and 0.200 MeV, respectively. The source photon with the greatest frequency for each spectrum is around 0.175 MeV and a little over 0.100 MeV for the narrow and wide, respectively. Therefore, the conversion coefficients determined with MCNP 5 seem reasonable.

The backscatter profiles of both photon spectrums remain relatively constant up to 5 cm. They then begin to drop off as the volume of surrounding material decreases, therefore decreasing the amount of backscatter.

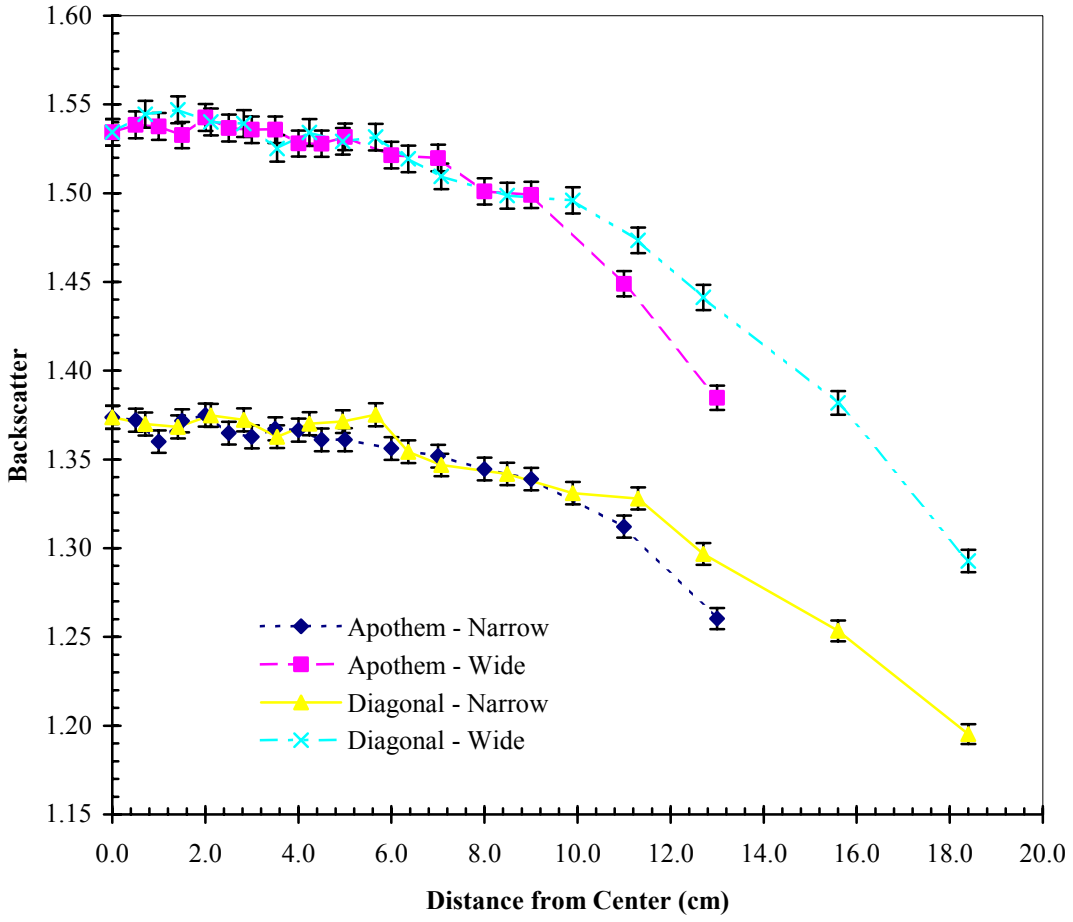

Fig. 17. Air kerma backscatter profiles along the apothem and diagonal on the front face of the ISO slab phantom for a narrow and wide spectrum of photons (normalized to one photon). The statistical error is ± one standard deviation.

PROBLEM SIX: CALIBRATION OF NEUTRON DETECTORS IN A BUNKER

Description of Problem

Direct contributions from a ^{252}Cf fission source are removed through the use of a shadow cone between the source and two detector positions in a neutron detector calibration bunker. Indirect contributions are then determined for energy fluence and spectral (angular) fluence at the two detector positions. This will indicate the amount of environmental contribution from the air and walls of the bunker. This contribution may even increase with the greater amounts of moisture in the air and concrete walls. To more accurately calibrate these detectors, this indirect contribution must be accounted for.

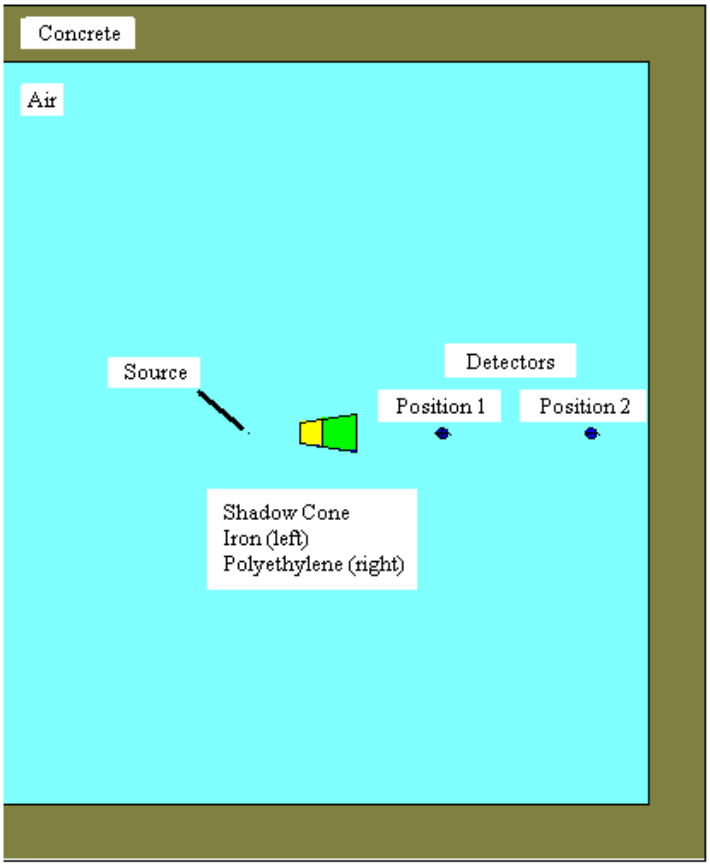

Fig. 18. Top view of MCNP geometry plot of neutron detector calibration bunker. The two detectors located behind the shadow should receive almost no direct contribution from the source. Instead, the indirect contribution is determined. The room is cut off to the left to better show the detectors, shadow cone and source.

Geometry Specifications

The ^{252}Cf source is a cylinder with diameter 0.5 cm and height 0.5 cm located so that the geometric center of the cylinder is at the origin. The cylinder axis extends into the y direction. The small end of the shadow cone is located 45 cm from the origin along the x-axis. The large end is located 95 cm from the origin with the separation between iron and polyethylene occurring at 65 cm. The cone is defined as kx -15.0 2.16263E-02 +1 by the author. The inside walls of the room are made of concrete at planes x= -350 cm and 350 cm, y= -350 cm and 350 cm, and finally z= -325 cm and 325 cm. The walls are 50 cm thick. The two detectors are located at 170,0,0 and 300,0,0 (Siebert 2003). A top view of the MCNP geometry plot is shown in Fig 18 on the previous page.

Source Specifications

This problem required a source with no self-shielding. This did not seem realistic and was therefore ignored. There were over 67 billion collisions in this problem, which ran for over 345 million histories of which there were a little over 21 million collisions in the source. Thus, about 0.03% of the collisions occurred in the source. These collisions would have had greater weight, but it seems reasonable to assume that the amount of self-shielding was negligible. In addition, the mean free path in the source was 3.6 cm while the source was a cylinder 0.5 cm long with a 0.5 cm diameter.

Tally Specifications

The energy bins used in the energy fluence spectrum are the same as those specified in the source definition at the author's request. The author, Dr. B.R.L. Siebert, also specified the cosine bins.

The energy fluence was determined by tallying particles cm^{-2} crossing the surfaces of cells approximating 12-inch diameter Bonner spheres at the two detector positions. These are common detectors that would be calibrated in this bunker. In addition, the 12-inch diameter Bonner sphere's response curve is similar to the dose equivalent delivered per neutron as a function of energy (Knoll 2000).

The cosine binning is tallied on surface 40, pz 0, which runs directly through the middle of the two spherical detectors. The spheres are cut in half by this surface making two cells, which are added together for the F4 tally. The surface is made part of a cell so the F1 tally will work. It is further designated with the FS card to perform the cosine tallying upon the surface at the two detector positions. The cosine binning will take place in the plane pz 0 at angles 0^o, 30^o, 60^o, 90^o, 120^o, 150^o, and 180^o with the reference vector normal to the positive sense of the surface.

Results

Not all of the energy bins in the determination of energy fluence passed all of the statistical checks. The bins with an average of 8.5 MeV and higher contained relative errors greater than 0.1 and are

noted in Table 10, below, which gives the energy fluence for detectors 1 and 2, 170,0,0 and 300,0,0, respectively. All results are normalized to one source particle.

Table 10. Energy fluence for source parallel to y-axis.

Energy Bins (MeV)			Average Energy in Bin (MeV)	Detector 1 (170,0,0)		Detector 2 (300,0,0)	
				Particles cm^{-2}	Standard Deviation (±)	Particles cm^{-2}	Standard Deviation (±)
0	-	4.14E-07	- - -	1.92E-06	2.3E-09	1.90E-06	2.3E-09
4.14E-07	-	1.00E-06	7.07E-07	7.02E-08	5.5E-10	7.06E-08	5.5E-10
1.00E-06	-	1.00E-05	5.5E-06	1.86E-07	9.1E-10	1.83E-07	9.0E-10
1.00E-05	-	5.00E-05	0.00003	1.36E-07	7.8E-10	1.36E-07	7.8E-10
5.00E-05	-	1.00E-04	0.000075	6.10E-08	5.2E-10	5.90E-08	5.1E-10
1.00E-04	-	2.00E-04	0.00015	6.14E-08	5.2E-10	6.10E-08	5.2E-10
2.00E-04	-	4.00E-04	0.0003	6.43E-08	5.3E-10	6.25E-08	5.3E-10
4.00E-04	-	7.00E-04	0.00055	5.25E-08	4.8E-10	5.11E-08	4.7E-10
7.00E-04	-	1.00E-03	0.00085	3.40E-08	3.9E-10	3.38E-08	3.9E-10
1.00E-03	-	3.00E-03	0.002	1.08E-07	6.9E-10	1.05E-07	6.8E-10
3.00E-03	-	6.00E-03	0.0045	7.27E-08	5.7E-10	7.07E-08	5.6E-10
6.00E-03	-	1.00E-02	0.008	5.59E-08	5.0E-10	5.38E-08	4.9E-10
1.00E-02	-	2.00E-02	0.015	8.00E-08	5.9E-10	7.67E-08	5.8E-10
2.00E-02	-	4.00E-02	0.03	8.98E-08	6.3E-10	8.70E-08	6.2E-10
4.00E-02	-	6.00E-02	0.05	6.06E-08	5.1E-10	5.73E-08	5.0E-10
6.00E-02	-	8.00E-02	0.07	4.71E-08	4.6E-10	4.34E-08	4.4E-10
8.00E-02	-	1.00E-01	0.09	4.08E-08	4.2E-10	3.88E-08	4.2E-10
1.00E-01	-	1.50E-01	0.125	9.17E-08	6.3E-10	8.69E-08	6.2E-10
1.50E-01	-	2.00E-01	0.175	7.91E-08	5.9E-10	7.46E-08	5.7E-10
2.00E-01	-	2.50E-01	0.225	5.96E-08	5.1E-10	5.64E-08	5.0E-10
2.50E-01	-	3.00E-01	0.275	5.81E-08	5.1E-10	5.43E-08	4.9E-10
3.00E-01	-	3.50E-01	0.325	5.47E-08	4.9E-10	4.95E-08	4.7E-10
3.50E-01	-	4.00E-01	0.375	3.16E-08	3.7E-10	2.97E-08	3.6E-10
4.00E-01	-	4.50E-01	0.425	2.30E-08	3.2E-10	2.19E-08	3.1E-10
4.50E-01	-	5.00E-01	0.475	3.36E-08	3.9E-10	3.04E-08	3.7E-10
5.00E-01	-	5.50E-01	0.525	3.43E-08	3.9E-10	3.17E-08	3.7E-10

Table 10. Continued.

Energy Bins (MeV)			Average Energy in Bin (MeV)	Detector 1 (170,0,0)		Detector 2 (300,0,0)	
				Particles cm^{-2}	Standard Deviation (±)	Particles cm^{-2}	Standard Deviation (±)
5.50E-01	-	6.00E-01	0.575	3.25E-08	3.8E-10	3.10E-08	3.7E-10
6.00E-01	-	7.00E-01	0.65	6.78E-08	5.5E-10	6.56E-08	5.4E-10
7.00E-01	-	8.00E-01	0.75	7.70E-08	5.9E-10	6.75E-08	5.5E-10
8.00E-01	-	9.00E-01	0.85	5.93E-08	5.1E-10	5.03E-08	4.7E-10
9.00E-01	-	1.00E+00	0.95	3.44E-08	3.9E-10	2.80E-08	3.5E-10
1.00E+00	-	1.20E+00	1.1	5.65E-08	5.0E-10	4.85E-08	4.6E-10
1.20E+00	-	1.40E+00	1.3	5.50E-08	4.9E-10	4.68E-08	4.5E-10
1.40E+00	-	1.60E+00	1.5	4.64E-08	4.5E-10	4.00E-08	4.2E-10
1.60E+00	-	1.80E+00	1.7	3.31E-08	3.8E-10	2.84E-08	3.5E-10
1.80E+00	-	2.00E+00	1.9	2.00E-08	2.9E-10	1.70E-08	2.7E-10
2.00E+00	-	2.30E+00	2.15	3.47E-08	3.9E-10	3.04E-08	3.6E-10
2.30E+00	-	2.60E+00	2.45	3.98E-08	4.1E-10	3.48E-08	3.9E-10
2.60E+00	-	3.00E+00	2.8	3.69E-08	4.0E-10	3.20E-08	3.7E-10
3.00E+00	-	3.50E+00	3.25	1.88E-08	2.8E-10	1.78E-08	2.7E-10
3.50E+00	-	4.00E+00	3.75	9.87E-09	2.0E-10	8.69E-09	1.9E-10
4.00E+00	-	4.50E+00	4.25	8.41E-09	1.8E-10	6.73E-09	1.6E-10
4.50E+00	-	5.00E+00	4.75	4.32E-09	1.3E-10	3.83E-09	1.2E-10
5.00E+00	-	6.00E+00	5.5	4.07E-09	1.2E-10	3.58E-09	1.2E-10
6.00E+00	-	7.00E+00	6.5	1.44E-09	7.1E-11	1.18E-09	6.6E-11
7.00E+00	-	8.00E+00	7.5	4.49E-10	3.9E-11	4.15E-10	3.8E-11
8.00E+00	-	9.00E+00	8.5	2.30E-10*	2.7E-11	1.27E-10*	2.0E-11
9.00E+00	-	1.00E+01	9.5	5.95E-11**	1.3E-11	6.10E-11**	1.4E-11
1.00E+01	-	1.10E+01	10.5	2.73E-11**	8.7E-12	2.82E-11**	9.8E-12
1.10E+01	-	1.20E+01	11.5	8.52E-12***	5.1E-12	2.31E-11**	9.4E-12
1.20E+01	-	1.30E+01	12.5	2.07E-12***	2.1E-12	0.00E+00	0.0E+00
1.30E+01	-	1.40E+01	13.5	3.60E-12***	3.6E-12	0.00E+00	0.0E+00
1.40E+01	-	1.50E+01	14.5	0.00E+00	0.0E+00	0.00E+00	0.0E+00
1.50E+01	-	1.60E+01	15.5	0.00E+00	0.0E+00	0.00E+00	0.0E+00

Table 10. Continued.

* These tally results had a relative error greater than 0.1 and questionable results
** These tally results had a relative error between 0.2 and 0.5 with the reported result possibly being off by a factor of a few
*** These tally results had a relative error greater than 0.5 and are not meaningful

Fig. 19 below plots the particles cm^{-2} versus the log of the average energies in the bins.

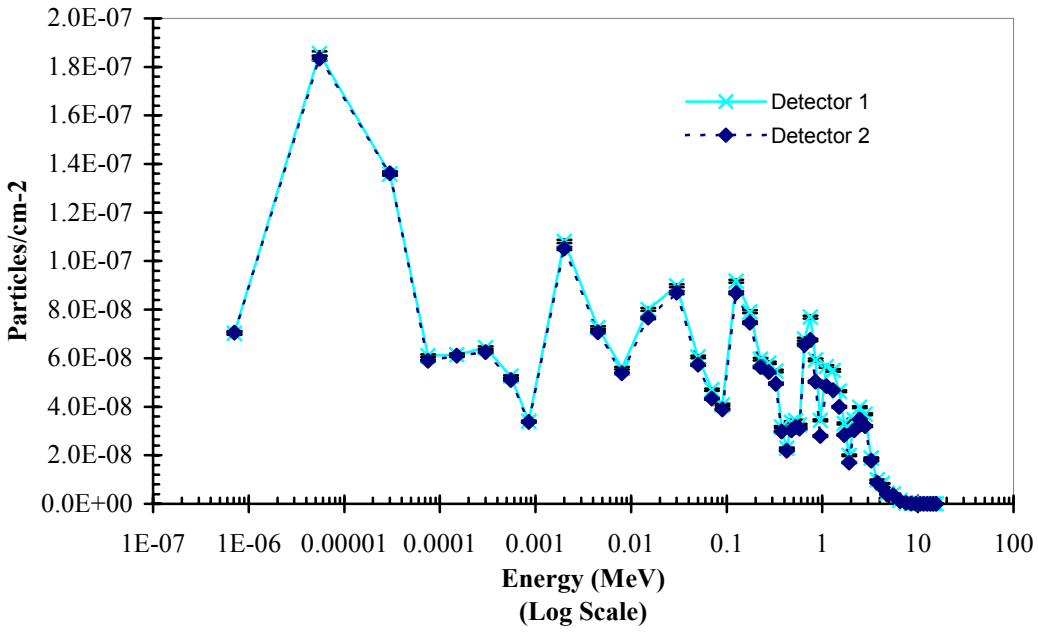

Fig. 19. Indirect neutron contribution to detector 1 at 170,0,0 and detector 2 at 300,0,0 for a source cylinder parallel to the y-axis. The statistical error indicates one standard deviation and may be smaller than the size of some of the data points.

A comparison of results between the two detectors showed a less than 10% difference for bins below 1 MeV. Above 1 MeV the difference would better be characterized as less than 20%. The error increases significantly above 8.5 MeV, when the relative error of the individual tallies increases above 0.1 and hence the tally result itself becomes questionable. This is shown in Fig. 20 on the next page.

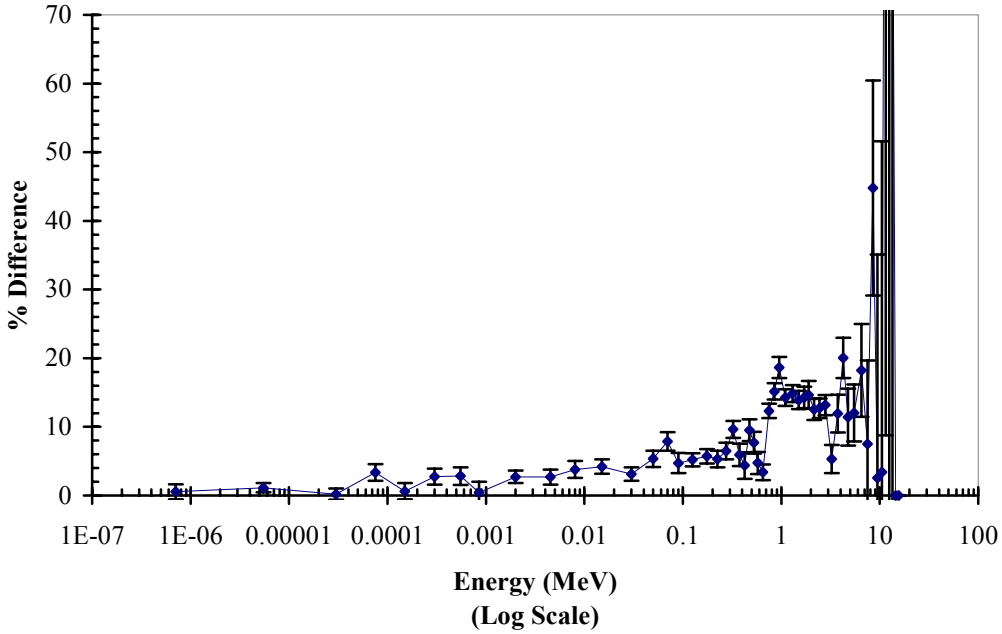

Fig. 20. Percent difference between energy fluence of the two detectors, calculated as the difference in tally results divided by the results for detector 1 times 100. To give greater clarity to the lower energy bins the scale was adjusted. Statistical error was calculated using error propagation and indicates one standard deviation. The error for the higher energy bins extends beyond this scale.

The cosine binning is tallied on a surface in the xy plane on the z-axis, pz 0. The positive sense of the surface is along the z-axis in the positive direction and these cosine bins are relative to that direction. For example, a polar angle with a cosine of –1 would indicate particles coming from 180^{o} from the reference vector, which would be along the z-axis below the surface. A polar angle with a cosine of 0 would indicate 90^{o} from the reference vector, which would be perpendicular to the reference vector and within the plane of the surface. Finally, a polar angle with a cosine of 1 would indicate particles coming from the direction of the reference vector. Table 11, on the next page, shows the results for the determination of spectral fluence in the two detectors. These results passed all statistical checks and are normalized to one source particle.

Table 11. Spectral fluence for source parallel to y-axis.

Cosine Bins			Average of Cosine Bin	Detector 1 (170,0,0)		Detector 2 (300,0,0)	
				Particles cm^{-2}	Standard Deviation (±)	Particles cm^{-2}	Standard Deviation (±)
-1	-	-0.866	-0.933	3.23E-06	1.1E-08	3.05E-06	1.1E-08
-0.866	-	-0.5	-0.683	6.02E-06	1.5E-08	6.09E-06	1.5E-08
-0.5	-	0	-0.25	3.08E-06	1.1E-08	2.86E-06	1.1E-08
0	-	0.5	0.25	3.09E-06	1.1E-08	2.86E-06	1.1E-08
0.5	-	0.866	0.683	6.06E-06	1.5E-08	6.05E-06	1.5E-08
0.866	-	1	0.933	3.23E-06	1.1E-08	3.06E-06	1.1E-08

Fig. 21, below, shows the spectral fluence as the particles cm^{-2} within the given cosine bin.

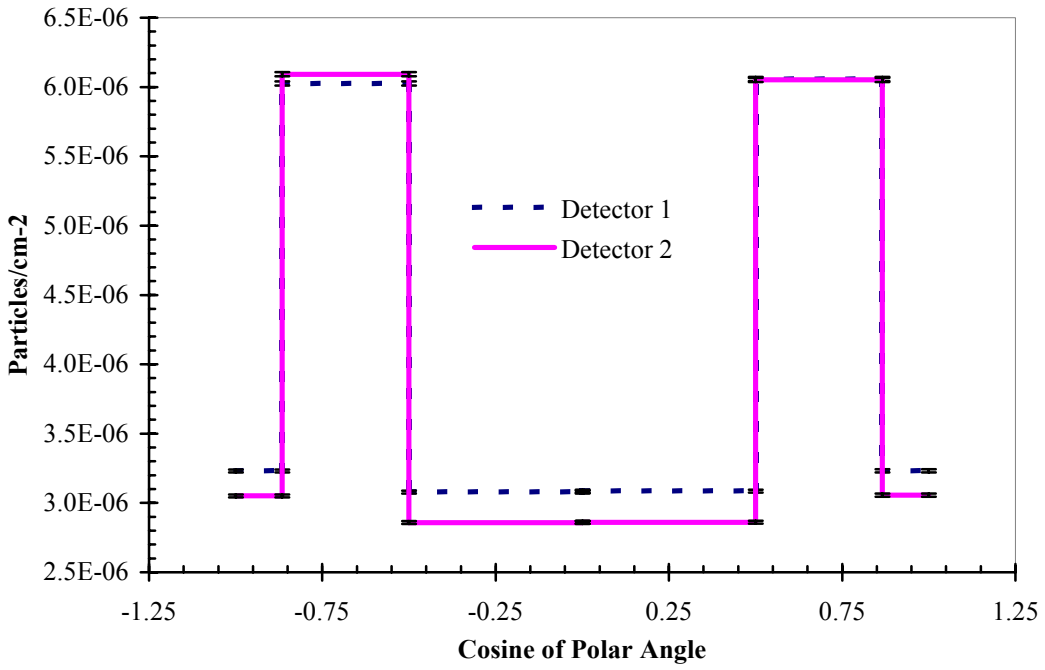

Fig. 21. Indirect spectral neutron contribution to detector 1 at 170,0,0 and detector 2 at 300,0,0 for a source cylinder parallel to the y-axis. The statistical error indicates one standard deviation and may be smaller than the size of some of the data points in some cases.

Discussion

Indirect contribution seems to be very small with the largest contribution coming from the low energy neutrons with an average polar angle of 47^{o} relative to particles crossing the surface, pz 0, along the z-axis from the positive side of the surface.

Source neutrons >0.8 MeV seem to produce a significant difference in indirect neutron contributions to the two detectors. However, this is also where the tally results began to have a large relative error, so this may not be true. There is little difference between the two detectors with low energy source neutrons.

PROBLEM SEVEN: PULSE HEIGHT DISTRIBUTIONS OF A GERMANIUM SPECTROMETER IN THE ENERGY RANGE BELOW 1 MeV

Description of Problem

Pulse height distributions at several photon energies are determined for a germanium detector using a beta version of MCNP 5. Some of the lower energy photon pulse height distributions used the Doppler broadening feature. These pulse height distributions may provide a full set of response functions for a given detector assuming the physical characteristics of the detector are accurately modeled, which would allow for a better calibration of the detector. Pulse height distributions at energies of 15 keV, 30 keV, 60 keV, 100 keV, 0.25 MeV, 0.5 MeV, 0.75 MeV and 1 MeV have been determined along with the estimated uncertainty due to source positioning and dead layer thickness with photon energies of 30 keV and 750 keV. Fig. 22, below, shows a MCNP plot of the side view of the Ge detector.

Peak positions in the pulse height distributions can be analytically derived and are compared to the peak positions in the pulse height distributions as an indication of the accuracy of MCNP 5. A comparison of the pulse height distributions with and without the Doppler broadening feature is also made.

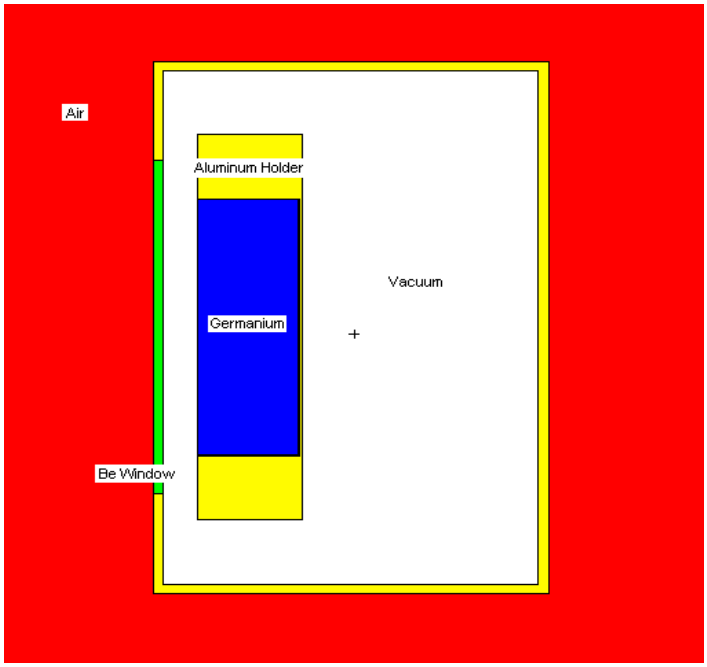

Fig. 22. MCNP geometry plot of the side view of the germanium detector. The germanium is the tally region. The source, which is not shown, would be to the left of the Be window within the air.

Geometry Specifications

The source is a disk located in air 2.0 cm in front of the detector's Be window. It has a radius of 0.25 cm. The cryostat containing the detector and vacuum is a cylinder with 0.15 cm thick aluminum of external radius 4.15 cm and a total height of 5.8 cm. A beryllium window of radius 2.6 cm and height 0.15 cm is located in the top face of the cryostat cylinder. 0.5 cm from the beryllium window is the germanium detector front surface. The germanium detector has an outer radius of 2.0 cm and a height of 1.5 cm. The dead layer of the germanium detector is 0.01 cm thick surrounding the entire outside of the germanium detector such that the radius of the core germanium is 1.99 cm and the height is 1.48 cm. The germanium detector is held in an aluminum holder with two parts. The back part has a radius of 3.0 cm and height of 0.5 cm. The lateral part has an outer radius of 3.0 cm, an inner radius of 2.0 cm, and a height of 1.5 cm (Siebert 2003).

Source Specifications

The source is a surface source emitting isotropically. The source does not consist of any material but is simply a disk in air so there is no self-shielding taking place, as specified by the author.

Tally Specifications

F8, *F8, and F6 tallies were all tried for these problems with the *F8 tally giving the most realistic pulse height distribution. The energy bins used in each pulse height distribution were specified by a detector resolution function. The resolution of the full energy peak was determined using the function and then this energy bin size was used for all of the energy bins. If the bins were not equal in size, then random peaks would result throughout the pulse height distributions.

Results

The Doppler broadening feature was used for photons with energy 15 keV, 30 keV, 60 keV, and 750 keV. Results of these photons without the Doppler broadening feature were also determined. Tables of all of the results are given in APPENDIX B. Determination of peak positions and all of the pulse height distributions are given in APPENDIX C. The peaks used in the comparison all had relative errors below 0.1 indicating good precision.

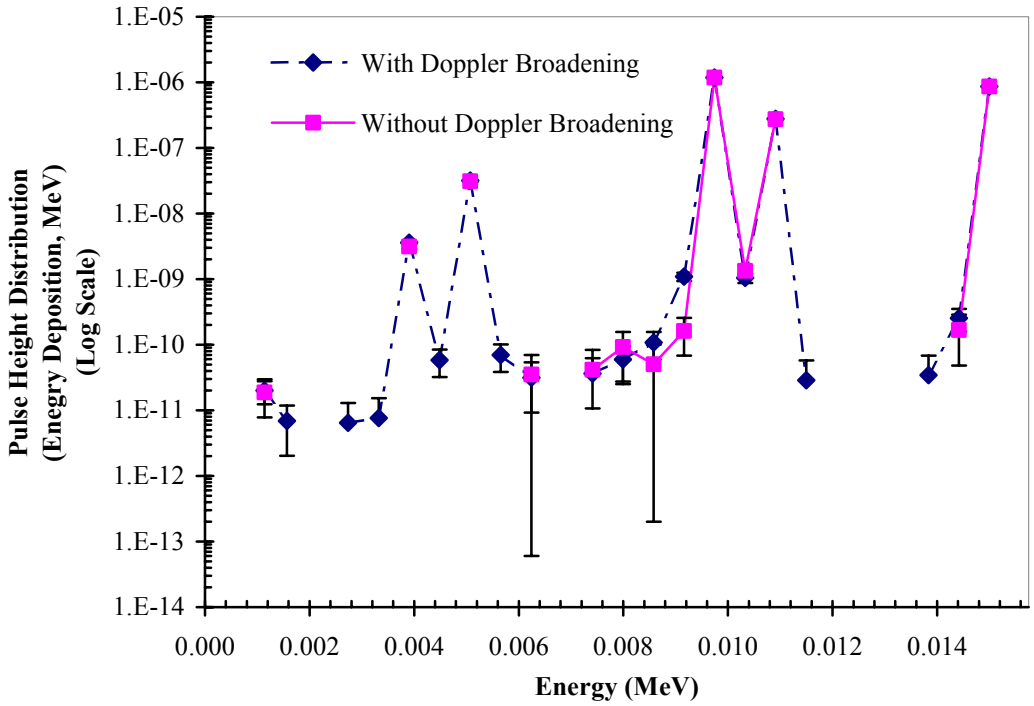

Fig. 23. Pulse height distribution spectrum for a 15 keV photon incident upon a Ge detector, with and without the Doppler broadening feature. Results have been normalized to one source particle. Missing points had zero tallies. Error bars indicate one standard deviation.

The first peak in Fig. 23, above, at 3.9 keV may be the Compton edge, while the second peak at 5.1 keV does not correspond to any predicted peaks. The peaks around 10 keV correspond to characteristic X-rays from Ge. The first of these two characteristic X-rays is an electron from the L shell filling a vacancy in the K shell. The second is an electron from the M shell again filling a vacancy in the K shell. The full energy peak is also present at 15 keV.

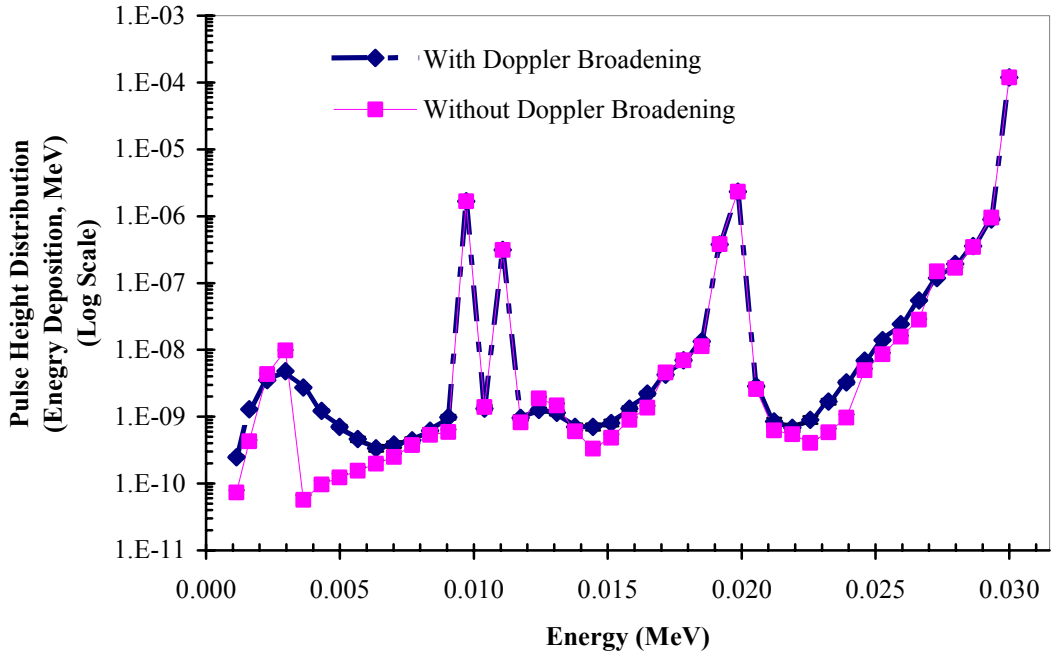

Fig. 24. Pulse height distribution spectrum for a 30 keV photon incident upon a Ge detector with and without the Doppler broadening feature. Results have been normalized to one source particle. Error bars indicate one standard deviation.

The first peak at 3 keV in Fig. 24, above, is the Compton edge. The peaks around 10 keV correspond to characteristic X-rays from Ge. The first of these two characteristic X-rays is an electron from the L shell filling a vacancy in the K shell. The second is an electron from the M shell again filling a vacancy in the K shell. The backscatter peak is located at 26.85 keV. There may be a small peak in the spectrum without the Doppler broadening feature, but no peak exists with the feature. The full energy peak is also present at 30 keV.

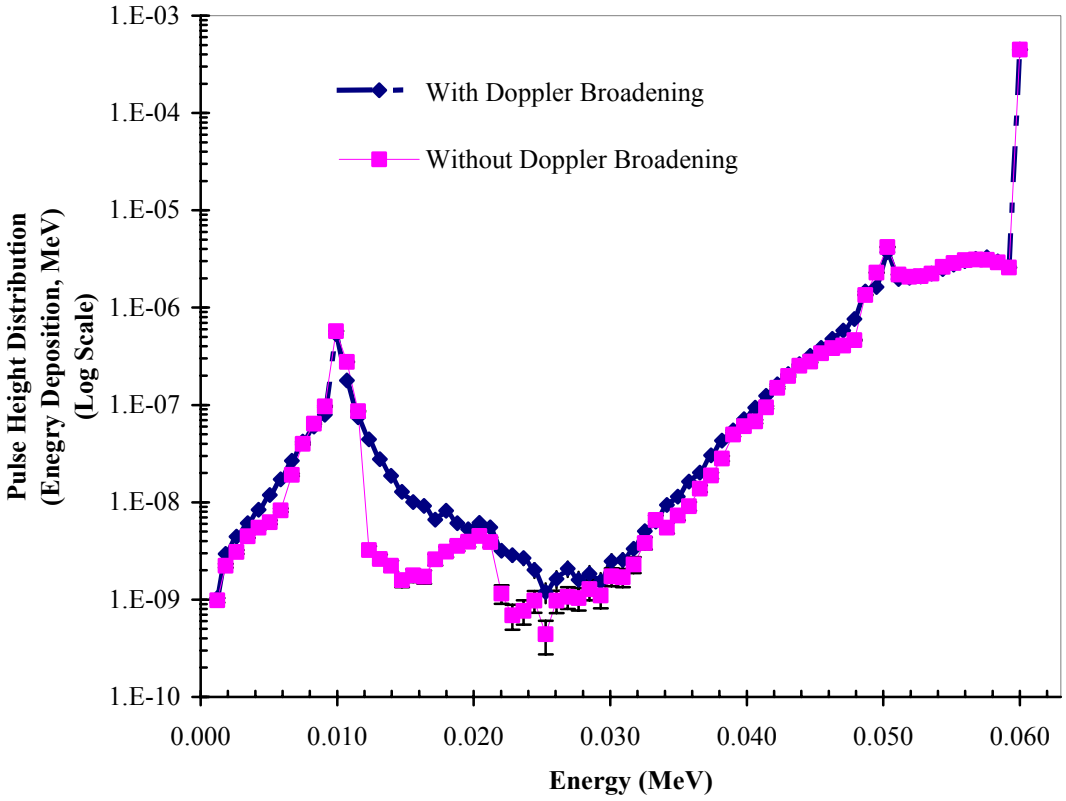

Fig. 25. Pulse height distribution spectrum for a 60 keV photon incident upon a Ge detector with and without the Doppler broadening feature. Results have been normalized to one source particle. Error bars indicate one standard deviation.

In Fig. 25, above, the peak at 10 keV is a mixture of the characteristic X-rays from Ge. This peak also includes the Compton edge. A peak seems to be present in the spectra without the Doppler broadening feature at 20 keV. This does not correspond to any predicted peaks however. The peak at 50 keV could be the backscatter peak, 48.59 keV, the Ge X-ray escape peak, 48.90 keV, or both in combination. The full energy peak is also present at 60 keV.

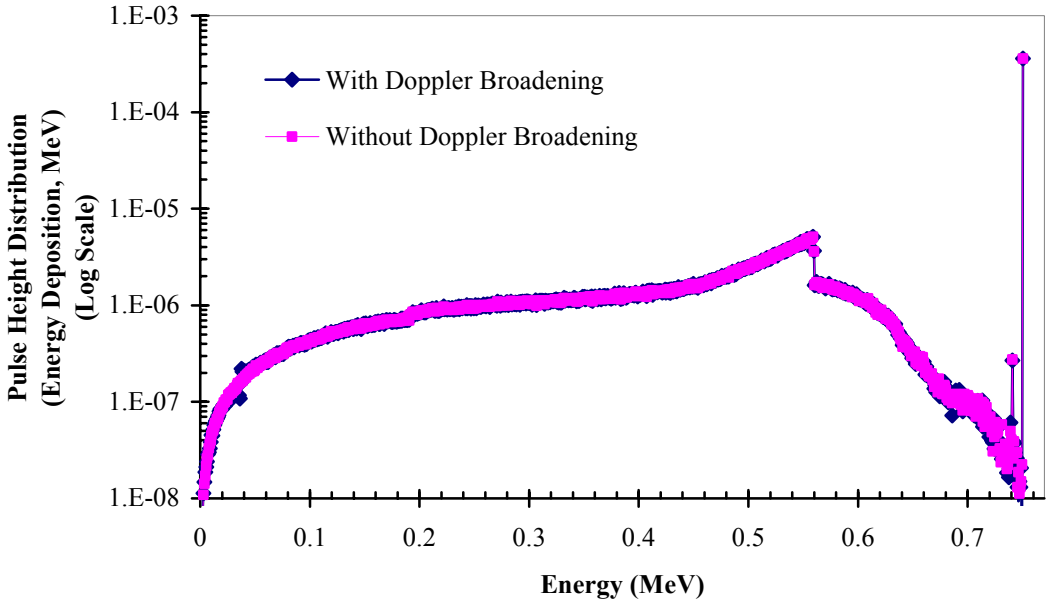

Fig. 26. Pulse height distribution spectrum for a 750 keV photon incident upon a Ge detector with and without the Doppler broadening feature. Results have been normalized to one source particle. Error bars indicate one standard deviation.

In Fig. 26, above, an error is evident at around 40 keV with the Doppler broadening. The Compton edge is located at 559 keV and the Ge X-ray escape peak is at 739 keV. The full energy peak is also present at 750 keV

The position of the backscatter peak, Ge X-ray escape peak, and the Compton edge are compared between the MCNP results and the analytically derived positions for the 15 keV, 30 keV, 60 keV and 750 keV source photons with and without the Doppler broadening feature. Table 12, on the following page, includes the comparison of backscatter peaks.

Table 12. Comparison of the analytically derived backscatter peak to results using a beta version of MCNP 5. The Doppler broadening feature did not have any affect upon the peak positions.

Source Photon Energy (keV)	Analytically Derived Backscatter Peak (keV)	Energy Bin of Backscatter Peak		Percent Error in Peak Location Using a Simple Average of the Energy in the Bin (%)
		Lower Limit (keV)	Upper Limit (keV)	
15	14.16	- - -	- - -	- - -
30	26.85	26.958	27.634	1.66
60	48.59	49.9	50.708	3.53
750	190.58	- - -	- - -	- - -

Backscatter peaks do not occur in the 15 keV and 750 keV spectra. The 30 keV spectra with the Doppler broadening feature did not have the backscatter peak, while the spectra without Doppler broadening had a small peak. The 60 keV source photon should have a Ge X-ray peak at 48.90 keV. So the single peak in the 60 keV spectra probably includes both the backscatter and Ge X-ray escape peaks, but both are in the wrong bin.

Table 13, below, compares the analytically derived Ge X-ray escape peaks to the results using the beta version of MCNP 5.

Table 13. Comparison of the analytically derived Ge X-ray escape peak to results using a beta version of MCNP 5. The Doppler broadening feature did not have any affect upon the peak positions.

Source Photon Energy (keV)	Analytically Derived Ge X-ray Escape Peak (keV)	Energy Bin of Ge X-ray Escape Peak		Percent Error in Peak Location Using a Simple Average of the Energy in the Bin (%)
		Lower Limit (keV)	Upper Limit (keV)	
15	3.90	3.612	4.196	- - -
30	18.90	18.846	20.198	- - -
60	48.90	49.9	50.708	2.87
750	738.90	739.93	740.74	0.19

The 30 keV comparison of Ge X-ray escape peaks was actually two bins wide. The error for each of the individual peaks was combined through error propagation. Peaks in the 60 kev and 750 keV spectra were almost identical. The 60 keV spectra probably includes both the backscatter and Ge X-ray escape peaks, which occur at 48.59 keV and 48.90 keV, but both are in the wrong bin.

Table 14, below, compares the position of the Compton edge. The Compton edge for a 15 keV source photon would occur at less than 1 keV, but the lower limit for photons is 1 keV so no Compton edge is evident. Also, the Compton edge for the 60 keV photon occurs at the same point as the characteristic X-ray peaks so again no comparison can be made. The Compton edge for the 30 keV and 750 keV photons occur in the correct bins.

Table 14. Comparison of the analytically derived Compton edge to results using a beta version of MCNP 5. The Doppler broadening feature did not have any affect upon the peak positions.

Source Photon Energy (keV)	Analytically Derived Compton Edge (keV)	Energy Bin of Compton Edge		Percent Error in Peak Location Using a Simple Average of the Energy in the Bin (%)
		Lower Limit (keV)	Upper Limit (keV)	
15	< 1	- - -	- - -	- - -
30	3.15	2.622	3.298	- - -
60	11.41	- - -	- - -	- - -
750	559.42	558.94	559.75	- - -

An examination of the uncertainty in dead layer thickness of ±50% for 30 keV and 750 keV photons is given in Table 15, on the following page. Variation of source positioning by ±0.5 mm gave no change in results for the same two photon energies.

Table 15. Comparison of uncertainty in dead layer thickness of Ge in the detector

	30 keV photon (energy deposition, MeV)	750 keV photon (energy deposition, MeV)
Normal thickness	3.96E-03 ± 6.3E-06	4.77E-04 ± 2.2E-06
-50% thickness	5.69E-03 ± 7.4E-06 43.6% increase	4.85E-04 ± 2.2E-06 1.8% increase
+50% thickness	2.75E-03 ± 5.2E-06 43.8% decrease	4.68E-04 ± 2.2E-06 1.7% decrease

Discussion

The positions of the peaks relative to the analytically derived positions indicates that MCNP is, in this problem, providing an overestimation of energy absorbed by the Ge. Using smaller energy bin sizes could help characterize the amount of error more accurately. Since the energy bin sizes were not the same for the different source particle energies in these problems, a comparison between the two cannot be made.

The fraction of absorbed energy within the given energy bins of the peaks was also compared between the results with and without the Doppler broadening feature. The results in percent-difference ranged from 0.1 ± 0.2% to 51.3 ± 8.9%. There was no trend to the difference such that the results with the feature were always lower. The Doppler feature seemed to alter the spectra by smoothing the peaks out and possibly decreasing the relative error for the baseline. This may actually be an indication of the error still present with the feature since this seems to reduce the peaks to nothing, as demonstrated by the absence of the 30 keV backscatter peak in Fig. 24 and Table 12.

The pulse height distribution of the 15 keV source photon seems to have an extra peak at 5.1 keV, Fig. 22, that did not correspond to any of the analytically derived peaks. The Ge X-ray escape peak appeared to contain more than one component. By decreasing the size of the energy bins, it is possible that the resolution could be improved for future comparisons.

Based on the present results, one must conclude that the Doppler broadening feature has proven not to work correctly as illustrated in part by this problem.

CONCLUSION

Anisotropic and radial dose profiles were determined for a ^{192}Ir brachytherapy device. The anisotropic profile showed the greatest dose to be on the transverse axis, 90^{o} relative to the axis of the source and cable, with the smallest dose on the axis of the source and cable. A comparison was made between the *F8 tally and the F6 tally. Results showed that for this problem, the results and standard deviation for the *F8 tally were outside of the results and standard deviation of the F6 tally. Also, the precision for the F6 tally was often smaller by half an order of magnitude than the *F8 tally.

A ^{32}P source was used in the second brachytherapy device. The radial dose profile was determined along with the dose rate 1 mm within the artery wall along the source longitudinal axis. This problem was an excellent demonstration of what can happen when the source is biased, resulting in erroneous results. With the source (over) biased, a drop in dose rate is present 1 mm within the artery wall along the center of the source cylinder longitudinal axis. The magnitude of error also increased significantly for the dose rate indicating the results were questionable. With no biasing, the dose rate profile 1 mm within the artery wall along the source longitudinal axis proved to be an even distribution of about 0.21 Gy s^{-1} for almost the entire length of the source cylinder.

Problem 4 was modeled to determine photon and neutron response for several different source energies to a TLD upon an ISO slab phantom. This problem included a comparison of results of the neutron physics with and without the S(α,β) cross sections. There was a significant difference between the results. The largest percent-difference occurred with the highest energy neutrons, but this difference had such a significant error that the results were not reliable. The use of the S(α,β) cross sections is limited to neutrons and only a few materials. These cross sections may potentially have a great effect upon the results of low energy photons. Hopefully, they will increase the accuracy of these results by improving the low energy physics to include resonances in the cross sections that will take into account molecular properties like bond vibrations and rotations.

When comparing MCNP versions 4C2 and 5beta3.23, with each run starting at the same random number and tracking to end at 50 million histories, it was found that the tally results, slope, vov, error, nrn, and collisions were identical. The only difference was the ctm, which ran 58% longer in version 5beta3.23 when compared to 4C2.

Air kerma backscatter profiles on the front face of an ISO slab phantom were determined along the apothem and diagonal of the front face. The results determined with MCNP were compared to experimental results found in ICRP 74 and give an indication of reasonable agreement between the two. Since the K_a (free in air) obtained in this problem used a spectrum of source photons, a direct comparison between ICRP 74, which used monoenergetic photons, was not considered practical.

Both the indirect spectral (angular distribution) and indirect energy fluence were determined for two 12-inch diameter Bonner spheres located in a neutron detector calibration room in problem 6. The indirect contribution was very small with the largest contribution coming from low energy photons at an average polar angle of 47^{o} relative to particles crossing a plane parallel to the floor.

The final problem looked at pulse height distribution spectra for a Ge detector. A comparison was made of spectra with the new Doppler broadening feature to spectra without the feature. The peaks within these spectra were also compared with analytically derived peaks for an indication of accuracy.

Spectra with the Doppler broadening feature compared very well with spectra without the feature in terms of peak positions. The positions of the peaks relative to the analytically derived positions indicates that MCNP, in this problem, provided an overestimation of energy absorbed by the Ge. Using smaller energy bin sizes could help to better characterize an associated amount of error. The magnitude of the tally results (peak sizes) with and without the Doppler broadening feature varied between $0.1 \pm 0.2\%$ to $51.3 \pm 8.9\%$. This will probably change when the feature, which is not working properly as shown in part by this problem, is corrected.

REFERENCES

Amols HI. Intravascular brachytherapy physics: introduction. Proceeding of the 22nd Annual EMBS International Conference. Chicago: EMBS; 2000: 1573-1576.

Attix FH. Introduction to radiological physics and radiation dosimetry. New York: John Wiley & Sons; 1986.

Bast RC, Kufe DW, Pollock RE, Weichselbaum RR, Holland JF, Frei E, Gansler TS. Cancer Medicine. Available at: http://www.ncbi.nlm.nih.gov/books/bv.fcgi?call=bv.View..ShowTOC&rid=cmed.TOC&depth=2: BC Decker Inc.; 2000. Accessed 22 January 2003.

Briesmeister JF. MCNP – a general monte carlo n-particle transport code, version 4C. Los Alamos: LA-13709-M; 2000.

Brown FB. MCNP version 5. ANS Winter Meeting. Washington D.C. 2002.

Gualdrini G. personal communication, QUADOS a concerted action of the European Commission. 30 January 2003.

Knoll GF. Radiation detection and measurement. New York: John Wiley & Sons; 2000.

Price R. ^{32}P Beta Spectrum. Available at: http://members.aol.com/rprice1495/data/P32. Accessed 1 June 2002.

Selcow EC, Goorley JT. Medical physics application of MCNP. Radiation Protection & Shielding Division of the American Nuclear Society, 12th Biennial RPSD Topical Meeting; Los Alamos: LA-UR-02-2043; 2002.

Siebert B. Intercomparison on the Usage of Computational Code in Radiation Dosimetry. Available at: http://www.nea.fr/download/quados/quados.html. Accessed 22 January 2003.

Sood A. Doppler energy broadening for incoherent scattering in MCNP, Part I. Los Alamos: X5:AS-02-16; 2002.

WebElements.com [online]. Available at: http://www.webelements.com/. Accessed 22 January 2003.

Wong T, Wallace S, Fernando W, Schumer W, Quong G. Dose errors in the near field of an HDR brachytherapy stepping source. Phys. Med. Biol. 44:357-363; 1999.

APPENDIX A

Problem 1, ^{192}Ir Brachytherapy Source

Message: outp=p1o.o runtpe=p1r.r mctal=p1m.m

```
Ir-192 Brachytherapy source
c Beginning of Cell Cards
c
c source
  1   2   -22.42   (-11 21 -23):
                   (-20 -21):
                   (-22 23)       imp:p,e 1
c steel capsule
  4   1   -8.02   -10 11 -1 25  imp:p,e 1  $ radius of capsule; 0.0325 to 0.045
  5   1   -8.02   -24 -25 -10      imp:p,e 1  $ cap of capsule
  6   1   -8.02   20 -21 25 -11 imp:p,e 1  $ space outside source cap on left
  7   1   -8.02   -1 23 22 -11  imp:p,e 1  $ space outside source cap on right
  8   1   -8.02    1 -2 -300    imp:p,e 1  $ inside of the cone; other cap
c
c woven steel cable
  9   4   -4.81   2 -150 -12    imp:p,e 1  $ woven steel cable
c                                  with radius 0.035
c
c axial fill material
c  10   3   -1.0   -10 12 -150 1 235
c  11   3   -1.0   1 300 -150 12 -10 235
c
c Dose Depth Cells
c radial depth by cylinders
c 15   3   -1.0   10  -100 -150   $ outside of the steel capsule
c                              to 1 cm radius cylinder
c 16   3   -1.0   100 -101 -150   $ 1 - 2 cm radius depth
c 17   3   -1.0   101 -102 -150   $ 2 - 3 cm radius depth
c 18   3   -1.0   102 -103 -150   $ 3 - 4 cm radius depth
c 19   3   -1.0   103 -104 -150   $ 4 - 5 cm radius depth
c
c wedges of a sphere centered at the origin with a radius of 5 cm
 20   3   -1.0   -150  235  201  10        imp:p,e 1     $   0 to  10
 22   3   -1.0   -150  235 -201  203 10     imp:p,e 1     $  10 to  20
 24   3   -1.0   -150 -203  205  235 10     imp:p,e 1     $  20 to  30
 26   3   -1.0   -150 -205  207  235 10     imp:p,e 1     $  30 to  40
 28   3   -1.0   -150 -207  209  235 10     imp:p,e 1     $  40 to  50
 30   3   -1.0   -150 -209  211  235 10     imp:p,e 1     $  50 to  60
 32   3   -1.0   -150 -211  213  235 10     imp:p,e 1     $  60 to  70
 34   3   -1.0   -150 -213  215  235 10     imp:p,e 1     $  70 to  80
 36   3   -1.0   -150 -215  217  235 10     imp:p,e 1     $  80 to  90
 38   3   -1.0   -150 -217 -219  235 10     imp:p,e 1     $  90 to 100
 40   3   -1.0   -150  219 -221  235 10     imp:p,e 1     $ 100 to 110
 42   3   -1.0   -150  221 -223  235 10     imp:p,e 1     $ 110 to 120
 44   3   -1.0   -150  223 -225  235 10     imp:p,e 1     $ 120 to 130
 46   3   -1.0   -150  225 -227  235 10     imp:p,e 1     $ 130 to 140
```

```
 48   3   -1.0   -150  227 -229  235 10     imp:p,e 1     $ 140 to 150
 50   3   -1.0   -150  229 -231  235 10     imp:p,e 1     $ 150 to 160
 52   3   -1.0   -150  231 -233  235 10     imp:p,e 1     $ 160 to 170
 54   3   -1.0   -150  233  235  10         imp:p,e 1     $ 170 to 180
c
c fill cells
 70   3   -1.0   (24 -10 -25 -150):(1 300 -2 -10 -150):(2 12 -10 -150)
                    imp:p,e 1
 71   3   -1.0   -150 -235 10     imp:p,e 1
c
c outside the known universe
 99   0            150      imp:p,e 0     $ outside of the problem
c
c End of Cell Cards

c Beginning of Surface Cards
c
  1   px   0.235    $ larger end of cone
  2   px   0.25     $ smaller end of cone
c  3   px   -0.2     $ end of catheter
c
 10   cx   0.045     $ outside radius of steel capsule
 11   cx   0.0325    $ inside radius of steel capsule; max radius of Ir-192
 12   cx   0.035     $ radius of woven steel cable
c
 20   sx  -0.1475  0.0325      $ sphere approximating Ir-192 core cap
 21   px  -0.1475     $ plane cuting sphere to approximate Ir-192 core cap
 22   sx   0.1475  0.0325      $ sphere approximating Ir-192 core cap
 23   px   0.1475     $ plane cuting sphere to approximate Ir-192 core cap
c
 24   sx  -0.139  0.061       $ sphere approximating end of steel encapsulation
 25   px  -0.18             $ plane cutting the sphere in half
c
c 100   cx   1
c 101   cx   2
c 102   cx   3
c 103   cx   4
c 104   cx   5
c
c 125   so   0.201        $ outside of device except cable
150   so   5           $ boundary of problem
c
c  200   p   0.08748866  -1 0 0     $   5 degrees
  201   p   0.176327    -1 0 0     $  10 degrees
c  202   p   0.267949    -1 0 0     $  15 degrees
  203   p   0.36397     -1 0 0     $  20 degrees
c  204   p   0.4663      -1 0 0     $  25 degrees
  205   p   0.57735     -1 0 0     $  30 degrees
c  206   p   0.7002      -1 0 0     $  35 degrees
  207   p   0.8391      -1 0 0     $  40 degrees
c  208   p   1          -1 0 0     $  45 degrees
  209   p   1.19175     -1 0 0     $  50 degrees
c  210   p   1.428148    -1 0 0     $  55 degrees
```

```
  211   p   1.732       -1 0 0     $  60 degrees
c  212   p   2.1445      -1 0 0     $  65 degrees
  213   p   2.7475      -1 0 0     $  70 degrees
c  214   p   3.73205     -1 0 0     $  75 degrees
  215   p   5.67128     -1 0 0     $  80 degrees
c  216   p   11.43       -1 0 0     $  85 degrees
  217   px  0                    $  90 degrees
c  218   p   -11.43      -1 0 0     $  95 degrees
  219   p   -5.67128    -1 0 0     $ 100 degrees
c  220   p   -3.73205    -1 0 0     $ 105 degrees
  221   p   -2.7475     -1 0 0     $ 110 degrees
c  222   p   -2.1445     -1 0 0     $ 115 degrees
  223   p   -1.732      -1 0 0     $ 120 degrees
c  224   p   -1.428148   -1 0 0     $ 125 degrees
  225   p   -1.19175    -1 0 0     $ 130 degrees
c  226   p   -1          -1 0 0     $ 135 degrees
  227   p   -0.8391     -1 0 0     $ 140 degrees
c  228   p   -0.7002     -1 0 0     $ 145 degrees
  229   p   -0.57735    -1 0 0     $ 150 degrees
c  230   p   -0.4663     -1 0 0     $ 155 degrees
  231   p   -0.36397    -1 0 0     $ 160 degrees
c  232   p   -0.267949   -1 0 0     $ 165 degrees
  233   p   -0.176327   -1 0 0     $ 170 degrees
c  234   p   -0.08748866 -1 0 0     $ 175 degrees
  235   py  0                    $ 0 or 180 degrees
c
c Cone joining the steel encapsulation with the woven steel cable
  300   kx   0.3025  0.444444 -1 $ -1 indicates cone opens in - dir
c
c End of Surface Cards

c Beginning of Data Cards
c
mode P
c
print
c prdmp 2j 1
c
nps 110000000
c
c input volume for tallying wedges
vol 7j 14.512589  14.544398  15r  14.512589  3j
c
c Source Definition
c Isotropic cylindrical volume source
sdef  pos=0 0 0  cel 1  axs=1 0 0  rad=d1  ext=d2  erg=d3  par 2
si1 0.0325
sp1 -21 1
c sb1 -21 4
si2 0.18
c sp2 -21 0
c sb2 -21 1
c These energies (MeV) and probabilities (normalized) are for the
```

```
c      photons after electron emission
c      http://members.aol.com/rprice1495/data/Ir192.pdf
si3 0 0.06149 0.06300 0.07130 0.07340 0.11009 0.13634 0.17698
      0.20131 0.20580 0.28004 0.28327 0.29596 0.30847 0.31651
      0.32931 0.37449 0.41647 0.42053 0.46807 0.48458 0.48530
      0.48904 0.58859 0.59337 0.59940 0.60442 0.61247 0.70398
      0.76600 0.88454 1.06148 1.08970 1.37830
c
sp3 0 0.00713192 0.00904863 0.00295484  0.000772031 0.0000565651
      0.000818388 0.0000191136 0.00210347 0.0147230 0.000103680
      0.00117097 0.0127795 0.0145714 0.369344 0.0000827303
      0.00321293 0.00296153 0.000327088 0.213200 0.0142059
      0.00000980639 0.00197599 0.0201254 0.000189531 0.0000172860
      0.0366937 0.0236646 0.0000238206 0.00000665052 0.00130113
      0.000235353 0.00000478285 0.00000553616
c
c Cell Importances
c
c imp:e 1 46r 1 0
c imp:p 1 46r 1 0
c
c Tallies
c
c Point detectors will give MeV/cm^2
c de and df card info from Attix, mass energy-absorption coefficient
c
c   f5:p        1        0  0   0    $ 1 cm from 0,0,0 -   0 degrees
c
c  f15:p  0.984808  0.173648  0   0    $ 1 cm from 0,0,0 -  10 degrees
c
c  f25:p  0.939693  0.342020  0   0    $ 1 cm from 0,0,0 -  20 degrees
c
c  f35:p  0.866025       0.5  0   0    $ 1 cm from 0,0,0 -  30 degrees
c
c  f45:p  0.766044  0.642788  0   0    $ 1 cm from 0,0,0 -  40 degrees
c
c  f55:p  0.642788  0.766044  0   0    $ 1 cm from 0,0,0 -  50 degrees
c
c  f65:p       0.5  0.866025  0   0    $ 1 cm from 0,0,0 -  60 degrees
c  de65   0.0100 0.015 0.02 0.03 0.04 0.05 0.06 0.08 0.1
c       0.15 0.2 0.3 0.4 0.5 0.6 0.8 1.0 1.5 2.0000
c  df65   4.79  1.28  0.512  0.149  0.0677  0.0418  0.0320
c       0.0262  0.0256  0.0277  0.0297  0.0319  0.0328
c       0.0330  0.0329 0.0321 0.0309 0.0282 0.0260
c  f75:p  0.342020  0.939693  0   0    $ 1 cm from 0,0,0 -  70 degrees
c  f85:p  0.173648  0.984808  0   0    $ 1 cm from 0,0,0 -  80 degrees
c  f95:p        0        1  0   0    $ 1 cm from 0,0,0 -  90 degrees
c  de95   0.0100 0.015 0.02 0.03 0.04 0.05 0.06 0.08 0.1
c       0.15 0.2 0.3 0.4 0.5 0.6 0.8 1.0 1.5 2.0000
c  df95   4.79  1.28  0.512  0.149  0.0677  0.0418  0.0320
c       0.0262  0.0256  0.0277  0.0297  0.0319  0.0328
c       0.0330  0.0329 0.0321 0.0309 0.0282 0.0260
c f105:p -0.173648  0.984808  0   0    $ 1 cm from 0,0,0 - 100 degrees
```

```
c f115:p -0.342020  0.939693  0   0    $ 1 cm from 0,0,0 - 110 degrees
c f125:p      -0.5  0.866025  0   0    $ 1 cm from 0,0,0 - 120 degrees
c  f135:p -0.642788  0.766044  0   0    $ 1 cm from 0,0,0 - 130 degrees
c de135   0.0100 0.015 0.02 0.03 0.04 0.05 0.06 0.08 0.1
c       0.15 0.2 0.3 0.4 0.5 0.6 0.8 1.0 1.5 2.0000
c df135   4.79  1.28  0.512  0.149  0.0677  0.0418  0.0320
c       0.0262  0.0256  0.0277  0.0297  0.0319  0.0328
c       0.0330  0.0329 0.0321 0.0309 0.0282 0.0260
c f145:p -0.766044  0.642788  0   0    $ 1 cm from 0,0,0 - 140 degrees
c f155:p -0.866025       0.5  0   0    $ 1 cm from 0,0,0 - 150 degrees
c f165:p -0.939693  0.342020  0   0    $ 1 cm from 0,0,0 - 160 degrees
c f175:p -0.984808  0.173648  0   0    $ 1 cm from 0,0,0 - 170 degrees
c f185:p       -1         0  0   0    $ 1 cm from 0,0,0 - 180 degrees
c
 fc6 Energy deposition (MeV/g) per source photon)
     f6 tallies are the anisotropic dose determination
 f6:p  20  22
 fm6   1.602e-10      $ convert MeV/g to Gy
 f16:p 24 26 28 30 32 34 36 38 40 42 44 46 48 50
 fm16  1.602e-10
 f26:p 52  54
 fm26 1.602e-10
c
 fc8 Total energy deposition (MeV) in each of the
     f8 tallies are the anisotropic dose determination
 *f8:p   20 22
 *f18:p  24 26 28 30 32 34 36 38 40 42 44 46 48 50
 *f28:p  52 54
c
c Beginning of Material Data Cards
c
c AISI Type 316L -- Stainless Steel
c rho = 8.02 g/cc
m1    025000  -0.02     014000  -0.01     024000  -0.17
      028000  -0.12     026000  -0.68
c
c Ir-192 pure cylindrical source
c rho = 22.42 g/cc
m2    077192   1
c
c Homogenous Liquid Water
c rho = 1.0 g/cc
m3    001000   1        008000  2
c
c Woven Steel Cable (assumed to be same steel as capsule)
c rho = 4.81 g/cc
m4    025000  -0.02     014000  -0.01     024000  -0.17
                  028000  -0.12     026000  -0.68
```

Problem 2, ^{32}P Brachytherapy Source

Message: outp=p1o.o runtpe=p1r.r mctal=p1m.m

```
Ir-192 Brachytherapy source
c Beginning of Cell Cards
c
c source
  1   2   -22.42   (-11 21 -23):
                   (-20 -21):
                   (-22 23)       imp:p,e 1
c steel capsule
  4   1   -8.02   -10 11 -1 25  imp:p,e 1  $ radius of capsule; 0.0325 to 0.045
  5   1   -8.02   -24 -25 -10      imp:p,e 1  $ cap of capsule
  6   1   -8.02   20 -21 25 -11 imp:p,e 1  $ space outside source cap on left
  7   1   -8.02   -1 23 22 -11  imp:p,e 1  $ space outside source cap on right
  8   1   -8.02    1 -2 -300    imp:p,e 1  $ inside of the cone; other cap
c
c woven steel cable
  9   4   -4.81   2 -150 -12    imp:p,e 1  $ woven steel cable
c                                  with radius 0.035
c
c axial fill material
c  10   3   -1.0   -10 12 -150 1 235
c  11   3   -1.0   1 300 -150 12 -10 235
c
c Dose Depth Cells
c radial depth by cylinders
c 15   3   -1.0   10  -100 -150   $ outside of the steel capsule
c                              to 1 cm radius cylinder
c 16   3   -1.0   100 -101 -150   $ 1 - 2 cm radius depth
c 17   3   -1.0   101 -102 -150   $ 2 - 3 cm radius depth
c 18   3   -1.0   102 -103 -150   $ 3 - 4 cm radius depth
c 19   3   -1.0   103 -104 -150   $ 4 - 5 cm radius depth
c
c wedges of a sphere centered at the origin with a radius of 5 cm
 20   3   -1.0   -150  235  201  10        imp:p,e 1     $   0 to  10
 22   3   -1.0   -150  235 -201  203 10     imp:p,e 1     $  10 to  20
 24   3   -1.0   -150 -203  205  235 10     imp:p,e 1     $  20 to  30
 26   3   -1.0   -150 -205  207  235 10     imp:p,e 1     $  30 to  40
 28   3   -1.0   -150 -207  209  235 10     imp:p,e 1     $  40 to  50
 30   3   -1.0   -150 -209  211  235 10     imp:p,e 1     $  50 to  60
 32   3   -1.0   -150 -211  213  235 10     imp:p,e 1     $  60 to  70
 34   3   -1.0   -150 -213  215  235 10     imp:p,e 1     $  70 to  80
 36   3   -1.0   -150 -215  217  235 10     imp:p,e 1     $  80 to  90
 38   3   -1.0   -150 -217 -219  235 10     imp:p,e 1     $  90 to 100
 40   3   -1.0   -150  219 -221  235 10     imp:p,e 1     $ 100 to 110
 42   3   -1.0   -150  221 -223  235 10     imp:p,e 1     $ 110 to 120
 44   3   -1.0   -150  223 -225  235 10     imp:p,e 1     $ 120 to 130
 46   3   -1.0   -150  225 -227  235 10     imp:p,e 1     $ 130 to 140
 48   3   -1.0   -150  227 -229  235 10     imp:p,e 1     $ 140 to 150
 50   3   -1.0   -150  229 -231  235 10     imp:p,e 1     $ 150 to 160
 52   3   -1.0   -150  231 -233  235 10     imp:p,e 1     $ 160 to 170
```

```
 54   3   -1.0   -150  233  235  10         imp:p,e 1     $ 170 to 180
c
c fill cells
 70   3   -1.0   (24 -10 -25 -150):(1 300 -2 -10 -150):(2 12 -10 -150)
                    imp:p,e 1
 71   3   -1.0   -150 -235 10     imp:p,e 1
c
c outside the known universe
 99   0            150      imp:p,e 0     $ outside of the problem
c
c End of Cell Cards

c Beginning of Surface Cards
c
  1   px   0.235    $ larger end of cone
  2   px   0.25     $ smaller end of cone
c  3   px   -0.2     $ end of catheter
c
 10   cx   0.045     $ outside radius of steel capsule
 11   cx   0.0325    $ inside radius of steel capsule; max radius of Ir-192
 12   cx   0.035     $ radius of woven steel cable
c
 20   sx  -0.1475  0.0325      $ sphere approximating Ir-192 core cap
 21   px  -0.1475     $ plane cuting sphere to approximate Ir-192 core cap
 22   sx   0.1475  0.0325      $ sphere approximating Ir-192 core cap
 23   px   0.1475     $ plane cuting sphere to approximate Ir-192 core cap
c
 24   sx  -0.139  0.061       $ sphere approximating end of steel encapsulation
 25   px  -0.18             $ plane cutting the sphere in half
c
c 100   cx   1
c 101   cx   2
c 102   cx   3
c 103   cx   4
c 104   cx   5
c
c 125   so   0.201        $ outside of device except cable
150   so   5          $ boundary of problem
c
c  200   p   0.08748866  -1 0 0     $   5 degrees
  201   p   0.176327    -1 0 0     $  10 degrees
c  202   p   0.267949    -1 0 0     $  15 degrees
  203   p   0.36397     -1 0 0     $  20 degrees
c  204   p   0.4663      -1 0 0     $  25 degrees
  205   p   0.57735     -1 0 0     $  30 degrees
c  206   p   0.7002      -1 0 0     $  35 degrees
  207   p   0.8391      -1 0 0     $  40 degrees
c  208   p   1          -1 0 0     $  45 degrees
  209   p   1.19175     -1 0 0     $  50 degrees
c  210   p   1.428148    -1 0 0     $  55 degrees
  211   p   1.732       -1 0 0     $  60 degrees
c  212   p   2.1445      -1 0 0     $  65 degrees
  213   p   2.7475      -1 0 0     $  70 degrees
```

```
c  214   p   3.73205     -1 0 0     $  75 degrees
  215   p   5.67128     -1 0 0     $  80 degrees
c  216   p   11.43       -1 0 0     $  85 degrees
  217   px   0                    $  90 degrees
c  218   p   -11.43      -1 0 0     $  95 degrees
  219   p   -5.67128    -1 0 0     $ 100 degrees
c  220   p   -3.73205    -1 0 0     $ 105 degrees
  221   p   -2.7475     -1 0 0     $ 110 degrees
c  222   p   -2.1445     -1 0 0     $ 115 degrees
  223   p   -1.732      -1 0 0     $ 120 degrees
c  224   p   -1.428148   -1 0 0     $ 125 degrees
  225   p   -1.19175    -1 0 0     $ 130 degrees
c  226   p   -1          -1 0 0     $ 135 degrees
  227   p   -0.8391     -1 0 0     $ 140 degrees
c  228   p   -0.7002     -1 0 0     $ 145 degrees
  229   p   -0.57735    -1 0 0     $ 150 degrees
c  230   p   -0.4663     -1 0 0     $ 155 degrees
  231   p   -0.36397    -1 0 0     $ 160 degrees
c  232   p   -0.267949   -1 0 0     $ 165 degrees
  233   p   -0.176327   -1 0 0     $ 170 degrees
c  234   p   -0.08748866 -1 0 0     $ 175 degrees
  235   py   0                     $ 0 or 180 degrees
c
c Cone joining the steel encapsulation with the woven steel cable
  300   kx   0.3025  0.444444 -1 $ -1 indicates cone opens in - dir
c
c End of Surface Cards

c Beginning of Data Cards
c
mode P
c
print
c prdmp 2j 1
c
nps 110000000
c
c input volume for tallying wedges
vol 7j 14.512589  14.544398  15r  14.512589  3j
c
c Source Definition
c Isotropic cylindrical volume source
sdef  pos=0 0 0  cel 1  axs=1 0 0  rad=d1  ext=d2  erg=d3  par 2
si1 0.0325
sp1 -21 1
c sb1 -21 4
si2 0.18
c sp2 -21 0
c sb2 -21 1
c These energies (MeV) and probabilities (normalized) are for the
c      photons after electron emission
c      http://members.aol.com/rprice1495/data/Ir192.pdf
si3 0 0.06149 0.06300 0.07130 0.07340 0.11009 0.13634 0.17698
```

```
      0.20131 0.20580 0.28004 0.28327 0.29596 0.30847 0.31651
      0.32931 0.37449 0.41647 0.42053 0.46807 0.48458 0.48530
      0.48904 0.58859 0.59337 0.59940 0.60442 0.61247 0.70398
      0.76600 0.88454 1.06148 1.08970 1.37830
c
sp3 0 0.00713192 0.00904863 0.00295484  0.000772031 0.0000565651
      0.000818388 0.0000191136 0.00210347 0.0147230 0.000103680
      0.00117097 0.0127795 0.0145714 0.369344 0.0000827303
      0.00321293 0.00296153 0.000327088 0.213200 0.0142059
      0.00000980639 0.00197599 0.0201254 0.000189531 0.0000172860
      0.0366937 0.0236646 0.0000238206 0.00000665052 0.00130113
      0.000235353 0.00000478285 0.00000553616
c
c Cell Importances
c
c imp:e 1 46r 1 0
c imp:p 1 46r 1 0
c
c Tallies
c
c Point detectors will give MeV/cm^2
c de and df card info from Attix, mass energy-absorption coefficient
c
c   f5:p        1        0  0   0    $ 1 cm from 0,0,0 -   0 degrees
c
c  f15:p  0.984808  0.173648  0   0    $ 1 cm from 0,0,0 -  10 degrees
c
c  f25:p  0.939693  0.342020  0   0    $ 1 cm from 0,0,0 -  20 degrees
c
c  f35:p  0.866025       0.5  0   0    $ 1 cm from 0,0,0 -  30 degrees
c
c  f45:p  0.766044  0.642788  0   0    $ 1 cm from 0,0,0 -  40 degrees
c
c  f55:p  0.642788  0.766044  0   0    $ 1 cm from 0,0,0 -  50 degrees
c
c  f65:p       0.5  0.866025  0   0    $ 1 cm from 0,0,0 -  60 degrees
c  de65   0.0100 0.015 0.02 0.03 0.04 0.05 0.06 0.08 0.1
c       0.15 0.2 0.3 0.4 0.5 0.6 0.8 1.0 1.5 2.0000
c  df65   4.79  1.28  0.512  0.149  0.0677  0.0418  0.0320
c       0.0262  0.0256  0.0277  0.0297  0.0319  0.0328
c       0.0330  0.0329 0.0321 0.0309 0.0282 0.0260
c  f75:p  0.342020  0.939693  0   0    $ 1 cm from 0,0,0 -  70 degrees
c  f85:p  0.173648  0.984808  0   0    $ 1 cm from 0,0,0 -  80 degrees
c  f95:p         0         1  0   0    $ 1 cm from 0,0,0 -  90 degrees
c  de95   0.0100 0.015 0.02 0.03 0.04 0.05 0.06 0.08 0.1
c       0.15 0.2 0.3 0.4 0.5 0.6 0.8 1.0 1.5 2.0000
c  df95   4.79  1.28  0.512  0.149  0.0677  0.0418  0.0320
c       0.0262  0.0256  0.0277  0.0297  0.0319  0.0328
c       0.0330  0.0329 0.0321 0.0309 0.0282 0.0260
c f105:p -0.173648  0.984808  0   0    $ 1 cm from 0,0,0 - 100 degrees
c f115:p -0.342020  0.939693  0   0    $ 1 cm from 0,0,0 - 110 degrees
c f125:p      -0.5  0.866025  0   0    $ 1 cm from 0,0,0 - 120 degrees
c  f135:p -0.642788  0.766044  0   0    $ 1 cm from 0,0,0 - 130 degrees
```

```
c de135   0.0100 0.015 0.02 0.03 0.04 0.05 0.06 0.08 0.1
c       0.15 0.2 0.3 0.4 0.5 0.6 0.8 1.0 1.5 2.0000
c df135   4.79  1.28  0.512  0.149  0.0677  0.0418  0.0320
c       0.0262  0.0256  0.0277  0.0297  0.0319  0.0328
c       0.0330  0.0329 0.0321 0.0309 0.0282 0.0260
c f145:p -0.766044  0.642788  0   0    $ 1 cm from 0,0,0 - 140 degrees
c f155:p -0.866025       0.5  0   0    $ 1 cm from 0,0,0 - 150 degrees
c f165:p -0.939693  0.342020  0   0    $ 1 cm from 0,0,0 - 160 degrees
c f175:p -0.984808  0.173648  0   0    $ 1 cm from 0,0,0 - 170 degrees
c f185:p        -1         0  0   0    $ 1 cm from 0,0,0 - 180 degrees
c
 fc6 Energy deposition (MeV/g) per source photon)
     f6 tallies are the anisotropic dose determination
 f6:p  20  22
 fm6   1.602e-10      $ convert MeV/g to Gy
 f16:p 24 26 28 30 32 34 36 38 40 42 44 46 48 50
 fm16  1.602e-10
 f26:p 52  54
 fm26 1.602e-10
c
 fc8 Total energy deposition (MeV) in each of the
     f8 tallies are the anisotropic dose determination
 *f8:p   20 22
 *f18:p  24 26 28 30 32 34 36 38 40 42 44 46 48 50
 *f28:p  52 54
c
c Beginning of Material Data Cards
c
c AISI Type 316L -- Stainless Steel
c rho = 8.02 g/cc
m1    025000  -0.02     014000  -0.01     024000  -0.17
      028000  -0.12     026000  -0.68
c
c Ir-192 pure cylindrical source
c rho = 22.42 g/cc
m2    077192   1
c
c Homogenous Liquid Water
c rho = 1.0 g/cc
m3    001000   1        008000  2
c
c Woven Steel Cable (assumed to be same steel as capsule)
c rho = 4.81 g/cc
m4    025000  -0.02     014000  -0.01     024000  -0.17
      028000  -0.12     026000  -0.68
```

Problem 4, Neutron and Photon Response of a TLD-Albedo Personal Dosemeter on an ISO Slab Phantom

Message: outp=p4nt.o runtpe=p4nt.r mctal=p4nt.m wwout=wwout

```
Neutron and Photon TLD Response on an ISO slab phantom
c Beginning of Cell Cards
c
c TLDs
  1   4   -2.54   5 -6 23 -24 37 -38 imp:n 7 $ Li-6F; chip 1; top left
  2   5   -2.64   7 -8 23 -24 37 -38 imp:n 7 $ Li-7F; chip 2; top right
  3   4   -2.54   5 -6 19 -20 37 -38 imp:n 7 $ Li-6F; chip 3; bottom left
  4   5   -2.64   7 -8 19 -20 37 -38 imp:n 7 $ Li-7F; chip 4; bottom right
c
c water phantom
c              Cell 10 is the PMMA cube
 10   1   -1.19   (1 -2 15 -28 40 -42):(11 -12 15 -28 40 -42)
               :(15 -16 1 -12 40 -42):(27 -28 1 -12 40 -42)
               :(39 -40 1 -12 15 -28):(41 -42 1 -12 15 -28)  imp:n 1
 11   3   -1.00   2 -11 16 -27 40 -41   imp:n 1 $ water inside ISO phantom
c
c Al plate
 20   2   -2.70   (4 -9 18 -19 37 -38):(4 -9 24 -25 37 -38)
               :(4 -5 18 -25 37 -38):(8 -9 18 -25 37 -38)
               :(6 -7 18 -25 37 -38):(20 -23 4 -9 37 -38)  imp:n 5
c
c Al disks
 25   2   -2.70   -52 36 -37  imp:n 30   $ in front of chip 3
 26   2   -2.70   -53 36 -37  imp:n 30   $ in front of chip 4
c
c vacuum disks
 30   0          -52 38 -39  imp:n 7 $ behind chip 3
 31   0          -53 38 -39  imp:n 7 $ behind chip 4
c
c holder
 35   6   -1.19   3 -10 38 -39 52 53 17 -26   imp:n 9 $ back with holes
 36   6   -1.19   (3 -4 17 -26 37 -38):(9 -10 17 -26 37 -38)
               :(3 -10 25 -26 37 -38):(3 -10 17 -18 37 -38)   imp:n 10
 37   6   -1.19   3 -10 17 -26 36 -37 50 51 52 53   imp:n 9
 38   6   -1.19   3 -10 17 -26 35 -36 50 51     imp:n 7
c
c source
 50   0          1 -12 15 -28 100 -101  imp:n 1
c
c outside of problem
 99   0   (-50 -37 101 -200):(-51 -37 101 -200):(-35 3 -10 17 -26 101 -200):
         (-3 -39 101 -200):(10 -39 101 -200):(-17 -39 101 -200):
         (26 -39 101 -200):((42:-1:12:-15:28:-100) -200)   imp:n 2
999   0   200   imp:n 0
c
c End of Cell Cards

c Beginning of Surface Cards
c
```

```
  1   px   -15     $ edge of water phantom; edge of PMMA
  2   px   -14     $ edge of PMMA; edge of water
  3   px   -1.75   $ edge of TLD; edge of polyethylene
  4   px   -1.25   $ edge of polyethylene; edge of Al
  5   px   -0.91   $ left edge of chips 1 and 3
  6   px   -0.59   $ right edge of chips 1 and 3
  7   px    0.59   $ left edge of chips 2 and 4
  8   px    0.91   $ right edge of chips 2 and 4
  9   px   1.25    $ edge of Al; edge of polyethylene
 10   px   1.75    $ edge of polyethylene; edge of TLD
 11   px    14     $ edge of water; edge of PMMA
 12   px    15     $ edge of PMMA; edge of water phantom
c
 15   py   -15     $ edge of water phantom; edge of PMMA
 16   py   -14     $ edge of PMMA; edge of water
 17   py   -2.75   $ edge of TLD; edge of polyethylene
 18   py   -2.25   $ edge of polyethylene; edge of Al
 19   py   -1.91   $ edge of Al; bottom edge of chips 3 and 4
 20   py   -1.59   $ top edge of chips 3 and 4; edge of Al
c 21   py   -1.25   $ edge of Al
c 22   py    1.25   $ edge of Al
 23   py    1.59   $ edge of Al; bottom edge of chips 1 and 2
 24   py    1.91   $ top edge of chips 1 and 2; edge of Al
 25   py    2.25   $ edge of Al; edge of polyethylene
 26   py    2.75   $ edge of polyethylene; edge of TLD
 27   py    14     $ edge of water; edge of PMMA
 28   py    15     $ edge of PMMA; edge of water phantom
c
 35   pz   -0.79   $ front edge of TLD; edge of polyethylene
 36   pz   -0.39   $ edge of polyethylene; edge of Al disk
 37   pz   -0.29   $ edge of Al disk; front edge LiF
 38   pz   -0.20   $ edge of LiF; edge of vacuum or polyethylene
 39   pz    0     $ back edge of TLD; edge of water phantom
 40   pz    0.25   $ edge of PMMA; edge of water
 41   pz    14     $ edge of water; edge of PMMA
 42   pz    15     $ edge of PMMA; back edge of water phantom
c
 50   c/z   -0.75  1.75 0.5    $ 1cm diameter hole centered on chip 1
 51   c/z    0.75  1.75 0.5    $ 1cm diameter hole centered on chip 2
 52   c/z   -0.75 -1.75 0.5    $ 1cm diameter hole centered on chip 3
 53   c/z    0.75 -1.75 0.5    $ 1cm diameter hole centered on chip 4
c
c source providing neutrons and photons at normal incidence
100   pz   -11
101   pz   -10
c
c surfaces to define the outside universe
200   so   30
c
c End of Surface Cards

c Beginning of Data Cards
c
```

```
mode n
c
print
c prdmp 2j 1
c
c ctme 180
nps 200000000
c phys:p 100 0 0
c phys:e 50 0 0 0 0 0
c
c Source Definition
c Plane source with direction normal to surface
sdef x=d1 y=d2 z=-10 sur=101 nrm=1 vec=0 0 -1 dir=-1 erg=0.0000000253 par 1
si1  -15  -2   2   15
sp1    0   1   1    1
sb1    0   1  20    1
si2  -15  -2.75  -0.5  0.5   2.75   15
sp2    0   1       1     1     1      1
sb2    0   1      20     1    20      1
c
c Cell importances
c
c imp:e 1 15r 1 0
c imp:p 1 15r 1 0
c
c Weight Window Generator
 wwp:n 10 1.1 5 0 -1
c wwg 14 0 0
 mesh geom=xyz ref=0 0 0 origin= -30 -30 -30
       imesh -2.0 2 30 iints 4 10 4
       jmesh -7 -3 3 7 30 jints 4 10 15 10 4
       kmesh -2 4 13 30  kints 4 10 7 4
c Tallies
c
c fc6 Energy deposition (MeV/g) per source photon)
c      f6 tallies are the cylindrical/radial dose depth
c f6:p  1 2 3 4 T
c
 fc4 n,t reactions in Li
 f4:n 1 3                              $ Li-6 TLDs
 fm4 (1.4534e24 7 105) (1.4534e24 7 105)
 f14:n 2 4                               $ Li-7 TLDs
 fm14 (9.0589e20 8 105) (9.0589e20 8 105)
c
c Beginning of Material Data Cards
c
c PMMA
c rho = 1.19 g/cc
m1    001001 -0.0805259   001002 -0.0000120807   $ naturally occurring H
      008016 -0.319490706637    008017 -0.00012169590664   $nat. O
      006012 -0.593190    006013 -0.00665831     $ naturally occurring C
c
c Aluminum
```

```
c rho = 2.70 g/cc
m2    013027 1
c
c Water
c rho = 1.00 g/cc
m3    001001 -0.111877   001002 -0.0000167841    $ naturally occurring H
      008016 -0.88776398262   008017 -0.0003381549598   $ nat. O
c
c Li-6F
c rho = 2.54 g/cc
m4    003006 -0.229      003007 -0.012      009019 -0.758
c
c Li-7F
c rho = 2.64 g/cc
m5    003006 -0.00016    003007 -0.270      009019 -0.730
c
c Holder
c rho = 1.19 g/cc
m6    001001 -0.079988   001002 -0.000012        $ naturally occurring H
      006012 -0.6279515   006013 -0.0070485      $ naturally occurring C
      005010 -0.056914   005011 -0.229086        $ naturally occurring B
c
c Li-6 TLD
m7    003006 1.4534e24     $ 003007 7.6163e22
c
c Li-7 TLD
m8    003006 9.0589e20     $ 003007 1.5287e24
```

Problem 5, Air Kerma Backscatter Profiles for two ISO Photon Expanded and Aligned Fields Impinging on an ISO Water Phantom

Message: outp=p5wnm.o runtpe=p5wnm.r mctal=p5wnm.m

```
Air Kerma Backscatter Profiles
c this is the tally segmented version that will determine
c backscatter profiles along the diagonal and apothem for
c the narrow spectrum with normal phantom materials
c using mass energy transfer coefficients for air
c
c using the *F2 Tally
c
c kerma is determined on the surface of the
c polyethylene using mass energy transfer coefficients for
c air.
c
c Beginning of Cell Cards
c
c water phantom
c               Cell 1 is the PMMA cube
  1   1   -1.19    (1 -2 10 -13 20 -23):(3 -4 10 -13 20 -23)
                  :(1 -4 10 -11 20 -23):(1 -4 12 -13 20 -23)
                  :(1 -4 10 -13 20 -21):(1 -4 10 -13 22 -23)
  2   2   -1      2 -3 11 -12 21 -22    $ water inside ISO phantom
c
c source
  50   0          1 -4 10 -13 100 -101
c
c vacuum
 100   0          (-200 -1):(-200 4):(-200 -10):(-200 13):
                 (-100 -200):(-200 23):
                 (-200 -20 101)
c
c outside of problem
999   0   200
c
c End of Cell Cards

c Beginning of Surface Cards
c
   1   px   -15     $ edge of water phantom; edge of PMMA
   2   px   -14     $ edge of PMMA; edge of water
   3   px    14     $ edge of water; edge of PMMA
   4   px    15     $ edge of PMMA; edge of water phantom
c
  10   py   -15     $ edge of water phantom; edge of PMMA
  11   py   -14     $ edge of PMMA; edge of water
  12   py    14     $ edge of water; edge of PMMA
  13   py    15     $ edge of PMMA; edge of water phantom
c
  20   pz     0     $ edge of water phantom
  21   pz    0.25   $ edge of PMMA; edge of water
```

```
 22   pz   14    $ edge of water; edge of PMMA
 23   pz   15    $ edge of PMMA; back edge of water phantom
c
c segmented tally surfaces
 30   so    0.2
 31   sx    0.5   0.2
 32   sx    1.0   0.2
 33   sx    1.5   0.2
 34   sx    2.0   0.2
 35   sx    2.5   0.2
 36   sx    3.0   0.2
 37   sx    3.5   0.2
 38   sx    4.0   0.2
 39   sx    4.5   0.2
 40   sx    5.0   0.2
 41   sx    6.0   0.2
 42   sx    7.0   0.2
 43   sx    8.0   0.2
 44   sx    9.0   0.2
 45   sx   11.0   0.2
 46   sx   13.0   0.2
c
 50    s    0.5   0.5   0   0.2
 51    s    1.0   1.0   0   0.2
 52    s    1.5   1.5   0   0.2
 53    s    2.0   2.0   0   0.2
 54    s    2.5   2.5   0   0.2
 55    s    3.0   3.0   0   0.2
 56    s    3.5   3.5   0   0.2
 57    s    4.0   4.0   0   0.2
 58    s    4.5   4.5   0   0.2
 59    s    5.0   5.0   0   0.2
 60    s    6.0   6.0   0   0.2
 61    s    7.0   7.0   0   0.2
 62    s    8.0   8.0   0   0.2
 63    s    9.0   9.0   0   0.2
 64    s   11.0  11.0   0   0.2
 65    s   13.0  13.0   0   0.2
c
c source providing neutrons and photons at normal incidence
100   pz   -11
101   pz   -10
c
c surfaces to define the outside universe
200   so   50
c
c End of Surface Cards

c Beginning of Data Cards
c
mode p
c
print
```

```
c prdmp 2j 1
c
nps 500000000
c
c Source Definition
c Plane source with direction normal to surface
sdef  x=d1 y=d2 z=-10 sur=101 nrm=1 vec=0 0 -1 dir=-1 erg=d3 ara=900 par 2
si1   -15 15
sp1   0 1
si2   -15 15
sp2   0 1
c si3   0.1030   0.1035   0.1040   0.1045   0.1050   0.1055   0.1060   0.1065
c     0.1070   0.1075   0.1080   0.1085   0.1090   0.1095   0.1100   0.1105
c     0.1110   0.1115   0.1120   0.1125   0.1130   0.1135   0.1140   0.1145
c     0.1150   0.1155   0.1160   0.1165   0.1170   0.1175   0.1180   0.1185
c     0.1190   0.1195   0.1200   0.1205   0.1210   0.1215   0.1220   0.1225
c     0.1230   0.1235   0.1240   0.1245   0.1250   0.1255   0.1260   0.1265
c     0.1270   0.1275   0.1280   0.1285   0.1290   0.1295   0.1300   0.1305
c     0.1310   0.1315   0.1320   0.1325   0.1330   0.1335   0.1340   0.1345
c     0.1350   0.1355   0.1360   0.1365   0.1370   0.1375   0.1380   0.1385
c     0.1390   0.1395   0.1400   0.1405   0.1410   0.1415   0.1420   0.1425
c     0.1430   0.1435   0.1440   0.1445   0.1450   0.1455   0.1460   0.1465
c     0.1470   0.1475   0.1480   0.1485   0.1490   0.1495   0.1500   0.1505
c     0.1510   0.1515   0.1520   0.1525   0.1530   0.1535   0.1540   0.1545
c     0.1550   0.1555   0.1560   0.1565   0.1570   0.1575   0.1580   0.1585
c     0.1590   0.1595   0.1600   0.1605   0.1610   0.1615   0.1620   0.1625
c     0.1630   0.1635   0.1640   0.1645   0.1650   0.1655   0.1660   0.1665
c     0.1670   0.1675   0.1680   0.1685   0.1690   0.1695   0.1700   0.1705
c     0.1710   0.1715   0.1720   0.1725   0.1730   0.1735   0.1740   0.1745
c     0.1750   0.1755   0.1760   0.1765   0.1770   0.1775   0.1780   0.1785
c     0.1790   0.1795   0.1800   0.1805   0.1810   0.1815   0.1820   0.1825
c     0.1830   0.1835   0.1840   0.1845   0.1850   0.1855   0.1860   0.1865
c     0.1870   0.1875   0.1880   0.1885   0.1890   0.1895   0.1900   0.1905
c     0.1910   0.1915   0.1920   0.1925   0.1930   0.1935   0.1940   0.1945
c     0.1950   0.1955   0.1960   0.1965   0.1970   0.1975   0.1980   0.1985
c     0.1990   0.1995   0.2000   0.2005   0.2010   0.2015   0.2020   0.2025
c sp3   0   0.1847   0.2263   0.294   0.3694   0.3217   0.411   0.5033
c     0.4664   0.5218   0.5464   0.6096   0.7081   0.6881   0.8266   0.782
c     0.8743   0.9236   0.9836   0.9913   1.056   1.121   1.191   1.288
c     1.415   1.447   1.387   1.599   1.205   1.375   1.662   1.838   1.826
c     1.778   1.967   1.952   2.192   2.164   2.189   2.389   2.387   2.463
c     2.658   2.846   2.946   3.142   3.316   3.416   3.499   3.556   3.597
c     3.853   3.908   4.308   4.567   4.749   4.784   5.115   5.221   5.461
c     5.458   5.879   5.723   6.183   6.3   6.428   6.853   6.487   6.885
c     7.319   7.453   7.353   7.884   8.14   8.691   8.879   9.191   9.036
c     9.103   9.964   9.905   10.46   10.35   10.27   11   10.68   11.46
c     11.27   11.78   11.9   12.63   12.59   12.89   12.91   13.46   13.7
c     13.69   14.32   14.14   14.93   14.97   15.59   15.1   16.16   15.66
c     15.76   16.44   16.68   16.61   16.86   17.01   16.84   17   17.16
c     17.48   17.3   17.2   18.23   18.54   18.29   18.47   18.09   19.04
c     18.93   18.52   19   19.37   18.97   19.91   19.45   20.12   19.45
c     19.64   19.33   20.23   19.75   19.21   19.8   20.16   20.03   19.53
c     20.7   20.52   19.85   19.11   20.05   19.78   19.15   18.84   20.16
```

c 19.05 18.65 19.22 20.03 18.86 18.45 18.36 18.01 17.87
c 17.86 17.63 17.22 17.31 16.6 16.58 15.9 15.45 15.67
c 14.99 15.31 14.87 15.29 13.35 13.4 13.7 13.42 11.83
c 11.74 11.2 10.72 10.11 9.283 8.565 8.321 7.846 6.893
c 6.39 5.846 5.406 4.455 3.885 3.24 2.666 1.889 1.379
c 0.7466 0.5172 0.2124 0.1185 0
si3 0.0495 0.05 0.0505 0.051 0.0515 0.052 0.0525 0.053
0.0535 0.054 0.0545 0.055 0.0555 0.056 0.0565 0.057
0.0575 0.058 0.0585 0.059 0.0595 0.06 0.0605 0.061
0.0615 0.062 0.0625 0.063 0.0635 0.064 0.0645 0.065
0.0655 0.066 0.0665 0.067 0.0675 0.068 0.0685 0.069
0.0695 0.07 0.0705 0.071 0.0715 0.072 0.0725 0.073
0.0735 0.074 0.0745 0.075 0.0755 0.076 0.0765 0.077
0.0775 0.078 0.0785 0.079 0.0795 0.08 0.0805 0.081
0.0815 0.082 0.0825 0.083 0.0835 0.084 0.0845 0.085
0.0855 0.086 0.0865 0.087 0.0875 0.088 0.0885 0.089
0.0895 0.09 0.0905 0.091 0.0915 0.092 0.0925 0.093
0.0935 0.094 0.0945 0.095 0.0955 0.096 0.0965 0.097
0.0975 0.098 0.0985 0.099 0.0995 0.1 0.1005 0.101
0.1015 0.102 0.1025 0.103 0.1035 0.104 0.1045 0.105
0.1055 0.106 0.1065 0.107 0.1075 0.108 0.1085 0.109
0.1095 0.11 0.1105 0.111 0.1115 0.112 0.1125 0.113
0.1135 0.114 0.1145 0.115 0.1155 0.116 0.1165 0.117
0.1175 0.118 0.1185 0.119 0.1195 0.12 0.1205 0.121
0.1215 0.122 0.1225 0.123 0.1235 0.124 0.1245 0.125
0.1255 0.126 0.1265 0.127 0.1275 0.128 0.1285 0.129
0.1295 0.13 0.1305 0.131 0.1315 0.132 0.1325 0.133
0.1335 0.134 0.1345 0.135 0.1355 0.136 0.1365 0.137
0.1375 0.138 0.1385 0.139 0.1395 0.14 0.1405 0.141
0.1415 0.142 0.1425 0.143 0.1435 0.144 0.1445 0.145
0.1455 0.146 0.1465 0.147 0.1475 0.148 0.1485 0.149
0.1495 0.15 0.1505 0.151
sp3 0 0.03499 0.14 0.2682 0.2566 0.3324 0.2828 0.4403
0.3645 0.5569 0.5802 0.6181 0.7464 0.2391 0.3528
0.8281 0.9359 2.429 3.77 1.639 8.73 4.828 1.662
1.458 1.621 1.735 2.114 2.271 2.315 2.417 2.618
2.846 3.032 3.373 3.598 7.779 14.99 6.173 4.388
6.537 8.852 5.467 4.881 5.079 5.155 5.502 5.992
6.528 6.485 6.817 6.75 7.592 8.027 7.546 7.887
8.257 8.671 8.47 9.12 9.584 9.75 9.695 10.67
10.89 10.86 11.06 11.44 12.01 12.13 12.42 13.27
13.2 13.16 13.58 13.55 13.97 14.15 13.87 13.58
13.85 14.13 14.17 14.26 14.58 14.5 14.83 14.79
15.27 15.25 15.38 15.82 15.1 16.34 15.99 15.64
15.75 16.01 16.21 15.99 15.96 16.53 16.74 16.07
16.46 17.17 16.92 16.87 16.72 17.35 17 16.37
16.49 16.85 16.46 17.14 16.7 16.73 16.67 17.06
16.58 16.74 16.5 17.21 16.41 16.36 16.86 15.81
16.26 15.88 16.22 16.16 16.03 15.78 16.13 15.61
15.56 15.79 15.09 15.6 15.48 15.45 15.26 14.79
14.3 14.6 14.55 13.96 13.93 13.72 13.29 12.93
13.29 13.09 13.11 13.25 12.61 12.32 12.4 12.09
12.05 11.73 11.05 11.12 11.06 10.48 10.2 10.19

```
      9.91   9.339   9.823   8.709   9.339   9.321   9.097   8.744
      7.957   8.208   8.193   7.228   7.178   6.77   6.613   6.779
      6.199   6.202   5.645   5.584   4.895   4.858   4.493   4.502
      3.869   3.63   3.376   3.015   2.607   2.598   2.003   1.691
      1.42   1.079   0.6677   0.2712   0
c
c Cell Importances
c
imp:p 1 3r 0
c
c Tallies
c
fc2 Surface tally at the center of the front face
*f2:p  20
c de and df are mass energy transfer or mass energy absorption coefficients
c from Attix they have the same values
fm2 1.602e-10      $ to convert to gray
de2 0.01  0.015  0.02  0.03  0.04  0.05  0.06  0.08  0.1  0.15  0.2  0.3
df2 4.533  1.242  0.4942  0.1395  0.0625  0.0382  0.0289  0.0236  0.0231
    0.0249  0.0267  0.0287
fs2   -30
sd2    0.12566   1
c
fc12 Surface tally that is segmented along the apothem
*f12:p  20
c de and df are mass energy transfer or mass energy absorption coefficients
c from Attix they have the same values
fm12 1.602e-10      $ to convert to gray
de12 0.01  0.015  0.02  0.03  0.04  0.05  0.06  0.08  0.1  0.15  0.2  0.3
df12 4.533  1.242  0.4942  0.1395  0.0625  0.0382  0.0289  0.0236  0.0231
    0.0249  0.0267  0.0287
fs12  -31
sd12  0.12566   1
c
fc22 Surface tally that is segmented along the apothem
*f22:p  20
c de and df are mass energy transfer or mass energy absorption coefficients
c from Attix they have the same values
fm22 1.602e-10      $ to convert to gray
de22 0.01  0.015  0.02  0.03  0.04  0.05  0.06  0.08  0.1  0.15  0.2  0.3
df22 4.533  1.242  0.4942  0.1395  0.0625  0.0382  0.0289  0.0236  0.0231
    0.0249  0.0267  0.0287
fs22  -32
sd22  0.12566   1
c
fc32 Surface tally that is segmented along the apothem
*f32:p  20
c de and df are mass energy transfer or mass energy absorption coefficients
c from Attix they have the same values
fm32 1.602e-10      $ to convert to gray
de32 0.01  0.015  0.02  0.03  0.04  0.05  0.06  0.08  0.1  0.15  0.2  0.3
df32 4.533  1.242  0.4942  0.1395  0.0625  0.0382  0.0289  0.0236  0.0231
    0.0249  0.0267  0.0287
```

```
fs32  -33
sd32  0.12566   1
c
fc42 Surface tally that is segmented along the apothem
*f42:p  20
c de and df are mass energy transfer or mass energy absorption coefficients
c from Attix they have the same values
fm42 1.602e-10      $ to convert to gray
de42 0.01  0.015  0.02  0.03  0.04  0.05  0.06  0.08  0.1  0.15  0.2  0.3
df42 4.533  1.242  0.4942  0.1395  0.0625  0.0382  0.0289  0.0236  0.0231
     0.0249  0.0267  0.0287
fs42  -34
sd42  0.12566   1
c
fc52 Surface tally that is segmented along the apothem
*f52:p  20
c de and df are mass energy transfer or mass energy absorption coefficients
c from Attix they have the same values
fm52 1.602e-10      $ to convert to gray
de52 0.01  0.015  0.02  0.03  0.04  0.05  0.06  0.08  0.1  0.15  0.2  0.3
df52 4.533  1.242  0.4942  0.1395  0.0625  0.0382  0.0289  0.0236  0.0231
     0.0249  0.0267  0.0287
fs52  -35
sd52  0.12566   1
c
fc62 Surface tally that is segmented along the apothem
*f62:p  20
c de and df are mass energy transfer or mass energy absorption coefficients
c from Attix they have the same values
fm62 1.602e-10      $ to convert to gray
de62 0.01  0.015  0.02  0.03  0.04  0.05  0.06  0.08  0.1  0.15  0.2  0.3
df62 4.533  1.242  0.4942  0.1395  0.0625  0.0382  0.0289  0.0236  0.0231
     0.0249  0.0267  0.0287
fs62  -36
sd62  0.12566   1
c
fc72 Surface tally that is segmented along the apothem
*f72:p  20
c de and df are mass energy transfer or mass energy absorption coefficients
c from Attix they have the same values
fm72 1.602e-10      $ to convert to gray
de72 0.01  0.015  0.02  0.03  0.04  0.05  0.06  0.08  0.1  0.15  0.2  0.3
df72 4.533  1.242  0.4942  0.1395  0.0625  0.0382  0.0289  0.0236  0.0231
     0.0249  0.0267  0.0287
fs72  -37
sd72  0.12566   1
c
fc82 Surface tally that is segmented along the apothem
*f82:p  20
c de and df are mass energy transfer or mass energy absorption coefficients
c from Attix they have the same values
fm82 1.602e-10      $ to convert to gray
de82 0.01  0.015  0.02  0.03  0.04  0.05  0.06  0.08  0.1  0.15  0.2  0.3
```

```
df82 4.533  1.242  0.4942  0.1395  0.0625  0.0382  0.0289  0.0236  0.0231
     0.0249  0.0267  0.0287
fs82  -38
sd82  0.12566   1
c
fc92 Surface tally that is segmented along the apothem
*f92:p  20
c de and df are mass energy transfer or mass energy absorption coefficients
c from Attix they have the same values
fm92 1.602e-10      $ to convert to gray
de92 0.01  0.015  0.02  0.03  0.04  0.05  0.06  0.08  0.1  0.15  0.2  0.3
df92 4.533  1.242  0.4942  0.1395  0.0625  0.0382  0.0289  0.0236  0.0231
     0.0249  0.0267  0.0287
fs92  -39
sd92  0.12566   1
c
fc102 Surface tally that is segmented along the apothem
*f102:p  20
c de and df are mass energy transfer or mass energy absorption coefficients
c from Attix they have the same values
fm102 1.602e-10      $ to convert to gray
de102 0.01  0.015  0.02  0.03  0.04  0.05  0.06  0.08  0.1  0.15  0.2  0.3
df102 4.533  1.242  0.4942  0.1395  0.0625  0.0382  0.0289  0.0236  0.0231
     0.0249  0.0267  0.0287
fs102  -40
sd102  0.12566   1
c
fc112 Surface tally that is segmented along the apothem
*f112:p  20
c de and df are mass energy transfer or mass energy absorption coefficients
c from Attix they have the same values
fm112 1.602e-10      $ to convert to gray
de112 0.01  0.015  0.02  0.03  0.04  0.05  0.06  0.08  0.1  0.15  0.2  0.3
df112 4.533  1.242  0.4942  0.1395  0.0625  0.0382  0.0289  0.0236  0.0231
     0.0249  0.0267  0.0287
fs112  -41
sd112  0.12566   1
c
fc122 Surface tally that is segmented along the apothem
*f122:p  20
c de and df are mass energy transfer or mass energy absorption coefficients
c from Attix they have the same values
fm122 1.602e-10      $ to convert to gray
de122 0.01  0.015  0.02  0.03  0.04  0.05  0.06  0.08  0.1  0.15  0.2  0.3
df122 4.533  1.242  0.4942  0.1395  0.0625  0.0382  0.0289  0.0236  0.0231
     0.0249  0.0267  0.0287
fs122  -42
sd122  0.12566   1
c
fc132 Surface tally that is segmented along the apothem
*f132:p  20
c de and df are mass energy transfer or mass energy absorption coefficients
c from Attix they have the same values
```

```
fm132 1.602e-10      $ to convert to gray
de132 0.01  0.015  0.02  0.03  0.04  0.05  0.06  0.08  0.1  0.15  0.2  0.3
df132 4.533  1.242  0.4942  0.1395  0.0625  0.0382  0.0289  0.0236  0.0231
     0.0249  0.0267  0.0287
fs132  -43
sd132  0.12566   1
c
fc142 Surface tally that is segmented along the apothem
*f142:p  20
c de and df are mass energy transfer or mass energy absorption coefficients
c from Attix they have the same values
fm142 1.602e-10      $ to convert to gray
de142 0.01  0.015  0.02  0.03  0.04  0.05  0.06  0.08  0.1  0.15  0.2  0.3
df142 4.533  1.242  0.4942  0.1395  0.0625  0.0382  0.0289  0.0236  0.0231
     0.0249  0.0267  0.0287
fs142  -44
sd142  0.12566   1
c
fc152 Surface tally that is segmented along the apothem
*f152:p  20
c de and df are mass energy transfer or mass energy absorption coefficients
c from Attix they have the same values
fm152 1.602e-10      $ to convert to gray
de152 0.01  0.015  0.02  0.03  0.04  0.05  0.06  0.08  0.1  0.15  0.2  0.3
df152 4.533  1.242  0.4942  0.1395  0.0625  0.0382  0.0289  0.0236  0.0231
     0.0249  0.0267  0.0287
fs152  -45
sd152  0.12566   1
c
fc162 Surface tally that is segmented along the apothem
*f162:p  20
c de and df are mass energy transfer or mass energy absorption coefficients
c from Attix they have the same values
fm162 1.602e-10      $ to convert to gray
de162 0.01  0.015  0.02  0.03  0.04  0.05  0.06  0.08  0.1  0.15  0.2  0.3
df162 4.533  1.242  0.4942  0.1395  0.0625  0.0382  0.0289  0.0236  0.0231
     0.0249  0.0267  0.0287
fs162  -46
sd162  0.12566   1
c
fc172 Surface tally that is segmented along the diagonal
*f172:p  20
c de and df are mass energy transfer or mass energy absorption coefficients
c from Attix they have the same values
fm172 1.602e-10      $ to convert to gray
de172 0.01  0.015  0.02  0.03  0.04  0.05  0.06  0.08  0.1  0.15  0.2  0.3
df172 4.533  1.242  0.4942  0.1395  0.0625  0.0382  0.0289  0.0236  0.0231
     0.0249  0.0267  0.0287
fs172  -50
sd172  0.12566   1
c
fc182 Surface tally that is segmented along the diagonal
*f182:p  20
```

```
c de and df are mass energy transfer or mass energy absorption coefficients
c from Attix they have the same values
fm182 1.602e-10      $ to convert to gray
de182 0.01  0.015  0.02  0.03  0.04  0.05  0.06  0.08  0.1  0.15  0.2  0.3
df182 4.533  1.242  0.4942  0.1395  0.0625  0.0382  0.0289  0.0236  0.0231
     0.0249  0.0267  0.0287
fs182  -51
sd182  0.12566   1
c
fc192 Surface tally that is segmented along the diagonal
*f192:p  20
c de and df are mass energy transfer or mass energy absorption coefficients
c from Attix they have the same values
fm192 1.602e-10      $ to convert to gray
de192 0.01  0.015  0.02  0.03  0.04  0.05  0.06  0.08  0.1  0.15  0.2  0.3
df192 4.533  1.242  0.4942  0.1395  0.0625  0.0382  0.0289  0.0236  0.0231
     0.0249  0.0267  0.0287
fs192  -52
sd192  0.12566   1
c
fc202 Surface tally that is segmented along the diagonal
*f202:p  20
c de and df are mass energy transfer or mass energy absorption coefficients
c from Attix they have the same values
fm202 1.602e-10      $ to convert to gray
de202 0.01  0.015  0.02  0.03  0.04  0.05  0.06  0.08  0.1  0.15  0.2  0.3
df202 4.533  1.242  0.4942  0.1395  0.0625  0.0382  0.0289  0.0236  0.0231
     0.0249  0.0267  0.0287
fs202  -53
sd202  0.12566   1
c
fc212 Surface tally that is segmented along the diagonal
*f212:p  20
c de and df are mass energy transfer or mass energy absorption coefficients
c from Attix they have the same values
fm212 1.602e-10      $ to convert to gray
de212 0.01  0.015  0.02  0.03  0.04  0.05  0.06  0.08  0.1  0.15  0.2  0.3
df212 4.533  1.242  0.4942  0.1395  0.0625  0.0382  0.0289  0.0236  0.0231
     0.0249  0.0267  0.0287
fs212  -54
sd212  0.12566   1
c
 fc222 Surface tally that is segmented along the diagonal
  *f222:p  20
c de and df are mass energy transfer or mass energy absorption coefficients
c from Attix they have the same values
 fm222 1.602e-10      $ to convert to gray
 de222 0.01  0.015  0.02  0.03  0.04  0.05  0.06  0.08  0.1  0.15  0.2  0.3
 df222 4.533  1.242  0.4942  0.1395  0.0625  0.0382  0.0289  0.0236  0.0231
     0.0249  0.0267  0.0287
 fs222  -55
 sd222  0.12566   1
c
```

```
 fc232 Surface tally that is segmented along the diagonal
  *f232:p  20
c de and df are mass energy transfer or mass energy absorption coefficients
c from Attix they have the same values
 fm232 1.602e-10      $ to convert to gray
 de232 0.01  0.015  0.02  0.03  0.04  0.05  0.06  0.08  0.1  0.15  0.2  0.3
 df232 4.533  1.242  0.4942  0.1395  0.0625  0.0382  0.0289  0.0236  0.0231
     0.0249  0.0267  0.0287
 fs232  -56
 sd232  0.12566   1
c
 fc242 Surface tally that is segmented along the diagonal
  *f242:p  20
c de and df are mass energy transfer or mass energy absorption coefficients
c from Attix they have the same values
 fm242 1.602e-10      $ to convert to gray
 de242 0.01  0.015  0.02  0.03  0.04  0.05  0.06  0.08  0.1  0.15  0.2  0.3
 df242 4.533  1.242  0.4942  0.1395  0.0625  0.0382  0.0289  0.0236  0.0231
     0.0249  0.0267  0.0287
 fs242  -57
 sd242  0.12566   1
c
 fc252 Surface tally that is segmented along the diagonal
  *f252:p  20
c mass energy transfer or mass energy absorption coefficients from Attix
c  they have the same values
 fm252 1.602e-10      $ to convert to gray
 de252 0.01  0.015  0.02  0.03  0.04  0.05  0.06  0.08  0.1  0.15  0.2  0.3
 df252 4.533  1.242  0.4942  0.1395  0.0625  0.0382  0.0289  0.0236  0.0231
     0.0249  0.0267  0.0287
 fs252  -58
 sd252  0.12566   1
c
 fc262 Surface tally that is segmented along the diagonal
  *f262:p  20
c de and df are mass energy transfer or mass energy absorption coefficients
c from Attix they have the same values
 fm262 1.602e-10      $ to convert to gray
 de262 0.01  0.015  0.02  0.03  0.04  0.05  0.06  0.08  0.1  0.15  0.2  0.3
 df262 4.533  1.242  0.4942  0.1395  0.0625  0.0382  0.0289  0.0236  0.0231
     0.0249  0.0267  0.0287
 fs262  -59
 sd262  0.12566   1
c
 fc272 Surface tally that is segmented along the diagonal
  *f272:p  20
c de and df are mass energy transfer or mass energy absorption coefficients
c from Attix they have the same values
 fm272 1.602e-10      $ to convert to gray
 de272 0.01  0.015  0.02  0.03  0.04  0.05  0.06  0.08  0.1  0.15  0.2  0.3
 df272 4.533  1.242  0.4942  0.1395  0.0625  0.0382  0.0289  0.0236  0.0231
     0.0249  0.0267  0.0287
 fs272  -60
```

```
 sd272  0.12566   1
c
 fc282 Surface tally that is segmented along the diagonal
  *f282:p  20
c de and df are mass energy transfer or mass energy absorption coefficients
c from Attix they have the same values
 fm282 1.602e-10      $ to convert to gray
 de282 0.01  0.015  0.02  0.03  0.04  0.05  0.06  0.08  0.1  0.15  0.2  0.3
 df282 4.533  1.242  0.4942  0.1395  0.0625  0.0382  0.0289  0.0236  0.0231
     0.0249  0.0267  0.0287
 fs282  -61
 sd282  0.12566   1
c
 fc292 Surface tally that is segmented along the diagonal
  *f292:p  20
c de and df are mass energy transfer or mass energy absorption coefficients
c from Attix they have the same values
 fm292 1.602e-10      $ to convert to gray
 de292 0.01  0.015  0.02  0.03  0.04  0.05  0.06  0.08  0.1  0.15  0.2  0.3
 df292 4.533  1.242  0.4942  0.1395  0.0625  0.0382  0.0289  0.0236  0.0231
     0.0249  0.0267  0.0287
 fs292  -62
 sd292  0.12566   1
c
 fc302 Surface tally that is segmented along the diagonal
  *f302:p  20
c de and df are mass energy transfer or mass energy absorption coefficients
c from Attix they have the same values
 fm302 1.602e-10      $ to convert to gray
 de302 0.01  0.015  0.02  0.03  0.04  0.05  0.06  0.08  0.1  0.15  0.2  0.3
 df302 4.533  1.242  0.4942  0.1395  0.0625  0.0382  0.0289  0.0236  0.0231
     0.0249  0.0267  0.0287
 fs302  -63
 sd302  0.12566   1
c
 fc312 Surface tally that is segmented along the diagonal
  *f312:p  20
c de and df are mass energy transfer or mass energy absorption coefficients
c from Attix they have the same values
 fm312 1.602e-10      $ to convert to gray
 de312 0.01  0.015  0.02  0.03  0.04  0.05  0.06  0.08  0.1  0.15  0.2  0.3
 df312 4.533  1.242  0.4942  0.1395  0.0625  0.0382  0.0289  0.0236  0.0231
     0.0249  0.0267  0.0287
 fs312  -64
 sd312  0.12566   1
c
 fc322 Surface tally that is segmented along the diagonal
  *f322:p  20
c de and df are mass energy transfer or mass energy absorption coefficients
c from Attix they have the same values
 fm322 1.602e-10      $ to convert to gray
 de322 0.01  0.015  0.02  0.03  0.04  0.05  0.06  0.08  0.1  0.15  0.2  0.3
 df322 4.533  1.242  0.4942  0.1395  0.0625  0.0382  0.0289  0.0236  0.0231
```

```
     0.0249  0.0267  0.0287
 fs322  -65
 sd322  0.12566   1
c
c Beginning of Material Data Cards
c
c PMMA
c rho = 1.19 g/cc
m1    001001 -0.0805259   001002 -0.0000120807   $ naturally occurring H
      008016 -0.318853    008017 -0.000121453   008018 -0.000639228 $nat.O
      006012 -0.593190    006013 -0.00665831     $ naturally occurring C
c
c Water
c rho = 1.00 g/cc
m2    001001 -0.1118772159   001002 -0.0000167841    $ naturally occurring H
      008016 -0.88599230772  008017 -0.00033748028  008018 -0.001776212 $nat.O
c
c Air
c density = 0.00120484
 m3  007000  -0.790
     008000  -0.210
```

Problem 6, Calibration of Neutron Detectors in a Bunker

Message: outp=p6o.o runtpe=p6r.r mctal=p6m.m

```
Calibration of Neutron Detectors in a Bunker
c 15.24 cm radius sphere to tally flux in approximating
c 12" rem ball
c
c Beginning of Cell Cards
c
c Source
  1   5   -15.100   -50 22 -23
c
c Shadow Cone
c  iron section
  5   3   -7.87   -60 3 -4
c  polyethylene section
  6   4   -0.94   -60 4 -5
c
c Air inside room
 10   2   -0.00120484   (60 3 -5 21 -24 31 -32):
                         (5 -6 21 -24 31 -32 75 76 ):
                         (2 -3 21 -22 31 -32):
                         (2 -3 23 -24 31 -32):
                         (2 -3 50 22 -23 31 -32)
c
c Bunker Wall
 20   1   -2.3   (1 -2 20 -25 30 -33):(6 -7 20 -25 30 -33):
                 (1 -7 20 -21 30 -33):(1 -7 24 -25 30 -33):
                 (1 -7 20 -25 30 -31):(1 -7 20 -25 32 -33)
c
c Tally Cells
c  50   2   -0.00120484   -75
c  51   2   -0.00120484   -76
c
c Outside world
 99   0          -1:7:-20:25:-30:33
c
c Phoney cells to do surface tallies with
100   2   -0.00120484   -75 -40
101   2   -0.00120484   -75  40
102   2   -0.00120484   -76 -40
103   2   -0.00120484   -76  40
c
c End of Cell Cards

c Beginning of Surface Cards
c
  1   px   -400    $ outside of bunker wall
  2   px   -350    $ inside of bunker wall
  3   px   45      $ front edge of iron
  4   px   65      $ back edge of iron; front edge of polyethylene
  5   px   95      $ back edge of polyethylene
```

```
  6   px   350     $ inside of bunker wall
  7   px   400     $ outside of bunker wall
c
 20   py   -400    $ outside of bunker wall
 21   py   -350    $ inside of bunker wall
 22   py   -0.25   $ bottom of source cylinder
 23   py    0.25   $ top of source cylinder
 24   py   350     $ inside of bunker wall
 25   py   400     $ outside of bunker wall
c
 30   pz   -375    $ outside of bunker wall
 31   pz   -325    $ inside of bunker wall
 32   pz    325    $ inside of bunker wall
 33   pz    375    $ outside of bunker wall
c
 40   pz    0      $ surface to cosine bin
 41   px  165    $ segment of 40 for position 1
 42   px  175    $ segment of 40 for position 1
 43   px  295    $ segment of 40 for position 2
 44   px  305    $ segment of 40 for position 2
 45   py   -5   $ segment of 40
 46   py    5   $ segment of 40
c
c source geometrically centered at 0,0,0
 50   cy   0.25
c
c tally spheres
 75   sx   170   15.24     $ sphere 170 cm from source
 76   sx   300   15.24     $ sphere 300 cm from source
c
c Shadow Cone
 60   kx   -15.0 2.16263e-2 +1
c
c End of Surface Cards

c Beginning of Data Cards
c
mode n
c
print
c prdmp 2j 1
c
nps 1000000000
c
c Source Definition
c Cylinder source with radius 0.25 cm and height 0.5 cm
sdef  pos=0 0 0 axs=0 1 0 rad=d1 ext=d2 erg=d3 par 1
si1 0.25
sp1 -21 1
si2 0.25
sp2 -21 0
si3   0.000000414 0.0000010 0.000010 0.000050 0.00010 0.00020
     0.00040 0.00070 0.0010 0.0030 0.0060 0.010 0.020 0.040
```

```
      0.060 0.080 0.10 0.15 0.20 0.25 0.30 0.35 0.40 0.45 0.50
      0.55 0.60 0.70 0.80 0.90 1 1.2 1.4 1.6 1.8 2.0 2.3 2.6
      3.0 3.5 4.0 4.5 5.0 6.0 7.0 8.0 9.0 10.0 11.0 12.0 13.0
      14.0 15.0 16.0
sp3   0 0.31e-9 1.11e-8 1.27e-7 2.76e-7 7.82e-7 2.21e-6 4.53e-6
      5.68e-6 5.51e-6 1.28e-4 2.30e-4 7.74e-4 2.17e-3 2.80e-3
      3.29e-3 3.68e-3 1.05e-2 1.21e-2 1.33e-2 1.42e-2 1.49e-2
      1.55e-2 1.60e-2 1.63e-2 1.66e-2 1.68e-2 3.38e-2 3.39e-2
      3.37e-2 3.33e-2 6.46e-2 6.12e-2 5.73e-2 5.31e-2 4.88e-2
      6.55e-2 5.67e-2 6.33e-2 6.21e-2 4.68e-2 3.49e-2 2.58e-2
      3.30e-2 1.74e-2 9.01e-3 4.61e-3 2.33e-3 1.17e-3 5.83e-4
      2.88e-4 1.42e-4 6.94e-5 0
c
c Cell Importances
c
imp:n 1 3r 1 0 1 1 1 1
c imp:p 1 5r 1 0 1
c
c Tallies
c
c Spherical detectors to compare
c cosine bins will not work with this either
c
   fc4  Spherical detector at position 1: 170,0,0
   f4:n   (100 101)
   e4   0.000000414 0.0000010 0.000010 0.000050 0.00010 0.00020
      0.00040 0.00070 0.0010 0.0030 0.0060 0.010 0.020 0.040
      0.060 0.080 0.10 0.15 0.20 0.25 0.30 0.35 0.40 0.45 0.50
      0.55 0.60 0.70 0.80 0.90 1 1.2 1.4 1.6 1.8 2.0 2.3 2.6
      3.0 3.5 4.0 4.5 5.0 6.0 7.0 8.0 9.0 10.0 11.0 12.0 13.0
      14.0 15.0 16.0
c
  fc14  Spherical detector at position2: 300,0,0
  f14:n   (102 103)
  e14   0.000000414 0.0000010 0.000010 0.000050 0.00010 0.00020
      0.00040 0.00070 0.0010 0.0030 0.0060 0.010 0.020 0.040
      0.060 0.080 0.10 0.15 0.20 0.25 0.30 0.35 0.40 0.45 0.50
      0.55 0.60 0.70 0.80 0.90 1 1.2 1.4 1.6 1.8 2.0 2.3 2.6
      3.0 3.5 4.0 4.5 5.0 6.0 7.0 8.0 9.0 10.0 11.0 12.0 13.0
      14.0 15.0 16.0
c
  fc1  Planar surfaces for cosine binning
       position 1: 170,0,0
       position 2: 300,0,0
  f1:n   40
  fs1  -75
  sd1  62.8318 1
  e1   0.000000414 0.0000010 0.000010 0.000050 0.00010 0.00020
      0.00040 0.00070 0.0010 0.0030 0.0060 0.010 0.020 0.040
      0.060 0.080 0.10 0.15 0.20 0.25 0.30 0.35 0.40 0.45 0.50
      0.55 0.60 0.70 0.80 0.90 1 1.2 1.4 1.6 1.8 2.0 2.3 2.6
      3.0 3.5 4.0 4.5 5.0 6.0 7.0 8.0 9.0 10.0 11.0 12.0 13.0
      14.0 15.0 16.0
```

```
 c1   -0.866  -0.5  0  0.5  0.866  1
c
 f11:n   40
 fs11  -76
 sd11  62.8318 1
 e11   0.000000414 0.0000010 0.000010 0.000050 0.00010 0.00020
     0.00040 0.00070 0.0010 0.0030 0.0060 0.010 0.020 0.040
     0.060 0.080 0.10 0.15 0.20 0.25 0.30 0.35 0.40 0.45 0.50
     0.55 0.60 0.70 0.80 0.90 1 1.2 1.4 1.6 1.8 2.0 2.3 2.6
     3.0 3.5 4.0 4.5 5.0 6.0 7.0 8.0 9.0 10.0 11.0 12.0 13.0
     14.0 15.0 16.0
 c11   -0.866  -0.5  0  0.5  0.866  1
c
c Beginning of Material Data Cards
c
c Concrete
c rho = 2.3 g/cc
m1    001001 0.11698245   001002 0.00001755
     008016 0.60796842   008017 0.000231579
     014028 0.25344804   014029 0.01283316   014030 0.0085188
c
c Air
c rho = 0.00120484 g/cc
m2    006012 -0.00012521867138   006013 -0.00000140552862
     007014 -0.762280494675   007015 -0.0028001953254
     008016 -0.23470328576   008017 -0.000089400020638
c
c Iron
c rho = 7.87 g/cc
m3    026054 0.05845   026056 0.91754   026057 0.02119   026058 0.00282
c
c Polyethylene
c rho = 0.94 g/cc
m4    006012 0.9889   006013 0.0111
     001001 1.9997   001002 0.0003
c
c Californium 252
c rho = 15.100
m5    098252 1
```

Problem 7, Pulse Height Distributions of a Germanium Spectrometer in the Energy Range Below 1 MeV

Message: outp=p7.o runtpe=p7.r mctal=p7.m

```
Germanium Detector - 15 keV
c Beginning of Cell Cards
c
c Source - cylinder filled with air
c         use surface 2 on cell 1 with a circular plane source in sdef
   1   1   -0.00120484   -50 1 -2
c
c Be window
   5   4   -1.848        -56 3 -4
c
c Cryostat
  10   3   -2.70   (-51 52 3 -11):(-51 56 3 -4):(-51 10 -11)
c
c Al Holder
  15   3   -2.70   (53 -55 5 -8):(8 -9 -55)
c
c Ge Crystal
c  dead layer
  20   2   -5.323  (-53 54 5 -8):(-53 5 -6):(-53 7 -8)
c  core
  21   2   -5.323  -54 6 -7
c
c Vacuum inside cryostat
  25   0          (-52 9 -10):(-52 55 5 -9):(-52 4 -5)
c
c Air outside cryostat
  30   1   -0.00120484   (11 -100):(-100 51 3 -11):(-100 2 -3):
                    (-100 50 1 -2):(-1 -100)
c
c Outside world
  99   0               100
c
c End of Cell Cards

c Beginning of Surface Cards
c
   1   px   -21     $ arbitrary farthest edge of source disk
   2   px   -20     $ closest edge of source disk
c                Assume this will be a disk surface source
c
   3   px     0     $ top of cryostat; front edge of Be window
   4   px  0.15     $ back edge of Be window; thickness of cryostat
   5   px  0.65     $ front edge of Germanium detector
   6   px  0.66     $ top of dead layer
   7   px  2.14     $ bottom dead layer
   8   px  2.15     $ back edge of Germanium detector
   9   px   2.2     $ bottom of Al holder
  10   px  5.65     $ thickness of cryostat
  11   px   5.8     $ bottom of cryotstat
```

```
c
c  20   py    0      $ to avoid symmetrical problems
c
c Cylinders
  50   cx    0.25     $ source disk
  51   cx    4.15     $ outside radius of cryostat
  52   cx    4        $ inside radius of cryostat
  53   cx    2        $ outer radius of Ge
  54   cx    1.99     $ core of Ge detector
  55   cx    3        $ back part of Al holder
  56   cx    2.6      $ Be window
c
 100   so    35       $ boundary of problem
c
c End of Surface Cards

c Beginning of Data Cards
c
mode p
c
print
c prdmp 2j 1
c
nps 400000000
c
c Source Definition
c surface 2 on cell 1 with a circular plane source
 sdef  pos=-20.5 0 0   sur=2   axs=1 0 0   rad=d1   ext=0   erg=0.015   par 2
 si1 0 0.25
 sp1 -21 1
c
c Cell Importances
c
imp:p 1 6r 1 0
c
c Weight Window Generator
c wwp:p 8 2 5 0 0.25
c wwg 8 21
c
c Tallies
c
 fc8 Energy deposition (MeV) per source photon)
 *f8:p  21
 e8            0.000108
         0.000692
         0.001276
         0.001860
         0.002444
         0.003028
         0.003612
         0.004196
         0.004780
         0.005364
```

```
        0.005948
        0.006532
        0.007116
        0.007700
        0.008284
        0.008868
        0.009452
        0.010036
        0.010620
        0.011204
        0.011788
        0.012372
        0.012956
        0.013540
        0.014124
        0.014708
        0.015292
        0.015876
c
 fc18 Pulses
 f18:p  21
e18       0.000108
        0.000692
        0.001276
        0.001860
        0.002444
        0.003028
        0.003612
        0.004196
        0.004780
        0.005364
        0.005948
        0.006532
        0.007116
        0.007700
        0.008284
        0.008868
        0.009452
        0.010036
        0.010620
        0.011204
        0.011788
        0.012372
        0.012956
        0.013540
        0.014124
        0.014708
        0.015292
        0.015876
c
c Beginning of Material Data Cards
c
c Air
```

```
c rho =       0.00120484 g/cc
m1    006000 -0.000125   007000 -0.755267
      008000 -0.231781   018000 -0.012827
c
c Germanium
c rho = 5.323 g/cc
m2    032000 1
c
c Al
c rho = 2.70 g/cc
m3    013000 1
c
c Be
c rho = 1.848 g/cc
m4    004000 1
```

APPENDIX B

Table A.1. R.F. histogram for 15 keV photon with/without Doppler broadening feature.

Energy (MeV)	P.H.D. in Energy Bin δE Without Doppler Broadening	Precision (one standard deviation) Without Doppler Broadening	P.H.D. in Energy Bin δE With Doppler Broadening	Precision (one standard deviation) With Doppler Broadening
1.000E-03	- - - - -	- - - - -	- - - - -	- - - - -
1.276E-03	1.88E-11	1.1E-11	2.01E-11	7.7E-12
1.860E-03	0.00E+00	0.0E+00	6.89E-12	4.9E-12
2.444E-03	0.00E+00	0.0E+00	0.00E+00	0.0E+00
3.028E-03	0.00E+00	0.0E+00	6.45E-12	6.5E-12
3.612E-03	0.00E+00	0.0E+00	7.67E-12	7.7E-12
4.196E-03	3.15E-09	2.7E-10	3.62E-09	1.9E-10
4.780E-03	0.00E+00	0.0E+00	5.81E-11	2.6E-11
5.364E-03	3.10E-08	9.6E-10	3.18E-08	6.4E-10
5.948E-03	0.00E+00	0.0E+00	7.00E-11	3.1E-11
6.532E-03	3.51E-11	3.5E-11	3.15E-11	2.2E-11
7.116E-03	0.00E+00	0.0E+00	0.00E+00	0.0E+00
7.700E-03	4.16E-11	4.2E-11	3.64E-11	2.6E-11
8.284E-03	9.24E-11	6.5E-11	5.97E-11	3.4E-11
8.868E-03	5.02E-11	5.0E-11	1.08E-10	4.8E-11
9.452E-03	1.63E-10	9.4E-11	1.09E-09	1.6E-10
1.004E-02	1.19E-06	8.2E-09	1.19E-06	5.5E-09
1.062E-02	1.34E-09	2.9E-10	1.04E-09	1.6E-10
1.120E-02	2.76E-07	4.2E-09	2.78E-07	2.8E-09
1.179E-02	0.00E+00	0.0E+00	2.88E-11	2.9E-11
1.237E-02	0.00E+00	0.0E+00	0.00E+00	0.0E+00
1.296E-02	0.00E+00	0.0E+00	0.00E+00	0.0E+00
1.354E-02	0.00E+00	0.0E+00	0.00E+00	0.0E+00
1.412E-02	0.00E+00	0.0E+00	3.43E-11	3.4E-11
1.471E-02	1.68E-10	1.2E-10	2.54E-10	9.6E-11
1.529E-02	8.67E-07	8.7E-09	8.67E-07	5.7E-09
1.588E-02	0.00E+00	0.0E+00	0.00E+00	0.0E+00

Table A.2. R.F. histogram for 30 keV photon with/without Doppler broadening feature.

Energy (MeV)	P.H.D. in Energy Bin δE Without Doppler Broadening	Precision (one standard deviation) Without Doppler Broadening	P.H.D. in Energy Bin δE With Doppler Broadening	Precision (one standard deviation) With Doppler Broadening
1.000E-03	- - - - -	- - - - -	- - - - -	- - - - -
1.270E-03	7.35E-11	6.2E-12	2.48E-10	1.3E-11
1.946E-03	4.28E-10	2.0E-11	1.29E-09	3.7E-11
2.622E-03	4.37E-09	7.2E-11	3.51E-09	7.1E-11
3.298E-03	9.80E-09	1.2E-10	4.78E-09	9.4E-11
3.974E-03	5.69E-11	1.0E-11	2.73E-09	7.8E-11
4.650E-03	9.74E-11	1.5E-11	1.22E-09	5.7E-11
5.326E-03	1.24E-10	1.7E-11	7.06E-10	4.7E-11
6.002E-03	1.55E-10	2.1E-11	4.62E-10	4.0E-11
6.678E-03	1.99E-10	2.5E-11	3.38E-10	3.6E-11
7.354E-03	2.49E-10	3.0E-11	3.85E-10	4.1E-11
8.030E-03	3.78E-10	3.8E-11	4.44E-10	4.6E-11
8.706E-03	5.32E-10	4.7E-11	6.19E-10	5.7E-11
9.382E-03	5.94E-10	5.2E-11	9.79E-10	7.5E-11
1.006E-02	1.67E-06	2.8E-09	1.67E-06	3.2E-09
1.073E-02	1.40E-09	8.6E-11	1.32E-09	9.3E-11
1.141E-02	3.14E-07	1.3E-09	3.13E-07	1.5E-09
1.209E-02	8.18E-10	7.0E-11	9.60E-10	8.4E-11
1.276E-02	1.88E-09	1.1E-10	1.27E-09	9.9E-11
1.344E-02	1.47E-09	9.8E-11	1.14E-09	9.7E-11
1.411E-02	6.07E-10	6.5E-11	7.05E-10	7.8E-11
1.479E-02	3.32E-10	4.9E-11	7.04E-10	8.0E-11
1.547E-02	4.85E-10	6.1E-11	8.06E-10	8.7E-11
1.614E-02	8.96E-10	8.4E-11	1.31E-09	1.1E-10
1.682E-02	1.36E-09	1.1E-10	2.23E-09	1.5E-10
1.749E-02	4.57E-09	2.0E-10	4.23E-09	2.1E-10
1.817E-02	7.00E-09	2.5E-10	6.99E-09	2.8E-10

Table A.2. Continued.

Energy (MeV)	P.H.D. in Energy Bin δE Without Doppler Broadening	Precision (one standard deviation) Without Doppler Broadening	P.H.D. in Energy Bin δE With Doppler Broadening	Precision (one standard deviation) With Doppler Broadening
1.885E-02	1.13E-08	3.2E-10	1.34E-08	3.9E-10
1.952E-02	3.83E-07	1.9E-09	3.79E-07	2.1E-09
2.020E-02	2.34E-06	4.9E-09	2.34E-06	5.4E-09
2.087E-02	2.60E-09	1.6E-10	2.86E-09	1.9E-10
2.155E-02	6.27E-10	8.2E-11	8.50E-10	1.1E-10
2.223E-02	5.48E-10	7.8E-11	6.85E-10	9.7E-11
2.290E-02	4.06E-10	6.8E-11	9.02E-10	1.1E-10
2.358E-02	5.82E-10	8.2E-11	1.69E-09	1.6E-10
2.425E-02	9.70E-10	1.1E-10	3.26E-09	2.2E-10
2.493E-02	4.98E-09	2.5E-10	6.93E-09	3.3E-10
2.561E-02	8.62E-09	3.3E-10	1.40E-08	4.7E-10
2.628E-02	1.58E-08	4.5E-10	2.41E-08	6.3E-10
2.696E-02	2.84E-08	6.2E-10	5.47E-08	9.6E-10
2.763E-02	1.50E-07	1.4E-09	1.19E-07	1.4E-09
2.831E-02	1.69E-07	1.5E-09	1.92E-07	1.8E-09
2.899E-02	3.47E-07	2.2E-09	3.58E-07	2.5E-09
2.966E-02	9.56E-07	3.7E-09	8.92E-07	4.0E-09
3.034E-02	1.19E-04	4.8E-08	1.19E-04	4.8E-08
3.101E-02	0.000E+00	0.0E+00	0.000E+00	0.0E+00
3.169E-02	0.000E+00	0.0E+00	0.000E+00	0.0E+00

Table A.3. R.F. histogram for 60 keV photon with/without Doppler broadening feature.

Energy (MeV)	P.H.D. in Energy Bin δE Without Doppler Broadening	Precision (one standard deviation) Without Doppler Broadening	P.H.D. in Energy Bin δE With Doppler Broadening	Precision (one standard deviation) With Doppler Broadening
1.000E-03	- - - - -	- - - - -	- - - - -	- - - - -
1.420E-03	9.86E-10	5.2E-11	1.04E-09	5.3E-11
2.228E-03	2.23E-09	1.0E-10	2.94E-09	1.2E-10
3.036E-03	3.08E-09	1.4E-10	4.43E-09	1.7E-10
3.844E-03	4.49E-09	2.0E-10	6.11E-09	2.3E-10
4.652E-03	5.50E-09	2.4E-10	8.40E-09	3.0E-10
5.460E-03	6.24E-09	2.8E-10	1.19E-08	3.9E-10
6.268E-03	8.28E-09	3.5E-10	1.72E-08	5.0E-10
7.076E-03	1.91E-08	5.7E-10	2.68E-08	6.7E-10
7.884E-03	3.98E-08	8.6E-10	4.20E-08	8.9E-10
8.692E-03	6.42E-08	1.2E-09	6.02E-08	1.1E-09
9.500E-03	9.66E-08	1.5E-09	7.95E-08	1.3E-09
1.031E-02	5.75E-07	3.8E-09	5.36E-07	3.6E-09
1.112E-02	2.77E-07	2.7E-09	1.78E-07	2.2E-09
1.192E-02	8.63E-08	1.6E-09	7.46E-08	1.5E-09
1.273E-02	3.23E-09	3.2E-10	4.42E-08	1.2E-09
1.354E-02	2.62E-09	2.9E-10	2.76E-08	9.5E-10
1.435E-02	2.23E-09	2.8E-10	1.87E-08	8.1E-10
1.516E-02	1.58E-09	2.4E-10	1.28E-08	6.9E-10
1.596E-02	1.78E-09	2.6E-10	1.01E-08	6.3E-10
1.677E-02	1.72E-09	2.7E-10	9.20E-09	6.1E-10
1.758E-02	2.59E-09	3.3E-10	6.61E-09	5.3E-10
1.839E-02	3.10E-09	3.7E-10	8.18E-09	6.1E-10
1.920E-02	3.57E-09	4.1E-10	6.11E-09	5.4E-10
2.000E-02	3.92E-09	4.4E-10	5.29E-09	5.1E-10
2.081E-02	4.49E-09	4.8E-10	6.13E-09	5.6E-10
2.162E-02	3.90E-09	4.5E-10	5.51E-09	5.4E-10

Table A.3. Continued.

Energy (MeV)	P.H.D. in Energy Bin δE Without Doppler Broadening	Precision (one standard deviation) Without Doppler Broadening	P.H.D. in Energy Bin δE With Doppler Broadening	Precision (one standard deviation) With Doppler Broadening
2.243E-02	1.15E-09	2.5E-10	3.19E-09	4.2E-10
2.324E-02	6.88E-10	2.0E-10	2.86E-09	4.0E-10
2.404E-02	7.67E-10	2.1E-10	2.66E-09	4.0E-10
2.485E-02	9.80E-10	2.5E-10	2.02E-09	3.5E-10
2.566E-02	4.40E-10	1.7E-10	1.19E-09	2.7E-10
2.647E-02	9.79E-10	2.5E-10	1.64E-09	3.3E-10
2.728E-02	1.07E-09	2.7E-10	2.08E-09	3.7E-10
2.808E-02	1.04E-09	2.7E-10	1.59E-09	3.3E-10
2.889E-02	1.28E-09	3.0E-10	1.85E-09	3.6E-10
2.970E-02	1.10E-09	2.8E-10	1.54E-09	3.4E-10
3.051E-02	1.73E-09	3.6E-10	2.49E-09	4.3E-10
3.132E-02	1.70E-09	3.6E-10	2.55E-09	4.4E-10
3.212E-02	2.30E-09	4.3E-10	3.34E-09	5.1E-10
3.293E-02	3.82E-09	5.6E-10	5.04E-09	6.4E-10
3.374E-02	6.59E-09	7.4E-10	6.33E-09	7.3E-10
3.455E-02	5.47E-09	6.8E-10	9.40E-09	9.0E-10
3.536E-02	7.34E-09	8.0E-10	1.15E-08	1.0E-09
3.616E-02	9.13E-09	9.0E-10	1.63E-08	1.2E-09
3.697E-02	1.38E-08	1.1E-09	2.01E-08	1.4E-09
3.778E-02	1.88E-08	1.3E-09	3.04E-08	1.7E-09
3.859E-02	2.82E-08	1.6E-09	4.29E-08	2.0E-09
3.940E-02	4.97E-08	2.2E-09	5.49E-08	2.3E-09
4.020E-02	6.05E-08	2.5E-09	7.15E-08	2.7E-09
4.101E-02	6.75E-08	2.6E-09	9.40E-08	3.1E-09
4.182E-02	9.45E-08	3.1E-09	1.24E-07	3.6E-09
4.263E-02	1.50E-07	4.0E-09	1.63E-07	4.2E-09
4.344E-02	1.99E-07	4.6E-09	2.08E-07	4.7E-09
4.424E-02	2.53E-07	5.3E-09	2.63E-07	5.4E-09

Table A.3. Continued.

Energy (MeV)	P.H.D. in Energy Bin δE Without Doppler Broadening	Precision (one standard deviation) Without Doppler Broadening	P.H.D. in Energy Bin δE With Doppler Broadening	Precision (one standard deviation) With Doppler Broadening
4.505E-02	2.79E-07	5.6E-09	3.20E-07	6.0E-09
4.586E-02	3.40E-07	6.2E-09	3.87E-07	6.6E-09
4.667E-02	3.83E-07	6.7E-09	4.79E-07	7.4E-09
4.748E-02	4.06E-07	6.9E-09	5.80E-07	8.2E-09
4.828E-02	4.62E-07	7.4E-09	7.61E-07	9.5E-09
4.909E-02	1.35E-06	1.3E-08	1.47E-06	1.3E-08
4.990E-02	2.29E-06	1.7E-08	1.63E-06	1.4E-08
5.071E-02	4.20E-06	2.3E-08	3.72E-06	2.2E-08
5.152E-02	2.18E-06	1.7E-08	1.96E-06	1.6E-08
5.232E-02	2.07E-06	1.6E-08	2.03E-06	1.6E-08
5.313E-02	2.11E-06	1.7E-08	2.09E-06	1.6E-08
5.394E-02	2.24E-06	1.7E-08	2.23E-06	1.7E-08
5.475E-02	2.61E-06	1.9E-08	2.49E-06	1.8E-08
5.556E-02	2.87E-06	2.0E-08	2.78E-06	1.9E-08
5.636E-02	3.07E-06	2.1E-08	3.00E-06	2.0E-08
5.717E-02	3.12E-06	2.1E-08	3.17E-06	2.1E-08
5.798E-02	3.09E-06	2.1E-08	3.30E-06	2.2E-08
5.879E-02	2.91E-06	2.1E-08	2.99E-06	2.1E-08
5.960E-02	2.58E-06	2.0E-08	2.65E-06	2.0E-08
6.040E-02	4.47E-04	2.7E-07	4.47E-04	2.7E-07
6.121E-02	0.00E+00	0.0E+00	0.00E+00	0.0E+00
6.202E-02	0.00E+00	0.0E+00	0.00E+00	0.0E+00
6.283E-02	0.00E+00	0.0E+00	0.00E+00	0.0E+00
6.364E-02	0.00E+00	0.0E+00	0.00E+00	0.0E+00

Table A.4. R.F. histogram for 100 keV photon without Doppler broadening feature.

Energy (MeV)	P.H.D. in energy bin δE	Precision (one standard deviation)
1.000E-03	- - - - -	- - - - -
1.914E-03	1.27E-08	2.2E-10
2.853E-03	2.30E-08	3.7E-10
3.791E-03	2.96E-08	5.0E-10
4.730E-03	3.82E-08	6.4E-10
5.669E-03	4.54E-08	7.7E-10
6.607E-03	5.17E-08	8.9E-10
7.546E-03	5.80E-08	1.0E-09
8.485E-03	6.21E-08	1.1E-09
9.423E-03	6.73E-08	1.2E-09
1.036E-02	2.13E-07	2.3E-09
1.130E-02	1.02E-07	1.7E-09
1.224E-02	7.90E-08	1.5E-09
1.318E-02	8.40E-08	1.6E-09
1.412E-02	8.61E-08	1.7E-09
1.506E-02	9.46E-08	1.9E-09
1.599E-02	1.02E-07	2.0E-09
1.693E-02	1.15E-07	2.2E-09
1.787E-02	1.44E-07	2.5E-09
1.881E-02	1.78E-07	2.9E-09
1.975E-02	2.18E-07	3.3E-09
2.069E-02	2.58E-07	3.6E-09
2.163E-02	3.16E-07	4.1E-09
2.256E-02	3.67E-07	4.5E-09
2.350E-02	4.31E-07	5.0E-09
2.444E-02	5.07E-07	5.5E-09
2.538E-02	5.96E-07	6.1E-09
2.632E-02	6.89E-07	6.7E-09
2.726E-02	8.12E-07	7.4E-09

Table A.4. Continued.

Energy (MeV)	P.H.D. in energy bin δE	Precision (one standard deviation)
2.820E-02	8.73E-07	7.8E-09
2.913E-02	5.17E-08	1.9E-09
3.007E-02	4.35E-08	1.8E-09
3.101E-02	4.15E-08	1.8E-09
3.195E-02	3.79E-08	1.7E-09
3.289E-02	3.39E-08	1.7E-09
3.383E-02	2.83E-08	1.5E-09
3.477E-02	2.57E-08	1.5E-09
3.571E-02	2.06E-08	1.3E-09
3.664E-02	2.02E-08	1.4E-09
3.758E-02	1.70E-08	1.3E-09
3.852E-02	1.22E-08	1.1E-09
3.946E-02	8.57E-09	9.1E-10
4.040E-02	7.58E-09	8.7E-10
4.134E-02	8.07E-09	9.1E-10
4.228E-02	6.26E-09	8.1E-10
4.321E-02	7.58E-09	9.0E-10
4.415E-02	9.18E-09	1.0E-09
4.509E-02	1.04E-08	1.1E-09
4.603E-02	1.22E-08	1.2E-09
4.697E-02	1.33E-08	1.2E-09
4.791E-02	2.04E-08	1.6E-09
4.885E-02	2.52E-08	1.7E-09
4.978E-02	3.65E-08	2.1E-09
5.072E-02	4.05E-08	2.3E-09
5.166E-02	4.99E-08	2.5E-09
5.260E-02	6.46E-08	2.9E-09
5.354E-02	6.68E-08	3.0E-09
5.448E-02	7.63E-08	3.2E-09
5.542E-02	7.97E-08	3.3E-09

Table A.4. Continued.

Energy (MeV)	P.H.D. in energy bin δE	Precision (one standard deviation)
5.636E-02	9.24E-08	3.6E-09
5.729E-02	1.22E-07	4.2E-09
5.823E-02	1.72E-07	5.0E-09
5.917E-02	2.18E-07	5.7E-09
6.011E-02	2.75E-07	6.4E-09
6.105E-02	3.10E-07	6.9E-09
6.199E-02	3.58E-07	7.4E-09
6.293E-02	3.82E-07	7.7E-09
6.386E-02	4.08E-07	8.0E-09
6.480E-02	4.36E-07	8.4E-09
6.574E-02	4.83E-07	8.9E-09
6.668E-02	5.10E-07	9.2E-09
6.762E-02	5.30E-07	9.4E-09
6.856E-02	5.73E-07	9.8E-09
6.950E-02	5.76E-07	1.0E-08
7.043E-02	6.03E-07	1.0E-08
7.137E-02	6.46E-07	1.1E-08
7.231E-02	9.64E-07	1.3E-08
7.325E-02	2.11E-06	2.0E-08
7.419E-02	2.64E-06	2.2E-08
7.513E-02	2.75E-06	2.3E-08
7.607E-02	2.64E-06	2.2E-08
7.700E-02	2.56E-06	2.2E-08
7.794E-02	2.49E-06	2.2E-08
7.888E-02	2.44E-06	2.2E-08
7.982E-02	2.39E-06	2.2E-08
8.076E-02	2.36E-06	2.2E-08
8.170E-02	2.42E-06	2.2E-08
8.264E-02	2.45E-06	2.3E-08
8.358E-02	2.51E-06	2.3E-08

Table A.4. Continued.

Energy (MeV)	P.H.D. in energy bin δE	Precision (one standard deviation)
8.451E-02	2.66E-06	2.4E-08
8.545E-02	2.76E-06	2.4E-08
8.639E-02	2.82E-06	2.5E-08
8.733E-02	2.82E-06	2.5E-08
8.827E-02	2.83E-06	2.5E-08
8.921E-02	3.02E-06	2.6E-08
9.015E-02	3.95E-06	3.0E-08
9.108E-02	2.79E-06	2.5E-08
9.202E-02	2.76E-06	2.5E-08
9.296E-02	2.65E-06	2.5E-08
9.390E-02	2.56E-06	2.4E-08
9.484E-02	2.50E-06	2.4E-08
9.578E-02	2.35E-06	2.4E-08
9.672E-02	2.25E-06	2.3E-08
9.765E-02	2.07E-06	2.2E-08
9.859E-02	1.96E-06	2.2E-08
9.953E-02	1.75E-06	2.1E-08
1.005E-01	7.42E-04	4.5E-07
1.014E-01	0.00E+00	0.0E+00
1.024E-01	0.00E+00	0.0E+00
1.033E-01	0.00E+00	0.0E+00
1.042E-01	0.00E+00	0.0E+00
1.052E-01	0.00E+00	0.0E+00

Table A.5. R.F. histogram for 0.25 MeV photon without Doppler broadening feature.

Energy (MeV)	P.H.D. in energy bin δE	Precision (one standard deviation)
1.000E-03	- - - - -	- - - - -
1.040E-03	1.04E-08	1.0E-10
2.320E-03	4.98E-08	3.5E-10
3.600E-03	9.33E-08	6.2E-10
4.880E-03	1.37E-07	8.9E-10
6.160E-03	1.83E-07	1.2E-09
7.440E-03	2.23E-07	1.4E-09
8.720E-03	2.65E-07	1.7E-09
1.000E-02	3.26E-07	2.1E-09
1.128E-02	3.47E-07	2.3E-09
1.256E-02	3.89E-07	2.5E-09
1.384E-02	4.22E-07	2.7E-09
1.512E-02	4.58E-07	3.0E-09
1.640E-02	4.90E-07	3.2E-09
1.768E-02	5.35E-07	3.5E-09
1.896E-02	5.67E-07	3.7E-09
2.024E-02	5.96E-07	4.0E-09
2.152E-02	6.33E-07	4.2E-09
2.280E-02	6.64E-07	4.5E-09
2.408E-02	6.98E-07	4.7E-09
2.536E-02	7.27E-07	4.9E-09
2.664E-02	7.55E-07	5.2E-09
2.792E-02	7.87E-07	5.4E-09
2.920E-02	8.02E-07	5.6E-09
3.048E-02	8.38E-07	5.9E-09
3.176E-02	8.54E-07	6.0E-09
3.304E-02	8.80E-07	6.2E-09
3.432E-02	9.22E-07	6.5E-09
3.560E-02	9.32E-07	6.6E-09

Table A.5. Continued.

Energy (MeV)	P.H.D. in energy bin δE	Precision (one standard deviation)
3.688E-02	9.59E-07	6.9E-09
3.816E-02	9.90E-07	7.1E-09
3.944E-02	1.00E-06	7.3E-09
4.072E-02	1.02E-06	7.5E-09
4.200E-02	1.05E-06	7.6E-09
4.328E-02	1.06E-06	7.9E-09
4.456E-02	1.07E-06	8.0E-09
4.584E-02	1.08E-06	8.2E-09
4.712E-02	1.11E-06	8.4E-09
4.840E-02	1.12E-06	8.5E-09
4.968E-02	1.13E-06	8.7E-09
5.096E-02	1.14E-06	8.9E-09
5.224E-02	1.15E-06	9.0E-09
5.352E-02	1.16E-06	9.2E-09
5.480E-02	1.16E-06	9.3E-09
5.608E-02	1.16E-06	9.4E-09
5.736E-02	1.17E-06	9.5E-09
5.864E-02	1.18E-06	9.7E-09
5.992E-02	1.19E-06	9.8E-09
6.120E-02	1.19E-06	9.9E-09
6.248E-02	1.23E-06	1.0E-08
6.376E-02	1.20E-06	1.0E-08
6.504E-02	1.22E-06	1.0E-08
6.632E-02	1.23E-06	1.0E-08
6.760E-02	1.26E-06	1.1E-08
6.888E-02	1.26E-06	1.1E-08
7.016E-02	1.27E-06	1.1E-08
7.144E-02	1.27E-06	1.1E-08
7.272E-02	1.29E-06	1.1E-08
7.400E-02	1.29E-06	1.1E-08

Table A.5. Continued.

Energy (MeV)	P.H.D. in energy bin δE	Precision (one standard deviation)
7.528E-02	1.31E-06	1.2E-08
7.656E-02	1.32E-06	1.2E-08
7.784E-02	1.33E-06	1.2E-08
7.912E-02	1.33E-06	1.2E-08
8.040E-02	1.38E-06	1.2E-08
8.168E-02	1.39E-06	1.2E-08
8.296E-02	1.39E-06	1.3E-08
8.424E-02	1.43E-06	1.3E-08
8.552E-02	1.47E-06	1.3E-08
8.680E-02	1.53E-06	1.3E-08
8.808E-02	1.58E-06	1.4E-08
8.936E-02	1.68E-06	1.4E-08
9.064E-02	1.74E-06	1.5E-08
9.192E-02	1.82E-06	1.5E-08
9.320E-02	1.94E-06	1.6E-08
9.448E-02	1.99E-06	1.6E-08
9.576E-02	2.10E-06	1.7E-08
9.704E-02	2.21E-06	1.7E-08
9.832E-02	2.26E-06	1.7E-08
9.960E-02	2.35E-06	1.8E-08
1.009E-01	2.46E-06	1.8E-08
1.022E-01	2.57E-06	1.9E-08
1.034E-01	2.66E-06	1.9E-08
1.047E-01	2.78E-06	2.0E-08
1.060E-01	2.94E-06	2.1E-08
1.073E-01	3.05E-06	2.1E-08
1.086E-01	3.21E-06	2.2E-08
1.098E-01	3.33E-06	2.2E-08
1.111E-01	3.47E-06	2.3E-08
1.124E-01	3.62E-06	2.4E-08

Table A.5. Continued.

Energy (MeV)	P.H.D. in energy bin δE	Precision (one standard deviation)
1.137E-01	3.74E-06	2.4E-08
1.150E-01	3.96E-06	2.5E-08
1.162E-01	4.10E-06	2.5E-08
1.175E-01	4.26E-06	2.6E-08
1.188E-01	4.48E-06	2.7E-08
1.201E-01	4.67E-06	2.8E-08
1.214E-01	4.93E-06	2.9E-08
1.226E-01	5.14E-06	2.9E-08
1.239E-01	4.51E-06	2.7E-08
1.252E-01	1.46E-06	1.6E-08
1.265E-01	1.49E-06	1.6E-08
1.278E-01	1.95E-06	1.8E-08
1.290E-01	2.07E-06	1.9E-08
1.303E-01	2.14E-06	1.9E-08
1.316E-01	2.18E-06	2.0E-08
1.329E-01	2.16E-06	2.0E-08
1.342E-01	2.13E-06	2.0E-08
1.354E-01	2.10E-06	2.0E-08
1.367E-01	2.04E-06	1.9E-08
1.380E-01	1.98E-06	1.9E-08
1.393E-01	1.94E-06	1.9E-08
1.406E-01	1.88E-06	1.9E-08
1.418E-01	1.84E-06	1.9E-08
1.431E-01	1.79E-06	1.9E-08
1.444E-01	1.80E-06	1.9E-08
1.457E-01	1.73E-06	1.8E-08
1.470E-01	1.72E-06	1.9E-08
1.482E-01	1.64E-06	1.8E-08
1.495E-01	1.63E-06	1.8E-08
1.508E-01	1.61E-06	1.8E-08

Table A.5. Continued.

Energy (MeV)	P.H.D. in energy bin δE	Precision (one standard deviation)
1.521E-01	1.57E-06	1.8E-08
1.534E-01	1.58E-06	1.8E-08
1.546E-01	1.51E-06	1.8E-08
1.559E-01	1.49E-06	1.8E-08
1.572E-01	1.45E-06	1.8E-08
1.585E-01	1.47E-06	1.8E-08
1.598E-01	1.44E-06	1.8E-08
1.610E-01	1.44E-06	1.8E-08
1.623E-01	1.42E-06	1.8E-08
1.636E-01	1.39E-06	1.8E-08
1.649E-01	1.38E-06	1.8E-08
1.662E-01	1.32E-06	1.7E-08
1.674E-01	1.31E-06	1.7E-08
1.687E-01	1.33E-06	1.7E-08
1.700E-01	1.32E-06	1.7E-08
1.713E-01	1.29E-06	1.7E-08
1.726E-01	1.30E-06	1.7E-08
1.738E-01	1.29E-06	1.7E-08
1.751E-01	1.26E-06	1.7E-08
1.764E-01	1.25E-06	1.7E-08
1.777E-01	1.23E-06	1.7E-08
1.790E-01	1.21E-06	1.7E-08
1.802E-01	1.18E-06	1.7E-08
1.815E-01	1.20E-06	1.7E-08
1.828E-01	1.17E-06	1.7E-08
1.841E-01	1.16E-06	1.7E-08
1.854E-01	1.15E-06	1.7E-08
1.866E-01	1.14E-06	1.7E-08
1.879E-01	1.07E-06	1.7E-08
1.892E-01	1.09E-06	1.7E-08

Table A.5. Continued.

Energy (MeV)	P.H.D. in energy bin δE	Precision (one standard deviation)
1.905E-01	1.06E-06	1.7E-08
1.918E-01	1.06E-06	1.7E-08
1.930E-01	1.02E-06	1.6E-08
1.943E-01	1.03E-06	1.6E-08
1.956E-01	9.57E-07	1.6E-08
1.969E-01	9.89E-07	1.6E-08
1.982E-01	9.41E-07	1.6E-08
1.994E-01	9.69E-07	1.6E-08
2.007E-01	9.43E-07	1.6E-08
2.020E-01	9.41E-07	1.6E-08
2.033E-01	9.02E-07	1.6E-08
2.046E-01	8.80E-07	1.6E-08
2.058E-01	8.81E-07	1.6E-08
2.071E-01	8.80E-07	1.6E-08
2.084E-01	8.49E-07	1.6E-08
2.097E-01	8.27E-07	1.5E-08
2.110E-01	7.92E-07	1.5E-08
2.122E-01	7.60E-07	1.5E-08
2.135E-01	7.52E-07	1.5E-08
2.148E-01	7.31E-07	1.5E-08
2.161E-01	6.94E-07	1.4E-08
2.174E-01	6.62E-07	1.4E-08
2.186E-01	6.56E-07	1.4E-08
2.199E-01	6.42E-07	1.4E-08
2.212E-01	6.10E-07	1.4E-08
2.225E-01	5.89E-07	1.3E-08
2.238E-01	5.89E-07	1.3E-08
2.250E-01	5.53E-07	1.3E-08
2.263E-01	5.73E-07	1.3E-08
2.276E-01	5.44E-07	1.3E-08

Table A.5. Continued.

Energy (MeV)	P.H.D. in energy bin δE	Precision (one standard deviation)
2.289E-01	5.35E-07	1.3E-08
2.302E-01	5.08E-07	1.3E-08
2.314E-01	4.75E-07	1.2E-08
2.327E-01	4.50E-07	1.2E-08
2.340E-01	4.49E-07	1.2E-08
2.353E-01	4.35E-07	1.2E-08
2.366E-01	4.22E-07	1.2E-08
2.378E-01	4.20E-07	1.2E-08
2.391E-01	4.92E-07	1.3E-08
2.404E-01	9.40E-07	1.7E-08
2.417E-01	3.91E-07	1.1E-08
2.430E-01	3.94E-07	1.1E-08
2.442E-01	3.90E-07	1.1E-08
2.455E-01	3.65E-07	1.1E-08
2.468E-01	3.32E-07	1.1E-08
2.481E-01	3.26E-07	1.0E-08
2.494E-01	3.09E-07	1.0E-08
2.506E-01	6.30E-04	4.4E-07
2.519E-01	0.00E+00	0.0E+00
2.532E-01	0.00E+00	0.0E+00
2.545E-01	0.00E+00	0.0E+00
2.557E-01	0.00E+00	0.0E+00
2.570E-01	0.00E+00	0.0E+00
2.583E-01	0.00E+00	0.0E+00
2.596E-01	0.00E+00	0.0E+00
2.609E-01	0.00E+00	0.0E+00
2.621E-01	0.00E+00	0.0E+00

Table A.6. R.F. histogram for 0.5 MeV photon without Doppler broadening feature.

Energy (MeV)	P.H.D. in energy bin δE	Precision (one standard deviation)
1.000E-03	- - - - -	- - - - -
1.170E-03	5.13E-09	1.2E-10
2.830E-03	2.97E-08	4.6E-10
4.490E-03	5.81E-08	8.5E-10
6.150E-03	8.86E-08	1.3E-09
7.810E-03	1.19E-07	1.7E-09
9.470E-03	1.49E-07	2.1E-09
1.113E-02	1.81E-07	2.5E-09
1.279E-02	2.08E-07	2.9E-09
1.445E-02	2.34E-07	3.3E-09
1.611E-02	2.65E-07	3.7E-09
1.777E-02	2.91E-07	4.0E-09
1.943E-02	3.16E-07	4.4E-09
2.109E-02	3.42E-07	4.8E-09
2.275E-02	3.67E-07	5.2E-09
2.441E-02	4.05E-07	5.6E-09
2.607E-02	4.27E-07	6.0E-09
2.773E-02	4.43E-07	6.3E-09
2.939E-02	4.80E-07	6.8E-09
3.105E-02	5.07E-07	7.1E-09
3.271E-02	5.34E-07	7.5E-09
3.437E-02	5.77E-07	8.0E-09
3.603E-02	5.89E-07	8.3E-09
3.769E-02	6.28E-07	8.8E-09
3.935E-02	6.64E-07	9.2E-09
4.101E-02	6.75E-07	9.5E-09
4.267E-02	6.97E-07	9.8E-09
4.433E-02	7.19E-07	1.0E-08
4.599E-02	7.28E-07	1.0E-08
4.765E-02	7.85E-07	1.1E-08

Table A.6. Continued.

Energy (MeV)	P.H.D. in energy bin δE	Precision (one standard deviation)
4.931E-02	8.12E-07	1.1E-08
5.097E-02	8.49E-07	1.2E-08
5.263E-02	8.48E-07	1.2E-08
5.429E-02	8.68E-07	1.2E-08
5.595E-02	8.99E-07	1.3E-08
5.761E-02	8.98E-07	1.3E-08
5.927E-02	9.52E-07	1.4E-08
6.093E-02	9.68E-07	1.4E-08
6.259E-02	9.91E-07	1.4E-08
6.425E-02	1.01E-06	1.5E-08
6.591E-02	1.03E-06	1.5E-08
6.757E-02	1.11E-06	1.6E-08
6.923E-02	1.06E-06	1.6E-08
7.089E-02	1.14E-06	1.6E-08
7.255E-02	1.14E-06	1.7E-08
7.421E-02	1.15E-06	1.7E-08
7.587E-02	1.18E-06	1.7E-08
7.753E-02	1.21E-06	1.8E-08
7.919E-02	1.22E-06	1.8E-08
8.085E-02	1.28E-06	1.8E-08
8.251E-02	1.29E-06	1.9E-08
8.417E-02	1.29E-06	1.9E-08
8.583E-02	1.29E-06	1.9E-08
8.749E-02	1.32E-06	1.9E-08
8.915E-02	1.39E-06	2.0E-08
9.081E-02	1.36E-06	2.0E-08
9.247E-02	1.40E-06	2.1E-08
9.413E-02	1.39E-06	2.1E-08
9.579E-02	1.44E-06	2.1E-08
9.745E-02	1.42E-06	2.1E-08

Table A.6. Continued.

Energy (MeV)	P.H.D. in energy bin δE	Precision (one standard deviation)
9.911E-02	1.46E-06	2.2E-08
1.008E-01	1.51E-06	2.2E-08
1.024E-01	1.54E-06	2.3E-08
1.041E-01	1.49E-06	2.3E-08
1.058E-01	1.55E-06	2.3E-08
1.074E-01	1.54E-06	2.3E-08
1.091E-01	1.57E-06	2.4E-08
1.107E-01	1.66E-06	2.5E-08
1.124E-01	1.65E-06	2.5E-08
1.141E-01	1.65E-06	2.5E-08
1.157E-01	1.68E-06	2.5E-08
1.174E-01	1.68E-06	2.5E-08
1.190E-01	1.76E-06	2.6E-08
1.207E-01	1.80E-06	2.7E-08
1.224E-01	1.75E-06	2.7E-08
1.240E-01	1.78E-06	2.7E-08
1.257E-01	1.83E-06	2.8E-08
1.273E-01	1.85E-06	2.8E-08
1.290E-01	1.79E-06	2.8E-08
1.307E-01	1.88E-06	2.9E-08
1.323E-01	1.91E-06	2.9E-08
1.340E-01	1.85E-06	2.9E-08
1.356E-01	1.91E-06	2.9E-08
1.373E-01	1.96E-06	3.0E-08
1.390E-01	2.02E-06	3.0E-08
1.406E-01	1.94E-06	3.0E-08
1.423E-01	1.96E-06	3.0E-08
1.439E-01	1.99E-06	3.1E-08
1.456E-01	1.96E-06	3.1E-08
1.473E-01	2.05E-06	3.2E-08

Table A.6. Continued.

Energy (MeV)	P.H.D. in energy bin δE	Precision (one standard deviation)
1.489E-01	2.03E-06	3.2E-08
1.506E-01	2.00E-06	3.2E-08
1.522E-01	2.07E-06	3.2E-08
1.539E-01	2.01E-06	3.2E-08
1.556E-01	1.94E-06	3.2E-08
1.572E-01	2.06E-06	3.3E-08
1.589E-01	2.05E-06	3.3E-08
1.605E-01	2.08E-06	3.3E-08
1.622E-01	2.13E-06	3.4E-08
1.639E-01	2.13E-06	3.4E-08
1.655E-01	2.13E-06	3.4E-08
1.672E-01	2.15E-06	3.5E-08
1.688E-01	2.14E-06	3.5E-08
1.705E-01	2.37E-06	3.6E-08
1.722E-01	2.50E-06	3.8E-08
1.738E-01	2.54E-06	3.8E-08
1.755E-01	2.56E-06	3.9E-08
1.771E-01	2.57E-06	3.9E-08
1.788E-01	2.58E-06	3.9E-08
1.805E-01	2.60E-06	3.9E-08
1.821E-01	2.64E-06	4.0E-08
1.838E-01	2.67E-06	4.0E-08
1.854E-01	2.68E-06	4.1E-08
1.871E-01	2.55E-06	4.0E-08
1.888E-01	2.71E-06	4.1E-08
1.904E-01	2.64E-06	4.1E-08
1.921E-01	2.70E-06	4.2E-08
1.937E-01	2.67E-06	4.1E-08
1.954E-01	2.65E-06	4.1E-08
1.971E-01	2.69E-06	4.2E-08

Table A.6. Continued.

Energy (MeV)	P.H.D. in energy bin δE	Precision (one standard deviation)
1.987E-01	2.75E-06	4.3E-08
2.004E-01	2.68E-06	4.2E-08
2.020E-01	2.79E-06	4.3E-08
2.037E-01	2.74E-06	4.3E-08
2.054E-01	2.72E-06	4.3E-08
2.070E-01	2.79E-06	4.4E-08
2.087E-01	2.78E-06	4.4E-08
2.103E-01	2.78E-06	4.4E-08
2.120E-01	2.78E-06	4.4E-08
2.137E-01	2.76E-06	4.4E-08
2.153E-01	2.74E-06	4.4E-08
2.170E-01	2.91E-06	4.6E-08
2.186E-01	2.90E-06	4.6E-08
2.203E-01	2.94E-06	4.6E-08
2.220E-01	2.87E-06	4.6E-08
2.236E-01	2.87E-06	4.6E-08
2.253E-01	2.90E-06	4.7E-08
2.269E-01	2.89E-06	4.7E-08
2.286E-01	2.98E-06	4.8E-08
2.303E-01	2.98E-06	4.8E-08
2.319E-01	2.85E-06	4.7E-08
2.336E-01	3.00E-06	4.8E-08
2.352E-01	2.96E-06	4.8E-08
2.369E-01	3.05E-06	4.9E-08
2.386E-01	3.07E-06	4.9E-08
2.402E-01	3.06E-06	5.0E-08
2.419E-01	3.10E-06	5.0E-08
2.435E-01	3.03E-06	4.9E-08
2.452E-01	3.18E-06	5.1E-08
2.469E-01	3.10E-06	5.1E-08

Table A.6. Continued.

Energy (MeV)	P.H.D. in energy bin δE	Precision (one standard deviation)
2.485E-01	3.17E-06	5.1E-08
2.502E-01	3.22E-06	5.2E-08
2.518E-01	3.12E-06	5.1E-08
2.535E-01	3.28E-06	5.3E-08
2.552E-01	3.31E-06	5.3E-08
2.568E-01	3.32E-06	5.3E-08
2.585E-01	3.43E-06	5.4E-08
2.601E-01	3.50E-06	5.5E-08
2.618E-01	3.47E-06	5.5E-08
2.635E-01	3.59E-06	5.6E-08
2.651E-01	3.68E-06	5.7E-08
2.668E-01	3.74E-06	5.8E-08
2.684E-01	3.88E-06	5.9E-08
2.701E-01	3.86E-06	5.9E-08
2.718E-01	4.02E-06	6.0E-08
2.734E-01	3.91E-06	5.9E-08
2.751E-01	4.15E-06	6.1E-08
2.767E-01	4.22E-06	6.3E-08
2.784E-01	4.24E-06	6.3E-08
2.801E-01	4.30E-06	6.3E-08
2.817E-01	4.41E-06	6.4E-08
2.834E-01	4.51E-06	6.5E-08
2.850E-01	4.66E-06	6.7E-08
2.867E-01	4.78E-06	6.7E-08
2.884E-01	4.90E-06	6.9E-08
2.900E-01	4.97E-06	6.9E-08
2.917E-01	5.11E-06	7.0E-08
2.933E-01	5.24E-06	7.1E-08
2.950E-01	5.29E-06	7.2E-08
2.967E-01	5.56E-06	7.4E-08

Table A.6. Continued.

Energy (MeV)	P.H.D. in energy bin δE	Precision (one standard deviation)
2.983E-01	5.64E-06	7.5E-08
3.000E-01	5.71E-06	7.5E-08
3.016E-01	5.79E-06	7.6E-08
3.033E-01	6.07E-06	7.8E-08
3.050E-01	6.22E-06	8.0E-08
3.066E-01	6.31E-06	8.0E-08
3.083E-01	6.51E-06	8.1E-08
3.099E-01	6.69E-06	8.3E-08
3.116E-01	6.88E-06	8.5E-08
3.133E-01	7.07E-06	8.6E-08
3.149E-01	7.19E-06	8.7E-08
3.166E-01	7.43E-06	8.8E-08
3.182E-01	7.54E-06	8.9E-08
3.199E-01	7.86E-06	9.1E-08
3.216E-01	8.10E-06	9.3E-08
3.232E-01	8.35E-06	9.4E-08
3.249E-01	8.60E-06	9.6E-08
3.265E-01	8.86E-06	9.8E-08
3.282E-01	9.39E-06	1.0E-07
3.299E-01	9.41E-06	1.0E-07
3.315E-01	7.23E-06	8.9E-08
3.332E-01	3.03E-06	5.8E-08
3.348E-01	3.10E-06	5.9E-08
3.365E-01	3.01E-06	5.8E-08
3.382E-01	2.88E-06	5.7E-08
3.398E-01	2.85E-06	5.7E-08
3.415E-01	2.76E-06	5.6E-08
3.431E-01	2.74E-06	5.6E-08
3.448E-01	2.74E-06	5.6E-08
3.465E-01	2.62E-06	5.5E-08

Table A.6. Continued.

Energy (MeV)	P.H.D. in energy bin δE	Precision (one standard deviation)
3.481E-01	2.55E-06	5.4E-08
3.498E-01	2.53E-06	5.4E-08
3.514E-01	2.57E-06	5.5E-08
3.531E-01	2.46E-06	5.4E-08
3.548E-01	2.32E-06	5.2E-08
3.564E-01	2.31E-06	5.2E-08
3.581E-01	2.33E-06	5.3E-08
3.597E-01	2.18E-06	5.1E-08
3.614E-01	2.18E-06	5.1E-08
3.631E-01	2.13E-06	5.1E-08
3.647E-01	2.07E-06	5.0E-08
3.664E-01	1.97E-06	4.9E-08
3.680E-01	1.97E-06	4.9E-08
3.697E-01	1.86E-06	4.8E-08
3.714E-01	1.84E-06	4.8E-08
3.730E-01	1.79E-06	4.7E-08
3.747E-01	1.59E-06	4.5E-08
3.763E-01	1.58E-06	4.4E-08
3.780E-01	1.52E-06	4.4E-08
3.797E-01	1.46E-06	4.3E-08
3.813E-01	1.38E-06	4.2E-08
3.830E-01	1.38E-06	4.2E-08
3.846E-01	1.32E-06	4.1E-08
3.863E-01	1.22E-06	4.0E-08
3.880E-01	1.24E-06	4.0E-08
3.896E-01	1.08E-06	3.7E-08
3.913E-01	1.06E-06	3.7E-08
3.929E-01	9.97E-07	3.6E-08
3.946E-01	9.15E-07	3.5E-08
3.963E-01	8.83E-07	3.4E-08

Table A.6. Continued.

Energy (MeV)	P.H.D. in energy bin δE	Precision (one standard deviation)
3.979E-01	8.02E-07	3.3E-08
3.996E-01	7.22E-07	3.1E-08
4.012E-01	6.70E-07	3.0E-08
4.029E-01	6.23E-07	2.9E-08
4.046E-01	5.84E-07	2.8E-08
4.062E-01	6.11E-07	2.9E-08
4.079E-01	5.87E-07	2.8E-08
4.095E-01	5.72E-07	2.8E-08
4.112E-01	5.33E-07	2.7E-08
4.129E-01	4.83E-07	2.6E-08
4.145E-01	4.99E-07	2.6E-08
4.162E-01	4.51E-07	2.5E-08
4.178E-01	4.32E-07	2.5E-08
4.195E-01	4.41E-07	2.5E-08
4.212E-01	4.04E-07	2.4E-08
4.228E-01	3.92E-07	2.4E-08
4.245E-01	3.83E-07	2.3E-08
4.261E-01	3.50E-07	2.2E-08
4.278E-01	4.03E-07	2.4E-08
4.295E-01	3.47E-07	2.2E-08
4.311E-01	3.30E-07	2.2E-08
4.328E-01	3.71E-07	2.3E-08
4.344E-01	3.68E-07	2.3E-08
4.361E-01	3.28E-07	2.2E-08
4.378E-01	3.13E-07	2.1E-08
4.394E-01	3.04E-07	2.1E-08
4.411E-01	3.20E-07	2.2E-08
4.427E-01	2.95E-07	2.1E-08
4.444E-01	2.93E-07	2.1E-08
4.461E-01	2.83E-07	2.1E-08

Table A.6. Continued.

Energy (MeV)	P.H.D. in energy bin δE	Precision (one standard deviation)
4.477E-01	2.41E-07	1.9E-08
4.494E-01	2.87E-07	2.1E-08
4.510E-01	2.70E-07	2.0E-08
4.527E-01	2.35E-07	1.9E-08
4.544E-01	2.89E-07	2.1E-08
4.560E-01	2.73E-07	2.0E-08
4.577E-01	2.48E-07	1.9E-08
4.593E-01	2.38E-07	1.9E-08
4.610E-01	2.12E-07	1.8E-08
4.627E-01	2.16E-07	1.8E-08
4.643E-01	2.43E-07	1.9E-08
4.660E-01	2.16E-07	1.8E-08
4.676E-01	2.52E-07	2.0E-08
4.693E-01	1.76E-07	1.7E-08
4.710E-01	1.77E-07	1.7E-08
4.726E-01	2.14E-07	1.8E-08
4.743E-01	1.78E-07	1.7E-08
4.759E-01	1.43E-07	1.5E-08
4.776E-01	1.46E-07	1.5E-08
4.793E-01	1.23E-07	1.4E-08
4.809E-01	1.25E-07	1.4E-08
4.826E-01	1.38E-07	1.5E-08
4.842E-01	9.67E-08	1.2E-08
4.859E-01	1.13E-07	1.4E-08
4.876E-01	1.18E-07	1.4E-08
4.892E-01	1.53E-07	1.6E-08
4.909E-01	4.12E-07	2.6E-08
4.925E-01	7.70E-08	1.1E-08
4.942E-01	7.07E-08	1.1E-08
4.959E-01	9.24E-08	1.2E-08

Table A.6. Continued.

Energy (MeV)	P.H.D. in energy bin δE	Precision (one standard deviation)
4.975E-01	8.44E-08	1.2E-08
4.992E-01	5.48E-08	9.5E-09
5.008E-01	4.20E-04	8.4E-07
5.025E-01	0.00E+00	0.0E+00
5.042E-01	0.00E+00	0.0E+00
5.058E-01	0.00E+00	0.0E+00
5.075E-01	0.00E+00	0.0E+00
5.091E-01	0.00E+00	0.0E+00
5.108E-01	0.00E+00	0.0E+00
5.125E-01	0.00E+00	0.0E+00
5.141E-01	0.00E+00	0.0E+00
5.158E-01	0.00E+00	0.0E+00
5.174E-01	0.00E+00	0.0E+00
5.191E-01	0.00E+00	0.0E+00
5.208E-01	0.00E+00	0.0E+00
5.224E-01	0.00E+00	0.0E+00
5.241E-01	0.00E+00	0.0E+00
5.257E-01	0.00E+00	0.0E+00

Table A.7. R.F. histogram for 0.75 MeV photon without Doppler broadening feature.

Energy (MeV)	P.H.D. in energy bin δE	Precision (one standard deviation)
1.000E-03	- - - - -	- - - - -
2.260E-03	1.15E-08	1.6E-10
4.220E-03	3.25E-08	3.9E-10
6.180E-03	5.35E-08	6.3E-10
8.140E-03	7.57E-08	8.7E-10
1.010E-02	1.01E-07	1.1E-09
1.206E-02	1.20E-07	1.4E-09
1.402E-02	1.40E-07	1.6E-09
1.598E-02	1.63E-07	1.8E-09
1.794E-02	1.83E-07	2.1E-09
1.990E-02	2.06E-07	2.3E-09
2.186E-02	2.33E-07	2.6E-09
2.382E-02	2.47E-07	2.8E-09
2.578E-02	2.70E-07	3.1E-09
2.774E-02	2.92E-07	3.3E-09
2.970E-02	3.10E-07	3.5E-09
3.166E-02	3.25E-07	3.7E-09
3.362E-02	3.53E-07	4.0E-09
3.558E-02	3.73E-07	4.2E-09
3.754E-02	3.91E-07	4.5E-09
3.950E-02	4.16E-07	4.7E-09
4.146E-02	4.36E-07	4.9E-09
4.342E-02	4.59E-07	5.2E-09
4.538E-02	4.83E-07	5.5E-09
4.734E-02	5.05E-07	5.7E-09
4.930E-02	5.17E-07	5.9E-09
5.126E-02	5.45E-07	6.2E-09
5.322E-02	5.61E-07	6.3E-09
5.518E-02	5.89E-07	6.7E-09
5.714E-02	6.07E-07	6.9E-09

Table A.7. Continued.

Energy (MeV)	P.H.D. in energy bin δE	Precision (one standard deviation)
5.910E-02	6.23E-07	7.1E-09
6.106E-02	6.36E-07	7.3E-09
6.302E-02	6.51E-07	7.5E-09
6.498E-02	6.91E-07	7.8E-09
6.694E-02	6.98E-07	8.0E-09
6.890E-02	7.08E-07	8.1E-09
7.086E-02	7.43E-07	8.5E-09
7.282E-02	7.46E-07	8.6E-09
7.478E-02	7.63E-07	8.9E-09
7.674E-02	7.87E-07	9.1E-09
7.870E-02	8.20E-07	9.3E-09
8.066E-02	8.57E-07	9.7E-09
8.262E-02	8.69E-07	9.9E-09
8.458E-02	8.87E-07	1.0E-08
8.654E-02	9.02E-07	1.0E-08
8.850E-02	9.25E-07	1.1E-08
9.046E-02	9.17E-07	1.1E-08
9.242E-02	9.67E-07	1.1E-08
9.438E-02	9.75E-07	1.1E-08
9.634E-02	9.87E-07	1.1E-08
9.830E-02	1.02E-06	1.2E-08
1.003E-01	1.06E-06	1.2E-08
1.022E-01	1.05E-06	1.2E-08
1.042E-01	1.07E-06	1.2E-08
1.061E-01	1.11E-06	1.3E-08
1.081E-01	1.12E-06	1.3E-08
1.101E-01	1.09E-06	1.3E-08
1.120E-01	1.14E-06	1.3E-08
1.140E-01	1.17E-06	1.4E-08
1.159E-01	1.18E-06	1.4E-08

Table A.7. Continued.

Energy (MeV)	P.H.D. in energy bin δE	Precision (one standard deviation)
1.179E-01	1.20E-06	1.4E-08
1.199E-01	1.25E-06	1.4E-08
1.218E-01	1.24E-06	1.4E-08
1.238E-01	1.27E-06	1.5E-08
1.257E-01	1.29E-06	1.5E-08
1.277E-01	1.30E-06	1.5E-08
1.297E-01	1.34E-06	1.5E-08
1.316E-01	1.34E-06	1.5E-08
1.336E-01	1.37E-06	1.6E-08
1.355E-01	1.40E-06	1.6E-08
1.375E-01	1.43E-06	1.6E-08
1.395E-01	1.41E-06	1.6E-08
1.414E-01	1.40E-06	1.7E-08
1.434E-01	1.45E-06	1.7E-08
1.453E-01	1.46E-06	1.7E-08
1.473E-01	1.44E-06	1.7E-08
1.493E-01	1.50E-06	1.7E-08
1.512E-01	1.53E-06	1.8E-08
1.532E-01	1.51E-06	1.8E-08
1.551E-01	1.55E-06	1.8E-08
1.571E-01	1.56E-06	1.8E-08
1.591E-01	1.55E-06	1.8E-08
1.610E-01	1.59E-06	1.9E-08
1.630E-01	1.62E-06	1.9E-08
1.649E-01	1.58E-06	1.9E-08
1.669E-01	1.68E-06	2.0E-08
1.689E-01	1.63E-06	1.9E-08
1.708E-01	1.68E-06	2.0E-08
1.728E-01	1.68E-06	2.0E-08
1.747E-01	1.68E-06	2.0E-08

Table A.7. Continued.

Energy (MeV)	P.H.D. in energy bin δE	Precision (one standard deviation)
1.767E-01	1.69E-06	2.0E-08
1.787E-01	1.65E-06	2.0E-08
1.806E-01	1.66E-06	2.0E-08
1.826E-01	1.69E-06	2.1E-08
1.845E-01	1.72E-06	2.1E-08
1.865E-01	1.74E-06	2.1E-08
1.885E-01	1.75E-06	2.1E-08
1.904E-01	1.79E-06	2.2E-08
1.924E-01	1.94E-06	2.3E-08
1.943E-01	1.98E-06	2.3E-08
1.963E-01	2.03E-06	2.3E-08
1.983E-01	2.02E-06	2.3E-08
2.002E-01	2.07E-06	2.4E-08
2.022E-01	2.11E-06	2.4E-08
2.041E-01	2.09E-06	2.4E-08
2.061E-01	2.07E-06	2.4E-08
2.081E-01	2.14E-06	2.5E-08
2.100E-01	2.20E-06	2.5E-08
2.120E-01	2.21E-06	2.5E-08
2.139E-01	2.12E-06	2.5E-08
2.159E-01	2.17E-06	2.5E-08
2.179E-01	2.18E-06	2.5E-08
2.198E-01	2.17E-06	2.6E-08
2.218E-01	2.21E-06	2.6E-08
2.237E-01	2.26E-06	2.6E-08
2.257E-01	2.21E-06	2.6E-08
2.277E-01	2.20E-06	2.6E-08
2.296E-01	2.21E-06	2.6E-08
2.316E-01	2.25E-06	2.7E-08
2.335E-01	2.28E-06	2.7E-08

Table A.7. Continued.

Energy (MeV)	P.H.D. in energy bin δE	Precision (one standard deviation)
2.355E-01	2.29E-06	2.7E-08
2.375E-01	2.23E-06	2.7E-08
2.394E-01	2.29E-06	2.7E-08
2.414E-01	2.32E-06	2.8E-08
2.433E-01	2.30E-06	2.8E-08
2.453E-01	2.35E-06	2.8E-08
2.473E-01	2.32E-06	2.8E-08
2.492E-01	2.35E-06	2.8E-08
2.512E-01	2.31E-06	2.8E-08
2.531E-01	2.35E-06	2.9E-08
2.551E-01	2.35E-06	2.9E-08
2.571E-01	2.40E-06	2.9E-08
2.590E-01	2.43E-06	2.9E-08
2.610E-01	2.37E-06	2.9E-08
2.629E-01	2.40E-06	3.0E-08
2.649E-01	2.42E-06	3.0E-08
2.669E-01	2.47E-06	3.0E-08
2.688E-01	2.44E-06	3.0E-08
2.708E-01	2.47E-06	3.0E-08
2.727E-01	2.55E-06	3.1E-08
2.747E-01	2.45E-06	3.0E-08
2.767E-01	2.50E-06	3.1E-08
2.786E-01	2.49E-06	3.1E-08
2.806E-01	2.57E-06	3.2E-08
2.825E-01	2.51E-06	3.1E-08
2.845E-01	2.56E-06	3.2E-08
2.865E-01	2.55E-06	3.2E-08
2.884E-01	2.57E-06	3.2E-08
2.904E-01	2.56E-06	3.2E-08
2.923E-01	2.54E-06	3.2E-08

Table A.7. Continued.

Energy (MeV)	P.H.D. in energy bin δE	Precision (one standard deviation)
2.943E-01	2.59E-06	3.2E-08
2.963E-01	2.60E-06	3.3E-08
2.982E-01	2.59E-06	3.3E-08
3.002E-01	2.65E-06	3.3E-08
3.021E-01	2.58E-06	3.3E-08
3.041E-01	2.60E-06	3.3E-08
3.061E-01	2.62E-06	3.3E-08
3.080E-01	2.59E-06	3.3E-08
3.100E-01	2.64E-06	3.4E-08
3.119E-01	2.69E-06	3.4E-08
3.139E-01	2.65E-06	3.4E-08
3.159E-01	2.68E-06	3.4E-08
3.178E-01	2.67E-06	3.4E-08
3.198E-01	2.70E-06	3.4E-08
3.217E-01	2.70E-06	3.5E-08
3.237E-01	2.75E-06	3.5E-08
3.257E-01	2.73E-06	3.5E-08
3.276E-01	2.71E-06	3.5E-08
3.296E-01	2.70E-06	3.5E-08
3.315E-01	2.78E-06	3.6E-08
3.335E-01	2.82E-06	3.6E-08
3.355E-01	2.80E-06	3.6E-08
3.374E-01	2.81E-06	3.6E-08
3.394E-01	2.75E-06	3.6E-08
3.413E-01	2.77E-06	3.6E-08
3.433E-01	2.79E-06	3.6E-08
3.453E-01	2.76E-06	3.6E-08
3.472E-01	2.83E-06	3.7E-08
3.492E-01	2.83E-06	3.7E-08
3.511E-01	2.92E-06	3.8E-08

Table A.7. Continued.

Energy (MeV)	P.H.D. in energy bin δE	Precision (one standard deviation)
3.531E-01	2.87E-06	3.7E-08
3.551E-01	2.89E-06	3.8E-08
3.570E-01	2.91E-06	3.8E-08
3.590E-01	2.91E-06	3.8E-08
3.609E-01	2.97E-06	3.8E-08
3.629E-01	2.87E-06	3.8E-08
3.649E-01	2.96E-06	3.9E-08
3.668E-01	2.91E-06	3.8E-08
3.688E-01	2.94E-06	3.9E-08
3.707E-01	2.89E-06	3.8E-08
3.727E-01	3.03E-06	3.9E-08
3.747E-01	2.97E-06	3.9E-08
3.766E-01	2.98E-06	3.9E-08
3.786E-01	3.04E-06	4.0E-08
3.805E-01	3.00E-06	4.0E-08
3.825E-01	3.06E-06	4.0E-08
3.845E-01	2.96E-06	4.0E-08
3.864E-01	3.13E-06	4.1E-08
3.884E-01	3.03E-06	4.0E-08
3.903E-01	3.02E-06	4.0E-08
3.923E-01	3.11E-06	4.1E-08
3.943E-01	3.15E-06	4.1E-08
3.962E-01	3.12E-06	4.1E-08
3.982E-01	3.22E-06	4.2E-08
4.001E-01	3.10E-06	4.1E-08
4.021E-01	3.19E-06	4.2E-08
4.041E-01	3.19E-06	4.2E-08
4.060E-01	3.27E-06	4.3E-08
4.080E-01	3.20E-06	4.3E-08
4.099E-01	3.27E-06	4.3E-08

Table A.7. Continued.

Energy (MeV)	P.H.D. in energy bin δE	Precision (one standard deviation)
4.119E-01	3.31E-06	4.3E-08
4.139E-01	3.28E-06	4.3E-08
4.158E-01	3.37E-06	4.4E-08
4.178E-01	3.33E-06	4.4E-08
4.197E-01	3.40E-06	4.4E-08
4.217E-01	3.33E-06	4.4E-08
4.237E-01	3.41E-06	4.5E-08
4.256E-01	3.43E-06	4.5E-08
4.276E-01	3.48E-06	4.5E-08
4.295E-01	3.40E-06	4.5E-08
4.315E-01	3.51E-06	4.6E-08
4.335E-01	3.50E-06	4.6E-08
4.354E-01	3.54E-06	4.6E-08
4.374E-01	3.60E-06	4.6E-08
4.393E-01	3.59E-06	4.7E-08
4.413E-01	3.62E-06	4.7E-08
4.433E-01	3.66E-06	4.7E-08
4.452E-01	3.81E-06	4.8E-08
4.472E-01	3.79E-06	4.8E-08
4.491E-01	3.84E-06	4.9E-08
4.511E-01	3.86E-06	4.9E-08
4.531E-01	3.88E-06	4.9E-08
4.550E-01	3.84E-06	4.9E-08
4.570E-01	3.88E-06	4.9E-08
4.589E-01	4.01E-06	5.1E-08
4.609E-01	4.11E-06	5.1E-08
4.629E-01	4.12E-06	5.1E-08
4.648E-01	4.23E-06	5.2E-08
4.668E-01	4.24E-06	5.2E-08
4.687E-01	4.41E-06	5.3E-08

Table A.7. Continued.

Energy (MeV)	P.H.D. in energy bin δE	Precision (one standard deviation)
4.707E-01	4.40E-06	5.3E-08
4.727E-01	4.48E-06	5.4E-08
4.746E-01	4.63E-06	5.5E-08
4.766E-01	4.72E-06	5.6E-08
4.785E-01	4.81E-06	5.6E-08
4.805E-01	4.83E-06	5.7E-08
4.825E-01	4.91E-06	5.7E-08
4.844E-01	5.16E-06	5.9E-08
4.864E-01	5.22E-06	5.9E-08
4.883E-01	5.22E-06	5.9E-08
4.903E-01	5.32E-06	6.0E-08
4.923E-01	5.64E-06	6.2E-08
4.942E-01	5.58E-06	6.2E-08
4.962E-01	5.81E-06	6.3E-08
4.981E-01	5.76E-06	6.3E-08
5.001E-01	6.04E-06	6.5E-08
5.021E-01	6.01E-06	6.4E-08
5.040E-01	6.22E-06	6.6E-08
5.060E-01	6.42E-06	6.7E-08
5.079E-01	6.55E-06	6.7E-08
5.099E-01	6.64E-06	6.8E-08
5.119E-01	6.75E-06	6.9E-08
5.138E-01	6.90E-06	7.0E-08
5.158E-01	7.13E-06	7.1E-08
5.177E-01	7.36E-06	7.2E-08
5.197E-01	7.52E-06	7.4E-08
5.217E-01	7.66E-06	7.4E-08
5.236E-01	7.88E-06	7.6E-08
5.256E-01	8.09E-06	7.7E-08
5.275E-01	8.11E-06	7.7E-08

Table A.7. Continued.

Energy (MeV)	P.H.D. in energy bin δE	Precision (one standard deviation)
5.295E-01	8.30E-06	7.8E-08
5.315E-01	8.61E-06	7.9E-08
5.334E-01	8.77E-06	8.1E-08
5.354E-01	8.90E-06	8.1E-08
5.373E-01	9.29E-06	8.3E-08
5.393E-01	9.54E-06	8.4E-08
5.413E-01	9.61E-06	8.5E-08
5.432E-01	9.92E-06	8.6E-08
5.452E-01	1.00E-05	8.7E-08
5.471E-01	1.04E-05	8.9E-08
5.491E-01	1.07E-05	9.0E-08
5.511E-01	1.07E-05	9.0E-08
5.530E-01	1.11E-05	9.2E-08
5.550E-01	1.17E-05	9.5E-08
5.569E-01	1.16E-05	9.4E-08
5.589E-01	1.22E-05	9.7E-08
5.609E-01	6.15E-06	6.9E-08
5.628E-01	4.10E-06	5.7E-08
5.648E-01	3.97E-06	5.6E-08
5.667E-01	4.03E-06	5.6E-08
5.687E-01	3.88E-06	5.5E-08
5.707E-01	3.79E-06	5.5E-08
5.726E-01	3.83E-06	5.5E-08
5.746E-01	3.76E-06	5.5E-08
5.765E-01	3.69E-06	5.4E-08
5.785E-01	3.55E-06	5.3E-08
5.805E-01	3.59E-06	5.3E-08
5.824E-01	3.52E-06	5.3E-08
5.844E-01	3.43E-06	5.2E-08
5.863E-01	3.32E-06	5.2E-08

Table A.7. Continued.

Energy (MeV)	P.H.D. in energy bin δE	Precision (one standard deviation)
5.883E-01	3.35E-06	5.2E-08
5.903E-01	3.27E-06	5.2E-08
5.922E-01	3.27E-06	5.2E-08
5.942E-01	3.18E-06	5.1E-08
5.961E-01	3.09E-06	5.0E-08
5.981E-01	3.02E-06	5.0E-08
6.001E-01	2.97E-06	5.0E-08
6.020E-01	2.83E-06	4.8E-08
6.040E-01	2.80E-06	4.8E-08
6.059E-01	2.69E-06	4.7E-08
6.079E-01	2.69E-06	4.8E-08
6.099E-01	2.64E-06	4.7E-08
6.118E-01	2.43E-06	4.5E-08
6.138E-01	2.39E-06	4.5E-08
6.157E-01	2.34E-06	4.5E-08
6.177E-01	2.12E-06	4.3E-08
6.197E-01	2.09E-06	4.2E-08
6.216E-01	2.06E-06	4.2E-08
6.236E-01	1.91E-06	4.1E-08
6.255E-01	1.85E-06	4.0E-08
6.275E-01	1.81E-06	4.0E-08
6.295E-01	1.76E-06	3.9E-08
6.314E-01	1.59E-06	3.7E-08
6.334E-01	1.55E-06	3.7E-08
6.353E-01	1.40E-06	3.5E-08
6.373E-01	1.29E-06	3.4E-08
6.393E-01	1.12E-06	3.1E-08
6.412E-01	1.05E-06	3.0E-08
6.432E-01	9.69E-07	2.9E-08
6.451E-01	9.37E-07	2.9E-08

Table A.7. Continued.

Energy (MeV)	P.H.D. in energy bin δE	Precision (one standard deviation)
6.471E-01	8.95E-07	2.8E-08
6.491E-01	7.80E-07	2.6E-08
6.510E-01	7.33E-07	2.6E-08
6.530E-01	7.66E-07	2.6E-08
6.549E-01	6.21E-07	2.4E-08
6.569E-01	6.62E-07	2.5E-08
6.589E-01	5.82E-07	2.3E-08
6.608E-01	5.81E-07	2.3E-08
6.628E-01	4.90E-07	2.1E-08
6.647E-01	4.76E-07	2.1E-08
6.667E-01	4.34E-07	2.0E-08
6.687E-01	4.20E-07	2.0E-08
6.706E-01	3.88E-07	1.9E-08
6.726E-01	3.48E-07	1.8E-08
6.745E-01	3.43E-07	1.8E-08
6.765E-01	3.05E-07	1.7E-08
6.785E-01	3.12E-07	1.7E-08
6.804E-01	3.06E-07	1.7E-08
6.824E-01	2.61E-07	1.6E-08
6.843E-01	2.71E-07	1.6E-08
6.863E-01	2.65E-07	1.6E-08
6.883E-01	2.60E-07	1.6E-08
6.902E-01	2.69E-07	1.6E-08
6.922E-01	2.42E-07	1.5E-08
6.941E-01	2.48E-07	1.5E-08
6.961E-01	2.20E-07	1.5E-08
6.981E-01	2.57E-07	1.6E-08
7.000E-01	2.45E-07	1.5E-08
7.020E-01	2.29E-07	1.5E-08
7.039E-01	2.05E-07	1.4E-08

Table A.7. Continued.

Energy (MeV)	P.H.D. in energy bin δE	Precision (one standard deviation)
7.059E-01	2.14E-07	1.4E-08
7.079E-01	2.04E-07	1.4E-08
7.098E-01	2.18E-07	1.5E-08
7.118E-01	2.01E-07	1.4E-08
7.137E-01	1.93E-07	1.4E-08
7.157E-01	1.85E-07	1.3E-08
7.177E-01	1.65E-07	1.3E-08
7.196E-01	1.46E-07	1.2E-08
7.216E-01	1.41E-07	1.2E-08
7.235E-01	1.31E-07	1.1E-08
7.255E-01	1.18E-07	1.1E-08
7.275E-01	1.24E-07	1.1E-08
7.294E-01	8.95E-08	9.5E-09
7.314E-01	9.08E-08	9.6E-09
7.333E-01	7.69E-08	8.8E-09
7.353E-01	7.00E-08	8.4E-09
7.373E-01	5.29E-08	7.3E-09
7.392E-01	1.12E-07	1.1E-08
7.412E-01	3.19E-07	1.8E-08
7.431E-01	7.38E-08	8.7E-09
7.451E-01	5.55E-08	7.6E-09
7.471E-01	3.81E-08	6.3E-09
7.490E-01	3.51E-08	6.0E-09
7.510E-01	3.60E-04	6.1E-07
7.529E-01	0.00E+00	0.0E+00
7.549E-01	0.00E+00	0.0E+00
7.569E-01	0.00E+00	0.0E+00
7.588E-01	0.00E+00	0.0E+00
7.608E-01	0.00E+00	0.0E+00
7.627E-01	0.00E+00	0.0E+00

Table A.7. Continued.

Energy (MeV)	P.H.D. in energy bin δE	Precision (one standard deviation)
7.647E-01	0.00E+00	0.0E+00
7.667E-01	0.00E+00	0.0E+00
7.686E-01	0.00E+00	0.0E+00
7.706E-01	0.00E+00	0.0E+00
7.725E-01	0.00E+00	0.0E+00
7.745E-01	0.00E+00	0.0E+00
7.765E-01	0.00E+00	0.0E+00
7.784E-01	0.00E+00	0.0E+00
7.804E-01	0.00E+00	0.0E+00
7.823E-01	0.00E+00	0.0E+00
7.843E-01	0.00E+00	0.0E+00
7.863E-01	0.00E+00	0.0E+00
7.882E-01	0.00E+00	0.0E+00

Table A.8. R.F. histogram for 1 MeV photon without Doppler broadening feature.

Energy (MeV)	P.H.D. in energy bin δE	Precision (one standard deviation)
1.000E-03	- - - - -	- - - - -
2.779E-03	5.94E-03	9.5E-06
4.987E-03	7.01E-06	3.4E-07
7.196E-03	7.30E-06	3.4E-07
9.405E-03	7.75E-06	3.5E-07
1.161E-02	8.25E-06	3.6E-07
1.382E-02	7.99E-06	3.6E-07
1.603E-02	7.64E-06	3.5E-07
1.824E-02	7.25E-06	3.4E-07
2.045E-02	7.81E-06	3.5E-07
2.266E-02	7.56E-06	3.5E-07
2.487E-02	8.07E-06	3.6E-07
2.707E-02	8.17E-06	3.6E-07
2.928E-02	7.20E-06	3.4E-07
3.149E-02	7.91E-06	3.6E-07
3.370E-02	8.31E-06	3.7E-07
3.591E-02	7.43E-06	3.5E-07
3.812E-02	8.17E-06	3.6E-07
4.033E-02	7.77E-06	3.5E-07
4.254E-02	7.72E-06	3.5E-07
4.474E-02	7.77E-06	3.5E-07
4.695E-02	7.81E-06	3.5E-07
4.916E-02	8.14E-06	3.6E-07
5.137E-02	8.01E-06	3.6E-07
5.358E-02	7.15E-06	3.4E-07
5.579E-02	7.80E-06	3.5E-07
5.800E-02	7.46E-06	3.5E-07
6.020E-02	8.47E-06	3.7E-07
6.241E-02	7.51E-06	3.5E-07
6.462E-02	7.83E-06	3.6E-07

Table A.8. Continued.

Energy (MeV)	P.H.D. in energy bin δE	Precision (one standard deviation)
6.683E-02	7.96E-06	3.6E-07
6.904E-02	7.49E-06	3.5E-07
7.125E-02	7.15E-06	3.4E-07
7.346E-02	6.99E-06	3.4E-07
7.567E-02	7.54E-06	3.5E-07
7.787E-02	7.75E-06	3.5E-07
8.008E-02	7.52E-06	3.5E-07
8.229E-02	8.07E-06	3.6E-07
8.450E-02	7.85E-06	3.6E-07
8.671E-02	7.22E-06	3.4E-07
8.892E-02	7.41E-06	3.5E-07
9.113E-02	7.99E-06	3.6E-07
9.334E-02	8.22E-06	3.6E-07
9.554E-02	7.56E-06	3.5E-07
9.775E-02	7.94E-06	3.6E-07
9.996E-02	8.22E-06	3.6E-07
1.022E-01	7.60E-06	3.5E-07
1.044E-01	7.14E-06	3.4E-07
1.066E-01	7.41E-06	3.5E-07
1.088E-01	7.73E-06	3.5E-07
1.110E-01	7.30E-06	3.4E-07
1.132E-01	7.85E-06	3.6E-07
1.154E-01	7.09E-06	3.4E-07
1.176E-01	8.85E-06	3.8E-07
1.198E-01	7.81E-06	3.5E-07
1.221E-01	7.94E-06	3.6E-07
1.243E-01	8.25E-06	3.6E-07
1.265E-01	8.38E-06	3.7E-07
1.287E-01	7.83E-06	3.6E-07
1.309E-01	7.88E-06	3.6E-07

Table A.8. Continued.

Energy (MeV)	P.H.D. in energy bin δE	Precision (one standard deviation)
1.331E-01	7.69E-06	3.5E-07
1.353E-01	7.91E-06	3.6E-07
1.375E-01	7.75E-06	3.5E-07
1.397E-01	8.33E-06	3.7E-07
1.419E-01	7.70E-06	3.5E-07
1.441E-01	7.86E-06	3.6E-07
1.463E-01	7.59E-06	3.5E-07
1.486E-01	7.85E-06	3.6E-07
1.508E-01	7.12E-06	3.4E-07
1.530E-01	7.78E-06	3.5E-07
1.552E-01	7.33E-06	3.4E-07
1.574E-01	7.17E-06	3.4E-07
1.596E-01	7.22E-06	3.4E-07
1.618E-01	7.78E-06	3.5E-07
1.640E-01	7.64E-06	3.5E-07
1.662E-01	6.99E-06	3.4E-07
1.684E-01	7.59E-06	3.5E-07
1.706E-01	7.41E-06	3.5E-07
1.729E-01	7.11E-06	3.4E-07
1.751E-01	7.17E-06	3.4E-07
1.773E-01	7.28E-06	3.4E-07
1.795E-01	7.31E-06	3.4E-07
1.817E-01	7.56E-06	3.5E-07
1.839E-01	7.75E-06	3.5E-07
1.861E-01	6.93E-06	3.3E-07
1.883E-01	6.83E-06	3.3E-07
1.905E-01	6.72E-06	3.3E-07
1.927E-01	6.90E-06	3.3E-07
1.949E-01	7.25E-06	3.4E-07
1.971E-01	7.52E-06	3.5E-07

Table A.8. Continued.

Energy (MeV)	P.H.D. in energy bin δE	Precision (one standard deviation)
1.994E-01	6.51E-06	3.2E-07
2.016E-01	7.57E-06	3.5E-07
2.038E-01	7.11E-06	3.4E-07
2.060E-01	7.75E-06	3.5E-07
2.082E-01	7.41E-06	3.5E-07
2.104E-01	7.57E-06	3.5E-07
2.126E-01	7.59E-06	3.5E-07
2.148E-01	7.51E-06	3.5E-07
2.170E-01	7.20E-06	3.4E-07
2.192E-01	7.67E-06	3.5E-07
2.214E-01	7.14E-06	3.4E-07
2.237E-01	7.11E-06	3.4E-07
2.259E-01	7.49E-06	3.5E-07
2.281E-01	7.85E-06	3.6E-07
2.303E-01	7.25E-06	3.4E-07
2.325E-01	7.64E-06	3.5E-07
2.347E-01	7.57E-06	3.5E-07
2.369E-01	7.40E-06	3.5E-07
2.391E-01	6.93E-06	3.3E-07
2.413E-01	7.57E-06	3.5E-07
2.435E-01	6.93E-06	3.3E-07
2.457E-01	7.25E-06	3.4E-07
2.479E-01	7.49E-06	3.5E-07
2.502E-01	6.78E-06	3.3E-07
2.524E-01	7.02E-06	3.4E-07
2.546E-01	7.77E-06	3.5E-07
2.568E-01	6.64E-06	3.3E-07
2.590E-01	7.43E-06	3.5E-07
2.612E-01	7.38E-06	3.4E-07
2.634E-01	7.22E-06	3.4E-07

Table A.8. Continued.

Energy (MeV)	P.H.D. in energy bin δE	Precision (one standard deviation)
2.656E-01	7.12E-06	3.4E-07
2.678E-01	7.12E-06	3.4E-07
2.700E-01	6.65E-06	3.3E-07
2.722E-01	7.23E-06	3.4E-07
2.745E-01	7.46E-06	3.5E-07
2.767E-01	6.69E-06	3.3E-07
2.789E-01	7.12E-06	3.4E-07
2.811E-01	6.41E-06	3.2E-07
2.833E-01	6.85E-06	3.3E-07
2.855E-01	7.36E-06	3.4E-07
2.877E-01	6.53E-06	3.2E-07
2.899E-01	6.72E-06	3.3E-07
2.921E-01	6.53E-06	3.2E-07
2.943E-01	6.17E-06	3.2E-07
2.965E-01	7.57E-06	3.5E-07
2.987E-01	6.67E-06	3.3E-07
3.010E-01	6.85E-06	3.3E-07
3.032E-01	6.57E-06	3.3E-07
3.054E-01	6.33E-06	3.2E-07
3.076E-01	7.14E-06	3.4E-07
3.098E-01	6.90E-06	3.3E-07
3.120E-01	6.73E-06	3.3E-07
3.142E-01	6.88E-06	3.3E-07
3.164E-01	6.91E-06	3.3E-07
3.186E-01	6.12E-06	3.1E-07
3.208E-01	7.09E-06	3.4E-07
3.230E-01	7.06E-06	3.4E-07
3.253E-01	7.09E-06	3.4E-07
3.275E-01	6.48E-06	3.2E-07
3.297E-01	6.57E-06	3.3E-07

Table A.8. Continued.

Energy (MeV)	P.H.D. in energy bin δE	Precision (one standard deviation)
3.319E-01	6.32E-06	3.2E-07
3.341E-01	6.72E-06	3.3E-07
3.363E-01	6.49E-06	3.2E-07
3.385E-01	6.57E-06	3.3E-07
3.407E-01	5.88E-06	3.1E-07
3.429E-01	6.07E-06	3.1E-07
3.451E-01	6.27E-06	3.2E-07
3.473E-01	6.46E-06	3.2E-07
3.495E-01	6.49E-06	3.2E-07
3.518E-01	6.19E-06	3.2E-07
3.540E-01	6.62E-06	3.3E-07
3.562E-01	6.53E-06	3.2E-07
3.584E-01	6.49E-06	3.2E-07
3.606E-01	6.77E-06	3.3E-07
3.628E-01	6.75E-06	3.3E-07
3.650E-01	6.73E-06	3.3E-07
3.672E-01	5.96E-06	3.1E-07
3.694E-01	6.19E-06	3.2E-07
3.716E-01	6.06E-06	3.1E-07
3.738E-01	6.75E-06	3.3E-07
3.761E-01	6.19E-06	3.2E-07
3.783E-01	5.57E-06	3.0E-07
3.805E-01	5.91E-06	3.1E-07
3.827E-01	6.09E-06	3.1E-07
3.849E-01	6.01E-06	3.1E-07
3.871E-01	6.11E-06	3.1E-07
3.893E-01	5.67E-06	3.0E-07
3.915E-01	6.19E-06	3.2E-07
3.937E-01	6.41E-06	3.2E-07
3.959E-01	6.38E-06	3.2E-07

Table A.8. Continued.

Energy (MeV)	P.H.D. in energy bin δE	Precision (one standard deviation)
3.981E-01	5.85E-06	3.1E-07
4.003E-01	5.62E-06	3.0E-07
4.026E-01	5.57E-06	3.0E-07
4.048E-01	6.64E-06	3.3E-07
4.070E-01	6.25E-06	3.2E-07
4.092E-01	6.22E-06	3.2E-07
4.114E-01	6.03E-06	3.1E-07
4.136E-01	6.09E-06	3.1E-07
4.158E-01	6.15E-06	3.2E-07
4.180E-01	6.03E-06	3.1E-07
4.202E-01	6.43E-06	3.2E-07
4.224E-01	6.06E-06	3.1E-07
4.246E-01	6.19E-06	3.2E-07
4.269E-01	5.80E-06	3.1E-07
4.291E-01	6.41E-06	3.2E-07
4.313E-01	6.19E-06	3.2E-07
4.335E-01	5.96E-06	3.1E-07
4.357E-01	6.35E-06	3.2E-07
4.379E-01	6.19E-06	3.2E-07
4.401E-01	6.17E-06	3.2E-07
4.423E-01	5.37E-06	2.9E-07
4.445E-01	5.41E-06	3.0E-07
4.467E-01	5.88E-06	3.1E-07
4.489E-01	6.06E-06	3.1E-07
4.511E-01	5.22E-06	2.9E-07
4.534E-01	5.77E-06	3.1E-07
4.556E-01	5.78E-06	3.1E-07
4.578E-01	6.25E-06	3.2E-07
4.600E-01	6.19E-06	3.2E-07
4.622E-01	5.56E-06	3.0E-07

Table A.8. Continued.

Energy (MeV)	P.H.D. in energy bin δE	Precision (one standard deviation)
4.644E-01	5.54E-06	3.0E-07
4.666E-01	5.93E-06	3.1E-07
4.688E-01	5.86E-06	3.1E-07
4.710E-01	5.88E-06	3.1E-07
4.732E-01	5.74E-06	3.0E-07
4.754E-01	6.27E-06	3.2E-07
4.777E-01	5.91E-06	3.1E-07
4.799E-01	5.46E-06	3.0E-07
4.821E-01	5.78E-06	3.1E-07
4.843E-01	5.57E-06	3.0E-07
4.865E-01	5.91E-06	3.1E-07
4.887E-01	6.24E-06	3.2E-07
4.909E-01	5.77E-06	3.1E-07
4.931E-01	5.80E-06	3.1E-07
4.953E-01	5.77E-06	3.1E-07
4.975E-01	5.49E-06	3.0E-07
4.997E-01	5.99E-06	3.1E-07
5.019E-01	6.12E-06	3.1E-07
5.042E-01	5.82E-06	3.1E-07
5.064E-01	5.96E-06	3.1E-07
5.086E-01	6.12E-06	3.1E-07
5.108E-01	5.48E-06	3.0E-07
5.130E-01	5.22E-06	2.9E-07
5.152E-01	5.62E-06	3.0E-07
5.174E-01	5.91E-06	3.1E-07
5.196E-01	5.57E-06	3.0E-07
5.218E-01	6.19E-06	3.2E-07
5.240E-01	6.17E-06	3.2E-07
5.262E-01	5.74E-06	3.0E-07
5.285E-01	5.49E-06	3.0E-07

Table A.8. Continued.

Energy (MeV)	P.H.D. in energy bin δE	Precision (one standard deviation)
5.307E-01	5.62E-06	3.0E-07
5.329E-01	5.80E-06	3.1E-07
5.351E-01	5.91E-06	3.1E-07
5.373E-01	6.03E-06	3.1E-07
5.395E-01	6.11E-06	3.1E-07
5.417E-01	5.99E-06	3.1E-07
5.439E-01	6.14E-06	3.1E-07
5.461E-01	6.83E-06	3.3E-07
5.483E-01	6.17E-06	3.2E-07
5.505E-01	5.83E-06	3.1E-07
5.527E-01	5.98E-06	3.1E-07
5.550E-01	6.07E-06	3.1E-07
5.572E-01	5.85E-06	3.1E-07
5.594E-01	5.54E-06	3.0E-07
5.616E-01	6.53E-06	3.2E-07
5.638E-01	6.07E-06	3.1E-07
5.660E-01	6.44E-06	3.2E-07
5.682E-01	5.11E-06	2.9E-07
5.704E-01	5.75E-06	3.0E-07
5.726E-01	5.90E-06	3.1E-07
5.748E-01	5.98E-06	3.1E-07
5.770E-01	6.35E-06	3.2E-07
5.793E-01	5.91E-06	3.1E-07
5.815E-01	6.25E-06	3.2E-07
5.837E-01	6.01E-06	3.1E-07
5.859E-01	5.56E-06	3.0E-07
5.881E-01	7.07E-06	3.4E-07
5.903E-01	6.04E-06	3.1E-07
5.925E-01	5.93E-06	3.1E-07
5.947E-01	6.46E-06	3.2E-07

Table A.8. Continued.

Energy (MeV)	P.H.D. in energy bin δE	Precision (one standard deviation)
5.969E-01	6.19E-06	3.2E-07
5.991E-01	6.24E-06	3.2E-07
6.013E-01	5.77E-06	3.1E-07
6.035E-01	5.51E-06	3.0E-07
6.058E-01	6.11E-06	3.1E-07
6.080E-01	6.56E-06	3.3E-07
6.102E-01	5.69E-06	3.0E-07
6.124E-01	6.20E-06	3.2E-07
6.146E-01	6.27E-06	3.2E-07
6.168E-01	6.25E-06	3.2E-07
6.190E-01	6.53E-06	3.2E-07
6.212E-01	6.86E-06	3.3E-07
6.234E-01	6.09E-06	3.1E-07
6.256E-01	6.59E-06	3.3E-07
6.278E-01	6.27E-06	3.2E-07
6.300E-01	5.86E-06	3.1E-07
6.323E-01	6.88E-06	3.3E-07
6.345E-01	6.36E-06	3.2E-07
6.367E-01	6.57E-06	3.3E-07
6.389E-01	6.01E-06	3.1E-07
6.411E-01	6.44E-06	3.2E-07
6.433E-01	6.56E-06	3.3E-07
6.455E-01	7.02E-06	3.4E-07
6.477E-01	5.83E-06	3.1E-07
6.499E-01	5.96E-06	3.1E-07
6.521E-01	6.62E-06	3.3E-07
6.543E-01	6.65E-06	3.3E-07
6.566E-01	6.77E-06	3.3E-07
6.588E-01	6.99E-06	3.4E-07
6.610E-01	6.35E-06	3.2E-07

Table A.8. Continued.

Energy (MeV)	P.H.D. in energy bin δE	Precision (one standard deviation)
6.632E-01	6.85E-06	3.3E-07
6.654E-01	6.24E-06	3.2E-07
6.676E-01	6.43E-06	3.2E-07
6.698E-01	7.41E-06	3.5E-07
6.720E-01	7.25E-06	3.4E-07
6.742E-01	6.93E-06	3.3E-07
6.764E-01	7.06E-06	3.4E-07
6.786E-01	7.12E-06	3.4E-07
6.809E-01	8.28E-06	3.7E-07
6.831E-01	7.15E-06	3.4E-07
6.853E-01	8.06E-06	3.6E-07
6.875E-01	7.36E-06	3.4E-07
6.897E-01	7.41E-06	3.5E-07
6.919E-01	8.14E-06	3.6E-07
6.941E-01	8.23E-06	3.6E-07
6.963E-01	8.17E-06	3.6E-07
6.985E-01	8.35E-06	3.7E-07
7.007E-01	8.78E-06	3.8E-07
7.029E-01	8.46E-06	3.7E-07
7.051E-01	8.44E-06	3.7E-07
7.074E-01	8.72E-06	3.7E-07
7.096E-01	9.17E-06	3.8E-07
7.118E-01	9.07E-06	3.8E-07
7.140E-01	8.56E-06	3.7E-07
7.162E-01	8.89E-06	3.8E-07
7.184E-01	8.78E-06	3.8E-07
7.206E-01	9.10E-06	3.8E-07
7.228E-01	8.88E-06	3.8E-07
7.250E-01	9.96E-06	4.0E-07
7.272E-01	9.83E-06	4.0E-07

Table A.8. Continued.

Energy (MeV)	P.H.D. in energy bin δE	Precision (one standard deviation)
7.294E-01	1.07E-05	4.2E-07
7.316E-01	1.03E-05	4.1E-07
7.339E-01	9.68E-06	4.0E-07
7.361E-01	1.03E-05	4.1E-07
7.383E-01	1.08E-05	4.2E-07
7.405E-01	1.04E-05	4.1E-07
7.427E-01	1.13E-05	4.3E-07
7.449E-01	1.11E-05	4.2E-07
7.471E-01	1.07E-05	4.2E-07
7.493E-01	1.22E-05	4.4E-07
7.515E-01	1.20E-05	4.4E-07
7.537E-01	1.17E-05	4.3E-07
7.559E-01	1.34E-05	4.6E-07
7.582E-01	1.29E-05	4.6E-07
7.604E-01	1.32E-05	4.6E-07
7.626E-01	1.30E-05	4.6E-07
7.648E-01	1.38E-05	4.7E-07
7.670E-01	1.34E-05	4.7E-07
7.692E-01	1.34E-05	4.6E-07
7.714E-01	1.41E-05	4.8E-07
7.736E-01	1.56E-05	5.0E-07
7.758E-01	1.47E-05	4.9E-07
7.780E-01	1.52E-05	5.0E-07
7.802E-01	1.53E-05	5.0E-07
7.824E-01	1.59E-05	5.1E-07
7.847E-01	1.72E-05	5.3E-07
7.869E-01	1.70E-05	5.2E-07
7.891E-01	1.69E-05	5.2E-07
7.913E-01	1.67E-05	5.2E-07
7.935E-01	1.76E-05	5.3E-07

Table A.8. Continued.

Energy (MeV)	P.H.D. in energy bin δE	Precision (one standard deviation)
7.957E-01	1.79E-05	5.4E-07
7.979E-01	1.01E-05	4.0E-07
8.001E-01	6.72E-06	3.3E-07
8.023E-01	5.85E-06	3.1E-07
8.045E-01	5.82E-06	3.1E-07
8.067E-01	5.62E-06	3.0E-07
8.090E-01	5.66E-06	3.0E-07
8.112E-01	5.99E-06	3.1E-07
8.134E-01	5.33E-06	2.9E-07
8.156E-01	5.64E-06	3.0E-07
8.178E-01	5.61E-06	3.0E-07
8.200E-01	5.67E-06	3.0E-07
8.222E-01	5.12E-06	2.9E-07
8.244E-01	5.35E-06	2.9E-07
8.266E-01	4.85E-06	2.8E-07
8.288E-01	5.32E-06	2.9E-07
8.310E-01	5.20E-06	2.9E-07
8.332E-01	5.51E-06	3.0E-07
8.355E-01	4.70E-06	2.8E-07
8.377E-01	4.66E-06	2.7E-07
8.399E-01	4.43E-06	2.7E-07
8.421E-01	4.35E-06	2.6E-07
8.443E-01	4.43E-06	2.7E-07
8.465E-01	4.37E-06	2.7E-07
8.487E-01	4.19E-06	2.6E-07
8.509E-01	3.71E-06	2.4E-07
8.531E-01	3.51E-06	2.4E-07
8.553E-01	3.37E-06	2.3E-07
8.575E-01	3.54E-06	2.4E-07
8.598E-01	3.56E-06	2.4E-07

Table A.8. Continued.

Energy (MeV)	P.H.D. in energy bin δE	Precision (one standard deviation)
8.620E-01	3.11E-06	2.2E-07
8.642E-01	3.61E-06	2.4E-07
8.664E-01	2.85E-06	2.1E-07
8.686E-01	3.35E-06	2.3E-07
8.708E-01	3.00E-06	2.2E-07
8.730E-01	2.84E-06	2.1E-07
8.752E-01	2.58E-06	2.0E-07
8.774E-01	2.50E-06	2.0E-07
8.796E-01	1.93E-06	1.8E-07
8.818E-01	1.77E-06	1.7E-07
8.840E-01	1.58E-06	1.6E-07
8.863E-01	1.66E-06	1.6E-07
8.885E-01	1.42E-06	1.5E-07
8.907E-01	1.11E-06	1.3E-07
8.929E-01	1.27E-06	1.4E-07
8.951E-01	1.37E-06	1.5E-07
8.973E-01	1.08E-06	1.3E-07
8.995E-01	1.05E-06	1.3E-07
9.017E-01	9.51E-07	1.2E-07
9.039E-01	9.02E-07	1.2E-07
9.061E-01	7.89E-07	1.1E-07
9.083E-01	6.28E-07	1.0E-07
9.106E-01	4.51E-07	8.5E-08
9.128E-01	6.28E-07	1.0E-07
9.150E-01	5.96E-07	9.8E-08
9.172E-01	4.67E-07	8.7E-08
9.194E-01	4.19E-07	8.2E-08
9.216E-01	3.71E-07	7.7E-08
9.238E-01	3.38E-07	7.4E-08
9.260E-01	3.38E-07	7.4E-08

Table A.8. Continued.

Energy (MeV)	P.H.D. in energy bin δE	Precision (one standard deviation)
9.282E-01	4.03E-07	8.1E-08
9.304E-01	3.87E-07	7.9E-08
9.326E-01	3.71E-07	7.7E-08
9.348E-01	3.54E-07	7.6E-08
9.371E-01	3.06E-07	7.0E-08
9.393E-01	3.06E-07	7.0E-08
9.415E-01	2.09E-07	5.8E-08
9.437E-01	3.38E-07	7.4E-08
9.459E-01	2.58E-07	6.4E-08
9.481E-01	3.54E-07	7.6E-08
9.503E-01	2.74E-07	6.6E-08
9.525E-01	2.74E-07	6.6E-08
9.547E-01	2.58E-07	6.4E-08
9.569E-01	1.93E-07	5.6E-08
9.591E-01	3.38E-07	7.4E-08
9.614E-01	1.61E-07	5.1E-08
9.636E-01	1.77E-07	5.3E-08
9.658E-01	1.45E-07	4.8E-08
9.680E-01	2.74E-07	6.6E-08
9.702E-01	2.09E-07	5.8E-08
9.724E-01	2.26E-07	6.0E-08
9.746E-01	8.06E-08	3.6E-08
9.768E-01	3.22E-08	2.3E-08
9.790E-01	6.44E-08	3.2E-08
9.812E-01	6.44E-08	3.2E-08
9.834E-01	4.83E-08	2.8E-08
9.856E-01	4.83E-08	2.8E-08
9.879E-01	4.83E-08	2.8E-08
9.901E-01	4.83E-08	2.8E-08
9.923E-01	3.87E-07	7.9E-08

Table A.8. Continued.

Energy (MeV)	P.H.D. in energy bin δE	Precision (one standard deviation)
9.945E-01	3.22E-08	2.3E-08
9.967E-01	1.61E-08	1.6E-08
9.989E-01	3.22E-08	2.3E-08
1.001E+00	3.32E-04	2.3E-06
1.003E+00	0.000E+00	0.0E+00
1.006E+00	0.000E+00	0.0E+00
1.008E+00	0.000E+00	0.0E+00
1.010E+00	0.000E+00	0.0E+00
1.012E+00	0.000E+00	0.0E+00
1.014E+00	0.000E+00	0.0E+00
1.017E+00	0.000E+00	0.0E+00
1.019E+00	0.000E+00	0.0E+00
1.021E+00	0.000E+00	0.0E+00
1.023E+00	0.000E+00	0.0E+00
1.025E+00	0.000E+00	0.0E+00
1.028E+00	0.000E+00	0.0E+00
1.030E+00	0.000E+00	0.0E+00
1.032E+00	0.000E+00	0.0E+00
1.034E+00	0.000E+00	0.0E+00
1.036E+00	0.000E+00	0.0E+00
1.039E+00	0.000E+00	0.0E+00
1.041E+00	0.000E+00	0.0E+00
1.043E+00	0.000E+00	0.0E+00
1.045E+00	0.000E+00	0.0E+00
1.048E+00	0.000E+00	0.0E+00
1.050E+00	0.000E+00	0.0E+00
1.052E+00	0.000E+00	0.0E+00
1.054E+00	0.000E+00	0.0E+00

APPENDIX C

Table B.1. Electron binding energies for materials in problem 7 (WebElements.com 2003).

Element	Shell	Atomic Orbital	Binding Energy (keV)
H	K	1s	0.0136
Ge	M5	3d5/2	0.0292
Ge	M4	3d3/2	0.0298
N	L1	2s	0.0373
O	L1	2s	0.0416
Al	L3	2p3/2	0.0725
Al	L2	2p1/2	0.0729
Be	K	1s	0.1115
Al	L1	2s	0.1178
Ge	M3	3p3/2	0.1208
Ge	M2	3p1/2	0.1249
Ge	M1	3s	0.1801
C	K	1s	0.2842
N	K	1s	0.4099
O	K	1s	0.5431
Ge	L3	2p3/2	1.217
Ge	L2	2p1/2	1.2481
Ge	L1	2s	1.4146
Al	K	1s	1.559
Ge	K	1s	11.103

Table B.2. Possible characteristic x-rays from Ge.

Shell Vacancy	Fill From	Characteristic x-ray (keV)
K	M5	11.074
	M4	11.073
	M3	10.982
	M2	10.978
	M1	10.923
	L3	9.886
	L2	9.855
	L1	9.688
L1	M5	1.385
	M4	1.385
	M3	1.294
	M2	1.290
	M1	1.235
	L3	0.198
	L2	0.167

Table B.3. Possible characteristic X-rays from Al.

Shell Vacancy	Fill From	Characteristic x-ray (keV)
K	L3	1.487
	L2	1.486
	L1	1.441

Table B.4. Ge X-ray escape peaks.

Source Photon Energy (keV)	Ge K X-ray escape peak from full energy peak (keV)	Ge L1 X-ray escape peak from full energy peak (keV)	Ge L2 X-ray escape peak from full energy peak (keV)	Ge K X-ray escape peak from Compton edge (keV)	Ge K X-ray escape peak from backscatter (keV)
15	3.90	13.59	13.75	-10.27	3.07
30	18.90	28.59	28.75	-7.95	15.74
60	48.90	58.59	58.75	0.31	37.49
100	88.90	98.59	98.75	17.03	60.77
250	238.90	248.59	248.75	112.54	115.26
500	488.90	498.59	498.75	319.80	157.99
750	738.90	748.59	748.75	548.32	179.47
1	988.90	998.59	998.75	785.39	192.40

Table B.5. Backscatter and Compton edge peaks.

Source Photon Energy (keV)	Backscatter (keV)	Compton Edge (keV)
15	14.17	0.83
30	26.85	3.15
60	48.59	11.41
100	71.87	28.13
250	126.36	123.64
500	169.09	330.91
750	190.58	559.42
1000	203.50	796.50

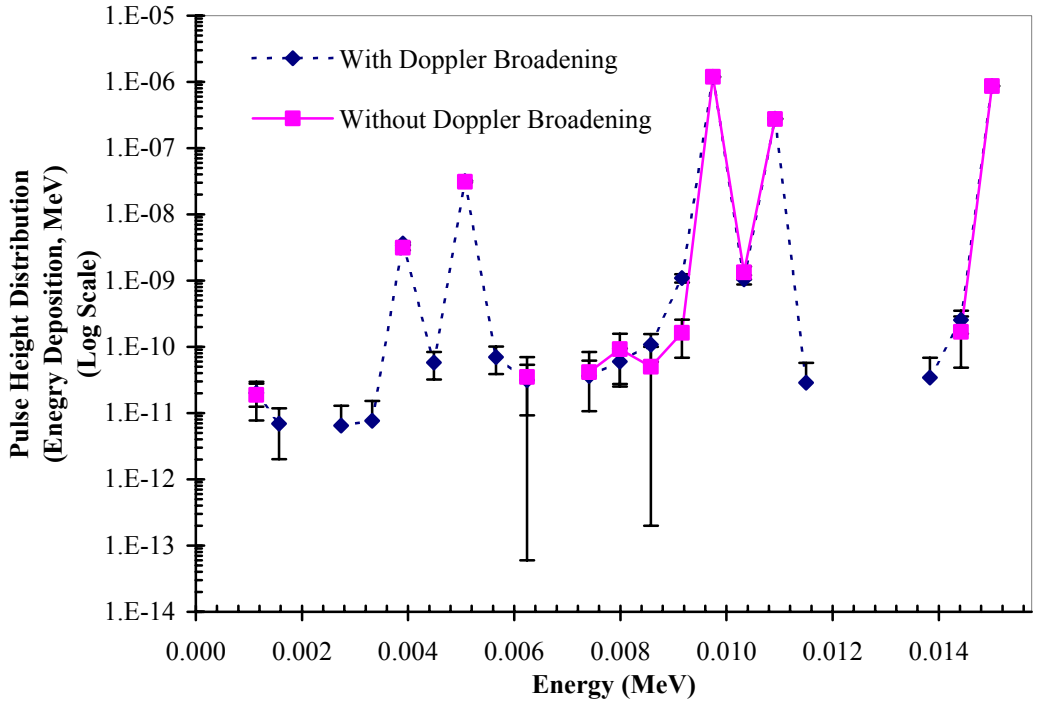

Fig. B.1. Pulse height distribution spectrum for a 15 keV photon incident upon a Ge detector, with and without the Doppler broadening feature. Results have been normalized to one source particle. Missing points had zero tallies. The first peak on the left at 3.9 keV may be the Compton edge, while the second peak at 5.1 keV does not correspond to any predicted peaks. The peaks around 10 keV correspond to characteristic X-rays from Ge. The characteristic X-ray at 9.8 keV is an electron from the L shell filling a vacancy in the K shell. The second characteristic X-ray peak at 11 keV is an electron from the M shell again filling a vacancy in the K shell. The full energy peak is also present at 15 keV. Error bars indicate one standard deviation.

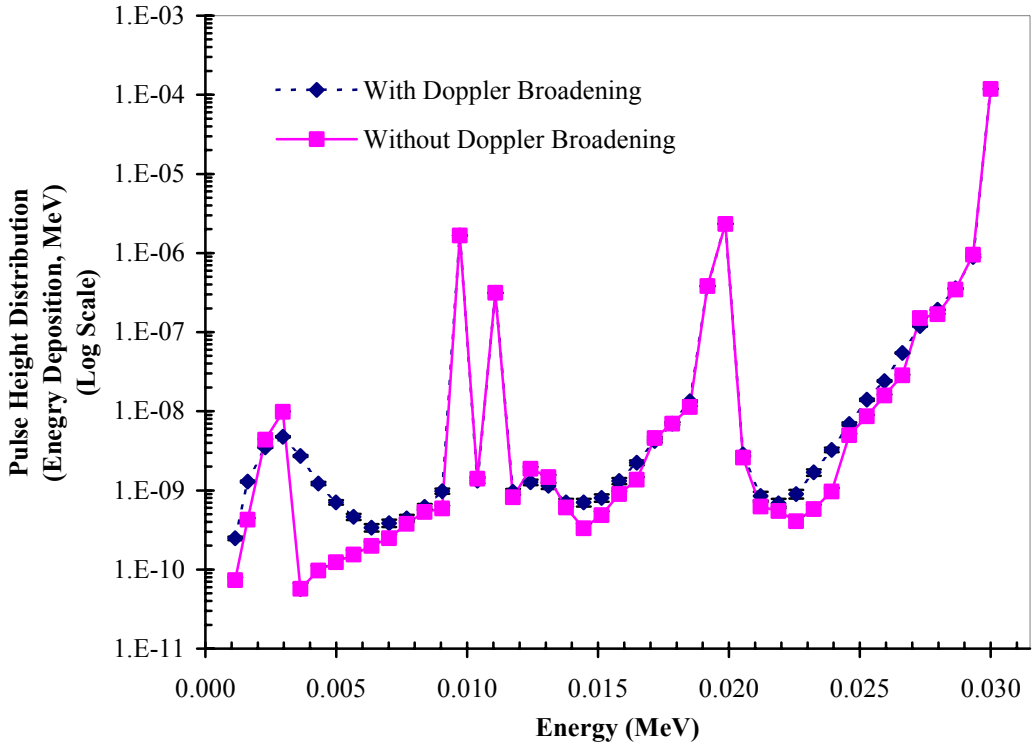

Fig. B.2. Pulse height distribution spectrum for a 30 keV photon incident upon a Ge detector with and without the Doppler broadening feature. Results have been normalized to one source particle. The peaks around 10 keV correspond to characteristic X-rays from Ge. The characteristic X-ray at 9.8 keV is an electron from the L shell filling a vacancy in the K shell. The second characteristic X-ray peak at 11 keV is an electron from the M shell again filling a vacancy in the K shell. The peak at 19 keV is an K shell X-ray escape peak from Ge. The backscatter peak is located at 26.85 keV. There may be a small peak in the spectrum without the Doppler broadening feature, but no peak exists with the feature. The full energy peak is also present at 30 keV. Error bars indicate one standard deviation.

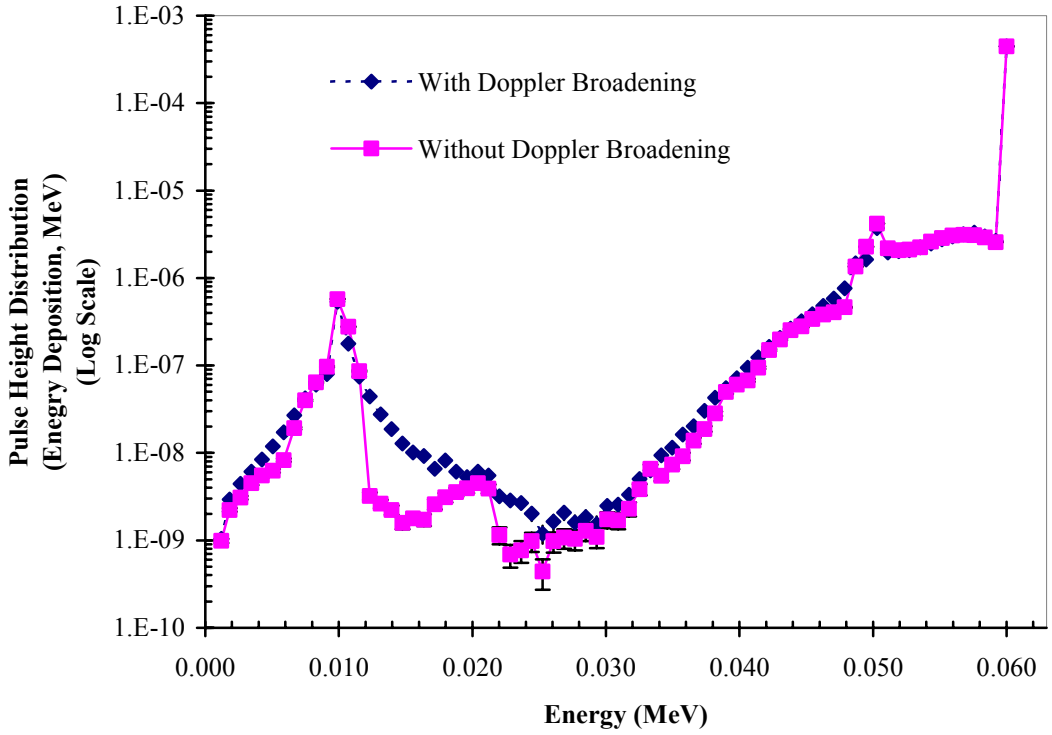

Fig. B.3. Pulse height distribution spectrum for a 60 keV photon incident upon a Ge detector with and without the Doppler broadening feature. Results have been normalized to one source particle. The peak at 10 keV is a mixture of characteristic X-rays from Ge. The peak at 50 keV could be the backscatter peak, 48.59 keV, or the Ge X-ray escape peak, 48.90 keV. The full energy peak is also present at 60 keV. Error bars indicate one standard deviation.

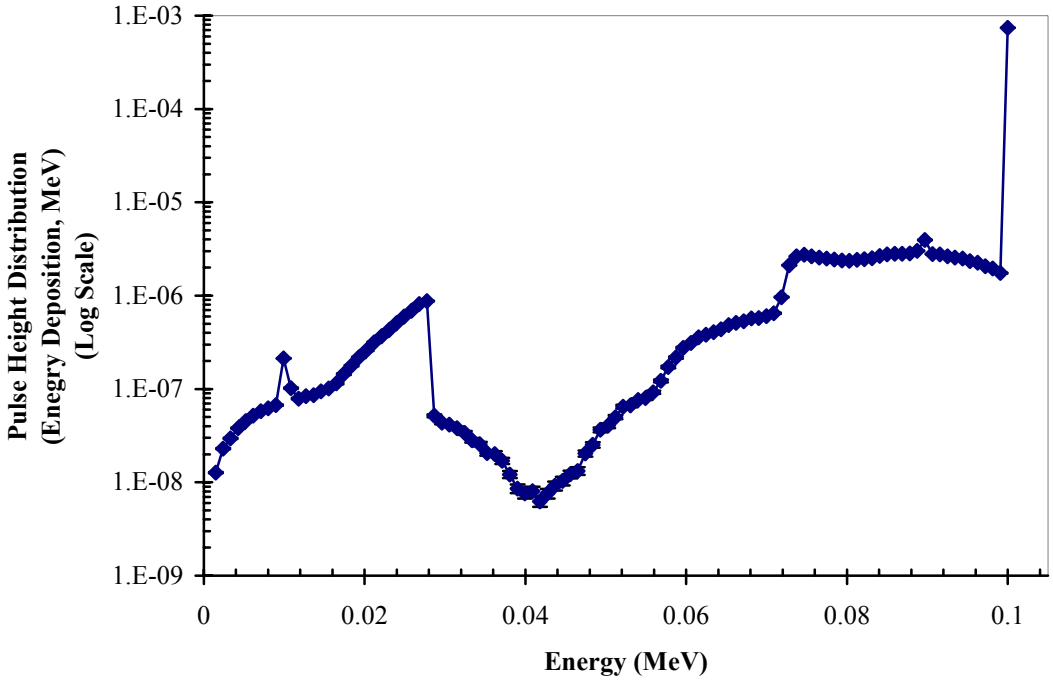

Fig. B.4. Pulse height distribution spectrum for a 100 keV photon incident upon a Ge detector. Results have been normalized to one source particle. The peak at 10 keV is a mixture of the characteristic X-rays from Ge. The Compton edge is located at 28 keV. A broad backscatter peak is at around 72 keV. The Ge K shell X-ray escape peak is at 89 keV. The full energy peak is also present at 100 keV. Error bars indicate one standard deviation.

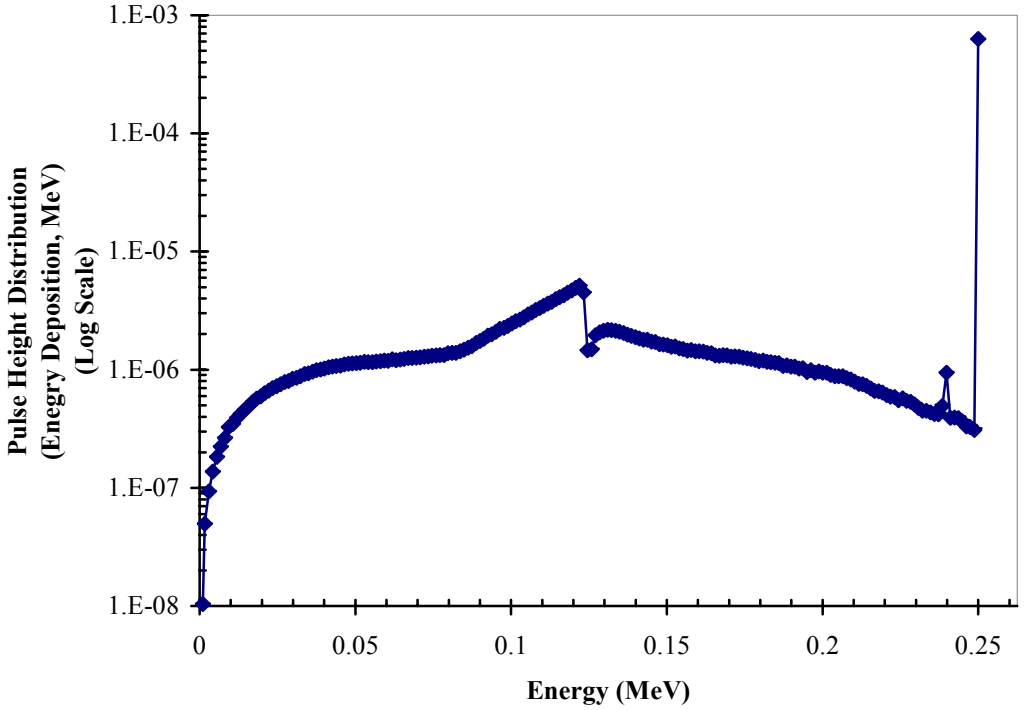

Fig. B.5. Pulse height distribution spectrum for a 250 keV photon incident upon a Ge detector. Results have been normalized to one source particle. The Compton edge is located at 124 keV. The Ge X-ray escape peak is at 239 keV. The full energy peak is also present at 250 keV. Error bars indicate one standard deviation.

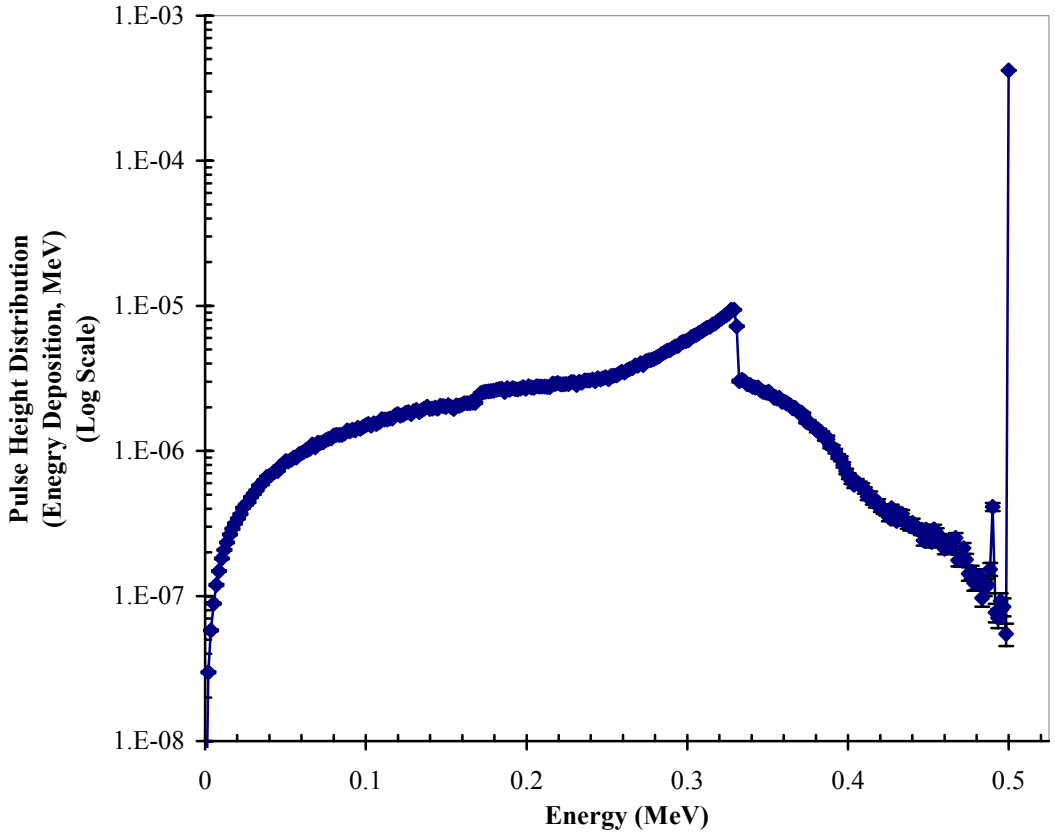

Fig. B.6. Pulse height distribution spectrum for a 500 keV photon incident upon a Ge detector. Results have been normalized to one source particle. A broad backscatter peak is located at around 169 keV, the Compton edge is located at 331 keV, and the Ge X-ray escape peak is at 489 keV. The full energy peak is also present at 500 keV. Error bars indicate one standard deviation.

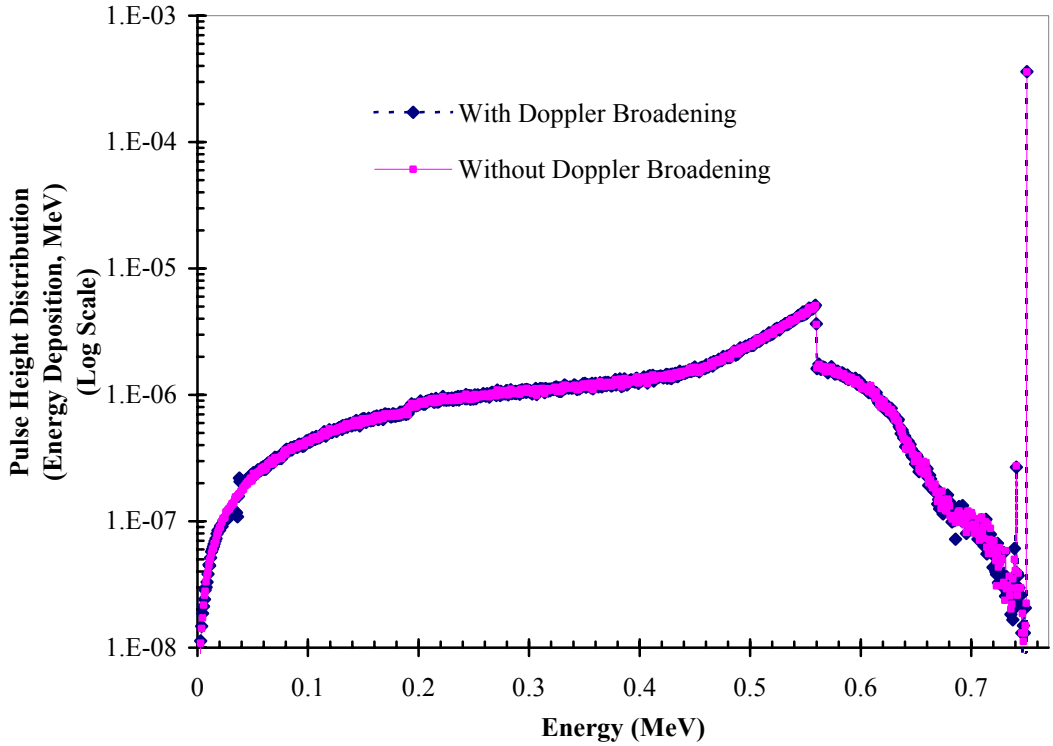

Fig. B.7. Pulse height distribution spectrum for a 750 keV photon incident upon a Ge detector with and without the Doppler broadening feature. Results have been normalized to one source particle. An error is evident at around 4 keV. A broad backscatter peak is located at around 190 keV, the Compton edge is located at 559 keV, and the Ge X-ray escape peak is at 739 keV. The full energy peak is also present at 750 keV. Error bars indicate one standard deviation.

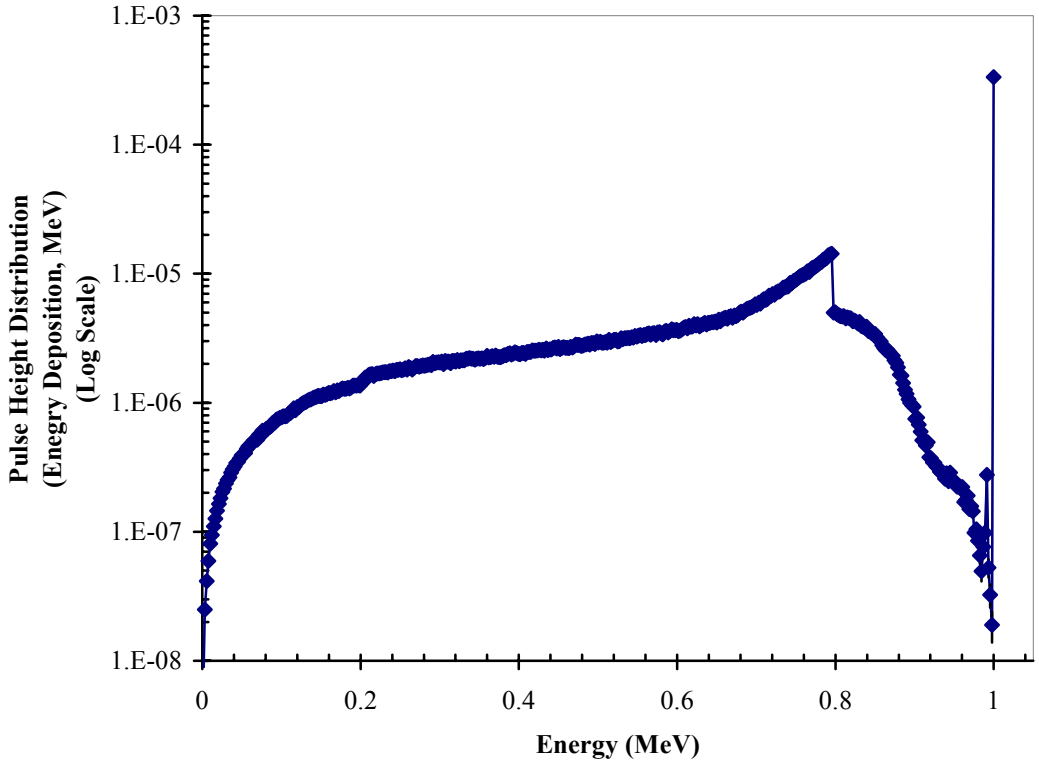

Fig. B.8. Pulse height distribution spectrum for a 1 MeV photon incident upon a Ge detector with and without the Doppler broadening feature. Results have been normalized to one source particle. A broad backscatter peak is located at around 204 keV, the Compton edge is located at 796 keV, and the Ge X-ray escape peak is at 989 keV. The full energy peak is also present at1 MeV. Error bars indicate one standard deviation.

VITA

R. Alex Redd received a Bachelor of Science degree in Chemistry from Texas A&M University on December 17, 1994. After graduation he attends to continue his education at Texas A&M University. His permanent address is 5247 Charing Way, Baton Rouge, LA 70817-2006.